

## FEATURE ARTICLE

## Meeting the Clean Energy Demand: Nanostructure Architectures for Solar Energy Conversion

Prashant V. Kamat\*

*Notre Dame Radiation Laboratory, Department of Chemistry & Biochemistry and Department of Chemical & Biomolecular Engineering, Notre Dame, Indiana 46556-5674**Received: October 23, 2006; In Final Form: December 6, 2006*

The increasing energy demand in the near future will force us to seek environmentally clean alternative energy resources. The emergence of nanomaterials as the new building blocks to construct light energy harvesting assemblies has opened up new ways to utilize renewable energy sources. This article discusses three major ways to utilize nanostructures for the design of solar energy conversion devices: (i) Mimicking photosynthesis with donor–acceptor molecular assemblies or clusters, (ii) semiconductor assisted photocatalysis to produce fuels such as hydrogen, and (iii) nanostructure semiconductor based solar cells. This account further highlights some of the recent developments in these areas and points out the factors that limit the efficiency optimization. Strategies to employ ordered assemblies of semiconductor and metal nanoparticles, inorganic-organic hybrid assemblies, and carbon nanostructures in the energy conversion schemes are also discussed. Directing the future research efforts toward utilization of such tailored nanostructures or ordered hybrid assemblies will play an important task in achieving the desired goal of cheap and efficient fuel production (e.g., solar hydrogen production) or electricity (photochemical solar cells).

## The Energy Challenge

The economic growth in many parts of the world during the past decade was able to be sustained because of the affordable energy prices. The dependence on oil and electricity has made energy a vital component of our everyday needs. The recent hike in oil and gas prices has prompted everyone to take a careful look at the issues dealing with our energy supply and demand. In the 20th century, the population quadrupled and our energy demand went up 16 times. The exponential energy demand is exhausting our fossil fuel supply at an alarming rate.<sup>1,2</sup> About 13 terawatts (TW) of energy is currently needed to sustain the lifestyle of 6.5 billion people worldwide. By year 2050, we will need an additional 10 TW of clean energy to maintain the current lifestyle.

**The End of Cheap Oil.** Emergence of more than a billion new consumers from 20 developing countries with a newly acquired spending capacity is increasing global CO<sub>2</sub> emission at an alarming rate.<sup>3</sup> For example, China and India, two countries with the largest numbers of new consumers have been adding new cars at an average annual increase of 19% and 14%, respectively. Motor vehicles alone account for more than 50% of air pollution in these countries.<sup>3</sup> Whereas the consumer growth in the developing countries is a good marker for predicting a brighter global economic outlook, it undermines the demand for additional energy resources and the overall impact on the environment. According to Hubbert,<sup>5–7</sup> the exponential growth we have seen in the last century is a *transient phenomenon*, and the fossil fuel production will follow the trend of a bell shaped curve. The peak oil production in the mainland

U.S. seen in 1970 followed this predicted curve thus giving the credibility to his model. His projected growth for the worldwide oil prediction was modified (Figure 1) by Campbell<sup>4,8,9</sup> and Deffeyes.<sup>10</sup> According to this prediction, the peak production will be attained within the next decade.

In the near term, we are not about to run out of oil, but the production will attain the peak. Of the 2000 billion barrels of net global oil reserve, we have already found 1800 billion barrels of which 875 billion barrels have been consumed.<sup>10</sup> For every billion barrels of new oil discovered, we are consuming 4 billion barrels. Undoubtedly, new technologies can facilitate the extraction of oil from hard to obtain areas and sustain the production of each site longer, but it will have no impact on the reserves themselves. Extraction of oil from tar sands and shale will not be cheaper as it will demand additional energy for the extraction of oil from these sources. Coal and natural gas are likely to supplement the energy needs but this fossil fuel production will follow the Hubbert peak before the end of this century. The flow of energy supply by various sources in sustaining the population growth from 1600 to 2200 is shown in Figure 2. The role of oil and gas as per this model will have a significant impact as a major energy source for only a short duration. Diversification of our energy supply and political and social compromise for conservation will become inevitable if we need to maintain a healthy global economic growth.<sup>1,2,11,12</sup>

**Green House Gas Emission.** Another important consideration of increasing the energy production based on fossil fuels is its impact on the environment. Global warming from the fossil fuel greenhouse gases which contribute to the climate changes is becoming a major concern.<sup>13</sup> Recent scientific reports point

\* E-mail: pkamat@nd.edu. Web site: <http://www.nd.edu/~pkamat>.



Prashant V. Kamat is currently a Professor of Chemistry and Biochemistry, a Senior Scientist at Radiation Laboratory, and a Concurrent Professor in the Department of Chemical and Biomolecular Engineering, University of Notre Dame. A native of Binaga, India, he earned his masters (1974) and doctoral degrees (1979) in Physical Chemistry from the Bombay University, and carried out his postdoctoral research at Boston University (1979–1981) and University of Texas at Austin (1981–1983). He joined Notre Dame Radiation Laboratory in 1983 and initiated the photoelectrochemical investigation of semiconductor nanoparticles. Dr. Kamat's research has made significant contributions to three areas: (1) photoinduced catalytic reactions using semiconductor and metal nanoparticles, nanostructures and nanocomposites, (2) advanced materials such as inorganic–organic hybrid assemblies for utilizing renewable energy resources, and (3) environmental remediation using advanced oxidation processes and chemical sensors. He has directed DOE funded solar photochemistry research for more than 20 years. He has published more than 300 peer-reviewed journal papers, review articles, and book chapters. He has edited two books in the area of nanoscale materials. He was a fellow of Japan Society for Promotion of Science during 1997 and 2003 and was presented the 2006 Honda-Fujishima Lectureship award by the Japan Photochemical Society.

out a higher global mean surface temperature and melting of arctic ice. The surface temperature of Atlantic Ocean today is higher than it has been for at least a millennium making the tropical storms and hurricanes stronger than ever. The United Nations Framework Convention on Climate Change calls for "stabilization of greenhouse-gas concentrations in the atmosphere at a level that would prevent dangerous anthropogenic interference with the climate system 10 TW ( $10 \times 10^{12}$  watts) of carbon-emission-free power needs to be produced by the year 2050, almost equivalent to the power provided by all of today's energy sources combined".<sup>14,15</sup>

**Meeting Clean Energy Demand.** In order to meet the increasing energy demand in the near future, we will be forced to seek environmentally clean alternative energy resources.<sup>11,16,17</sup> Three major options are at our disposal to tackle the 10 TW clean energy generation in the coming years. These include carbon neutral energy (fossil fuel in conjunction with carbon sequestration), nuclear power, and renewable energy. If we have to produce 10 TW energy using fossil fuels without affecting the environment, we need to find secure storage for 25 billion metric tons of CO<sub>2</sub> produced annually (equal to the volume of 12500 km<sup>3</sup> or the volume of Lake Superior!). Should nuclear power be the alternate source of energy, we will require construction of a new 1 GW (gigawatt)-electric nuclear fission plant everyday for the next 50 years somewhere on this planet. Renewable energy can be tapped from the available resources: hydroelectric resource (0.5 TW), from all tides & ocean currents (2 TW), geothermal integrated over all of the land area (12 TW), globally extractable wind power (2–4 TW), and solar energy striking the earth (120,000 TW). Among these options solar energy stands out as the most viable choice to meet our energy

demand. Despite this vast resource, the energy produced from solar remains less than 0.01% of the total energy demand.

Although renewable energy such as solar radiation is ideal to meet the projected demand, it requires new initiatives to harvest incident photons with greater efficiency.<sup>18,19</sup> The single-crystal silicon based photovoltaic devices that are commercially available for installation deliver power with a 15% efficiency. These *first generation* devices suffer from high cost of manufacturing and installation. The *second generation* devices consisting of CuInGaSe<sub>2</sub> (CIGS) polycrystalline semiconductor thin films can bring down the price significantly, but their efficiency needs to be enhanced in order to make them practically viable. Now being aimed are the *third generation* devices that can deliver high efficiency devices at an economically viable cost. Our ability to design nanostructured semiconductors, organic–inorganic hybrid assemblies, and molecular assemblies opens up new ways to design such third generation light energy conversion devices.

### Nanotechnology to the Rescue?

During the past decade, nanomaterials have emerged as the new building blocks to construct light energy harvesting assemblies. Organic and inorganic hybrid structures that exhibit improved selectivity and efficiency toward catalytic processes have been designed. Size dependent properties such as size quantization effects in semiconductor nanoparticles and quantized charging effects in metal nanoparticles provide the basis for developing new and effective systems.<sup>20–26</sup> These nanostructures provide innovative strategies for designing next generation energy conversion devices.<sup>27–32</sup> Recent efforts to synthesize nanostructures with well-defined geometrical shapes (e.g., solid and hollow spheres, prisms, rods, and wires) and their assembly as 2- and 3-dimensional assemblies has further expanded the possibility of developing new strategies for light energy conversion.<sup>33–45</sup>

There are three major ways that one can utilize nanostructures for the design of solar energy conversion devices (Figure 3). The first one is to mimic photosynthesis with donor–acceptor molecular assemblies and clusters. The second one is the semiconductor assisted photocatalysis to produce fuels such as hydrogen. The third and most promising category is the nanostructure semiconductor based solar cells. This account highlights some of the recent developments in these areas and points out the factors that limit the efficiency optimization. Strategies to employ ordered assemblies of semiconductor and metal nanoparticles, inorganic-organic hybrid assemblies, and carbon nanostructures in the energy conversion schemes are discussed in the following sections.

#### 1. Donor–Acceptor Hybrid Assemblies

In photosynthesis, light energy is converted into chemical energy by green plants. The essential roles of chlorophyll *a*, (Chl*a*) are to capture solar energy, transfer the excitation energy to special locations, the reaction centers, and bring about the charge separation for the subsequent electron-transfer processes. Based on the principle of photosynthesis, a variety of donor–acceptor dyads and triads have been synthesized as light harvesting assemblies.<sup>46–53</sup> Of particular interest has been the study of donor–acceptor systems containing Chl*a* and porphyrins that can mimic the photoinduced electron-transfer process of natural photosynthesis. Despite the success of achieving long-lived charge separation, the use of dyads and triads in solar cells is rather limited.<sup>48,54–56</sup> A better understanding of the underlying physical principles of light absorption, energy transfer, radiative and nonradiative excited-state decay, electron

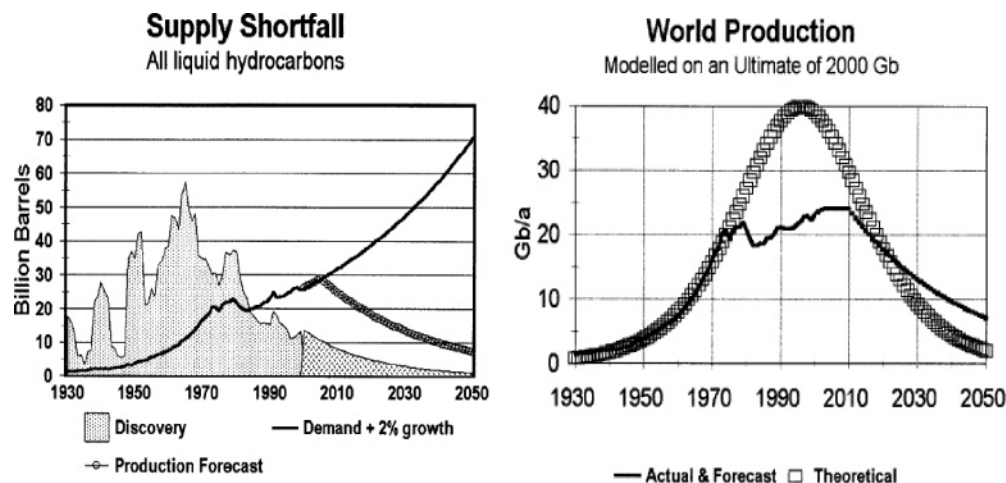


**Figure 1.** Left: Discovery trend. Oil discovery peaked in the 1960s, when we were finding more than we used. Now, the situation is reversed, meaning that the historic trend of growth at about 2% a year cannot be maintained as we consume our inheritance from past discovery. Right: World production of oil. Production has to mirror discovery, starting and ending at zero, with a peak in between at the halfway point. Production matched the theoretical curve well until the oil shock of the 1970s meaning that peak is lower and later than would otherwise have been the case, but decline is inevitable given a finite total. (From ref 4. Reprinted with permission from Springer.)

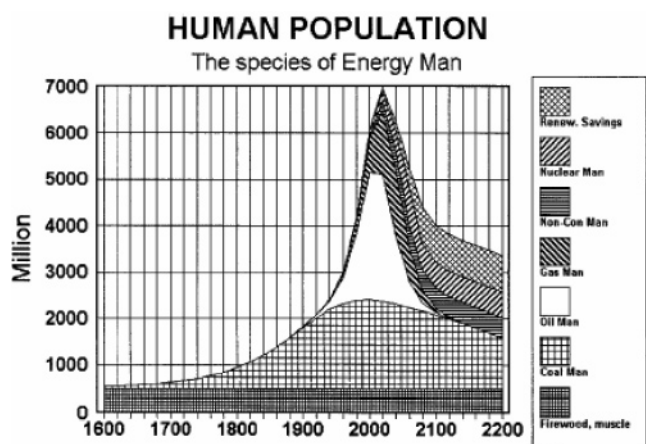


**Figure 2.** Sustaining the population with different energy resources. Each source of energy supports a corresponding population. The impact on population of oil and gas has been dramatic but is short-lived. (From ref 4 Reprinted with permission of Springer.)

transfer, proton-coupled electron transfer, and catalysis are important in designing molecular assemblies for energy conversion.<sup>57</sup> New approaches have to be considered to harvest the separated charges in a donor–acceptor molecular system.

Tailoring the optoelectronic properties of metal nanoparticles by organizing chromophores of specific properties and functions on gold nanoparticles can yield photoresponsive organic–inorganic nanohybrid materials. The organization of a densely packed photoresponsive shell encapsulating the nanoparticle core offers exciting opportunities for the design of novel photon-based devices for sensing, switching, and drug delivery<sup>58–61</sup> Metal hybrids of organic molecules assembled as two- or three-dimensional architectures provide routes to the design of materials with novel electrical, optical, and photochemical properties having potential applications in nanophotonics, lithography, and sensing.<sup>30,62–69</sup> The possibility of tailoring the optoelectronic properties of metal nanoparticles by organizing chromophores of specific properties and functions on gold nanoparticles prompts one to design photoresponsive organic–inorganic nanohybrids. Such an organization of a densely packed photoresponsive shell encapsulating the nanoparticle core offers exciting opportunities for the design of light energy conversion

devices.<sup>29</sup> Gold nanoparticles are widely used as probes for bimolecular labeling and as immunoprobes.<sup>70,71</sup>

Organized inorganic–organic nanohybrids, with hierarchical superiority in architecture, can be developed by assembling monolayers of organic molecules containing functional groups, such as amines, thiols, isothiocyanate, and silanes, on to the three-dimensional surface of metal nanoparticles.<sup>59,72</sup> Such monolayer protected metal clusters (MPCs) prepared by adopting the “two-phase extraction” procedure<sup>73,74</sup> can be functionalized with chromophores by “place exchange” reactions.<sup>75–77</sup> For example, porphyrin–alkanethiolate monolayer protected-gold nanoclusters (H<sub>2</sub>PC<sub>n</sub>MPC) form spherical shape clusters that can be employed as light harvesting antenna (Figure 4). They exhibit efficient light-harvesting capability and suppress undesirable energy transfer quenching of the porphyrin singlet excited-state by the gold surface relative to the bulk gold.

**a. Excited State Interactions.** The close vicinity of a metal nanoreactor alters the excited deactivation pathways of the surface-bound molecules. For example, Drexhage and co-workers have observed a distance-dependent quenching of excited states of chromophores on metal surfaces.<sup>78</sup> One of the noticeable properties of the fluorophore molecules when bound to metal surfaces is the decrease in singlet lifetime as a result of energy transfer from excited dye molecules to bulk metal films.<sup>79–81</sup> Total quenching of the singlet-excited-state of the chromophores can limit the application of chromophore-labeled metal nanoparticles in optoelectronic devices and photonic materials. Interestingly, recent studies on the photophysical properties of chromophore-linked gold nanoparticles from our group<sup>82–87</sup> and others<sup>88–94</sup> have suggested a dramatic suppression in the quenching of the singlet-excited-state when these chromophores are densely packed on Au nanoparticle surfaces. A better understanding of the excited-state processes will enable effective utilization of chromophore-functionalized metal nanostructures for light-harvesting and other specialized applications. Possible deactivation pathways of the photoexcited fluorophore bound to a gold nanoparticle, viz., (A) intermolecular interactions, (B) energy transfer, (C) electron transfer, and (D) emission from the chromophores bound on the metal nanoparticles, are summarized in Figure 5.

In the case of hybrid assemblies having metal nanoparticles as the core, the energy transfer depends critically on the size and shape of the nanoparticles, the distance between the dye

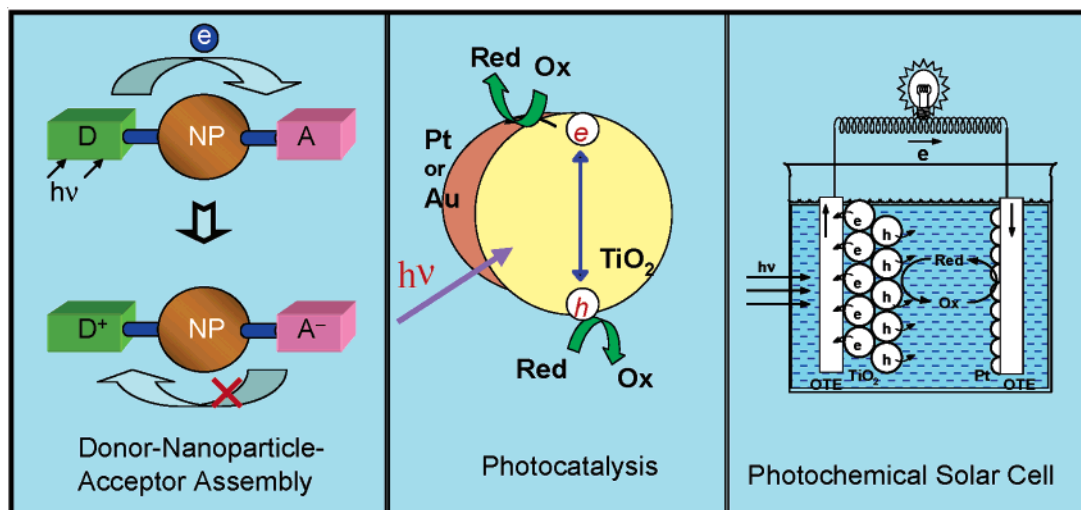


Figure 3. Strategies to employ nanostructured assemblies for light energy conversion.

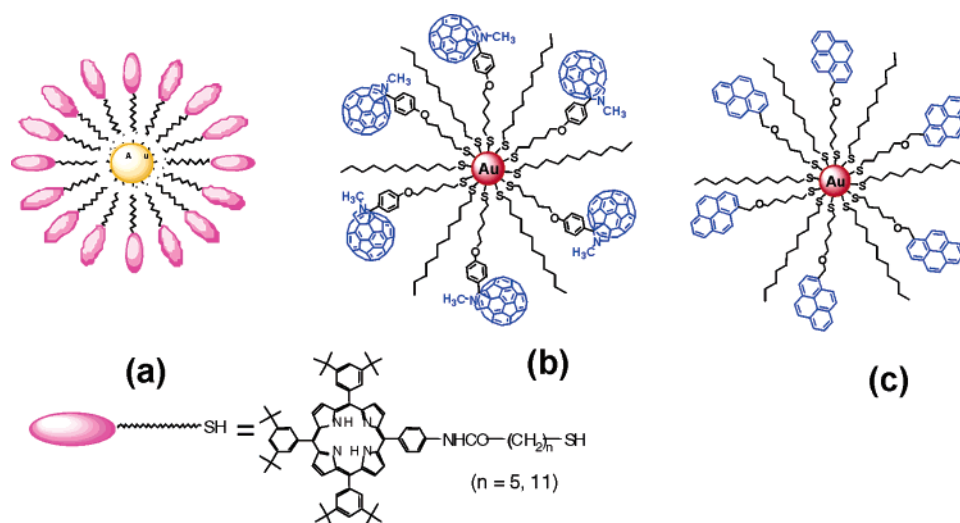


Figure 4. Examples of gold nanoparticles functionalized with (a) porphyrin, (b)  $C_{60}$ , and (c) pyrene (from ref 29).

molecule and the nanoparticle, the orientation of the molecular dipole with respect to the dye–nanoparticle axis, and the overlap of the chromophore emission with the nanoparticle absorption.<sup>95</sup> Energy transfer processes were found to dominate the deactivation of the excited-state in fullerene-functionalized gold clusters ( $C_{60}$ –R–S–Au).<sup>96</sup> Clusters of  $C_{60}$ –R–S–Au can be visualized as antenna systems containing a gold nanoparticle as the central nanocore and appended fullerene moieties as the photoreceptive hydrophobic shell.  $C_{60}$ –R–SH emission is totally quenched when the fullerene is anchored to the gold nanocore. Near field optical microscopy further aids in elucidating the photoinduced energy transfer to metal particles.<sup>97–99</sup>

The low singlet as well as triplet yields of the fullerene moiety in excited  $C_{60}$ –R–S–Au nanohybrids confirm that most of the excited-state energy is quickly dissipated to the Au core via energy transfer. Dulkieth et al.<sup>95</sup> isolated the resonant energy transfer rate from the decay rates of excited lissamine dye molecules by chemically attaching them to gold nanoparticles of different size. The increase in lifetime with decreasing particle size (particle diameter range of 1–30 nm) was indicative of decreased efficiency of energy transfer in smaller size particles. Heeger and co-workers<sup>100</sup> investigated the role of energy as well as electron transfer in the quenching of emission of conjugated polymers in the presence of gold nanoparticles of varying size. They concluded that resonance energy transfer dominates when

the diameter of Au nanoparticle is  $>2$  nm. Using the principle of energy transfer, attempts are being made to develop biosensors.<sup>101,102</sup>

**b. Photoinduced Electron Transfer.** Semiconductor nanoparticles are known to accept electrons from an excited sensitizer and transfer the electrons to another acceptor molecule bound to the surface. The demonstration of semiconductor particle mediated electron transfer between donor and acceptor molecules bound to its surface was demonstrated in our early studies.<sup>103–105</sup> The nonmetallic property of ultrasmall metallic particles can also be utilized to capture electrons from an excited sensitizer and thus mediate a photoinduced electron-transfer process.

In polar solvents, pyrene-linked Au nanoparticles ( $Py$ – $R_1$ –S–Au) exhibit noticeably lower yields compared to unbound pyrene thiol ( $Py$ – $R_1$ –SH).<sup>82</sup> Transient absorption experiments using pulsed laser irradiation (337 nm) of  $Py$ – $R_1$ –S–Au nanoparticle, in polar solvents such as tetrahydrofuran or acetonitrile confirm the electron transfer between gold nanoparticle and pyrene (Figure 6). The charge-separated states in  $Py$ – $R_1$ –S–Au assemblies are fairly long-lived as indicated by the longer lifetime of the pyrene cation radical (4.5  $\mu$ s). These observations demonstrate the ability of gold nanoparticles as electron acceptors.

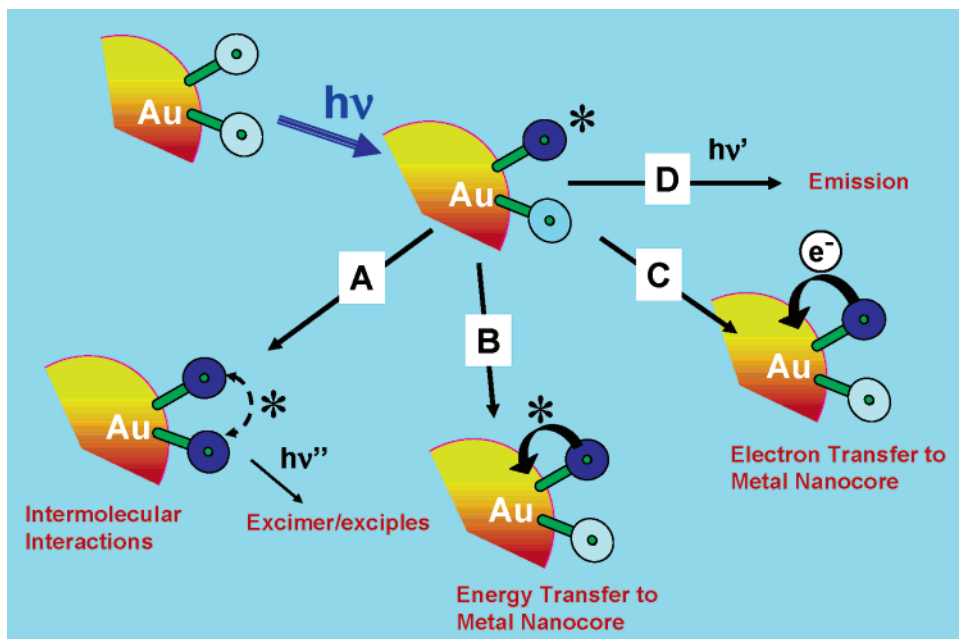


**Figure 5.** Photoexcitation of the chromophore bound to gold nanoparticles followed by its deactivation via energy transfer, electron transfer, and intermolecular interactions (from ref 29).

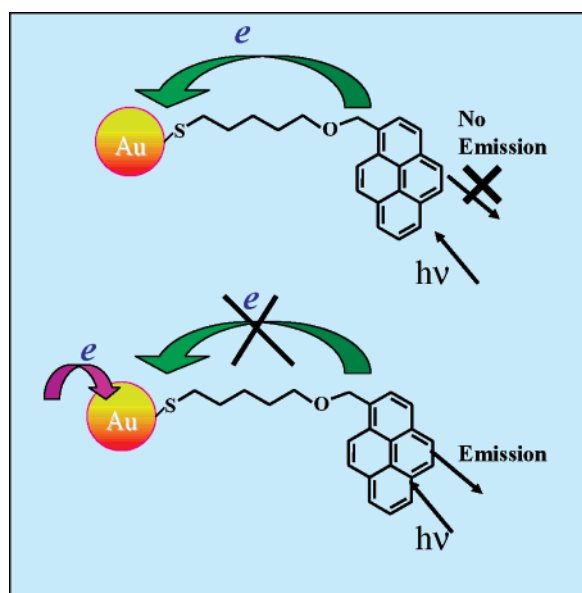


**Figure 6.** Modulation of photoinduced electron transfer between excited chromophore and gold nanoparticles (from ref 83).

Controlled charging of the Au nanoassembly enables one to modulate the excited-state interaction between the gold nanoparticle and a surface-bound fluorophore.<sup>83,87</sup> For example, a bifunctional surface-linking molecule such as mercaptopropionic acid was used to link the gold nanoparticle to the TiO<sub>2</sub> surface (thiol group to gold and carboxylic group to TiO<sub>2</sub>). Spectroelectrochemical experiments carried out using a thin layer electrochemical cell showed the emission spectra of pyrene modified gold particles which were linked to TiO<sub>2</sub> film cast on an optically transparent electrode (OTE/TiO<sub>2</sub>/-OOC-R<sub>2</sub>-S-(Au)-S-R<sub>1</sub>-Py) and subjected to different applied potentials (Figure 7). As the electrode is biased to negative potentials, an increase in the emission yield was observed. The overall shape of the emission band remains the same suggesting that the photoactive molecule contributing to the emission is unperturbed. At potentials more negative than -1.0 V, 90% of the quenched emission is restored by charging the gold nanopar-

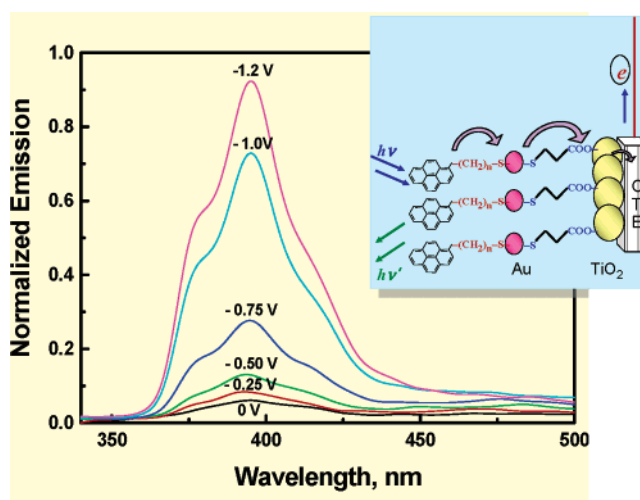


**Figure 7.** Modulation of photoinduced charge transfer in a pyrene modified gold particles linked to TiO<sub>2</sub> film cast on an optically transparent electrode (OTE). (From ref 83.)

ticles. The quantized charging effects studied with organic-capped gold nanoparticles suggest that the potential shift amounts to about 0.1 V per accumulated electron.<sup>106</sup> The electron transfer from excited pyrene molecules to gold nanoparticle experiences a barrier as we charge them with negative electrochemical bias.

The photoinduced electron-transfer mechanism in chlorophyll *a* bound gold nanoparticles was also confirmed from the electrochemical modulation of fluorescence of Chl<sub>a</sub>.<sup>87</sup> In the absence of an applied bias, Chlorophyll *a* cast on gold particulate films, as a result of electron transfer, exhibits a very weak fluorescence emission. However, upon negatively charging the gold nanoparticle by external bias, the fluorescence intensity increases. Charging the gold nanoparticles increases the energy barrier and thus suppresses direct electron transfer. This suppressed electron-transfer pathway at negative bias increases in radiative process. In addition to this indirect evidence for the electron transfer between excited chlorophyll *a* and gold nanoparticles, direct evidence for electron transfer was also

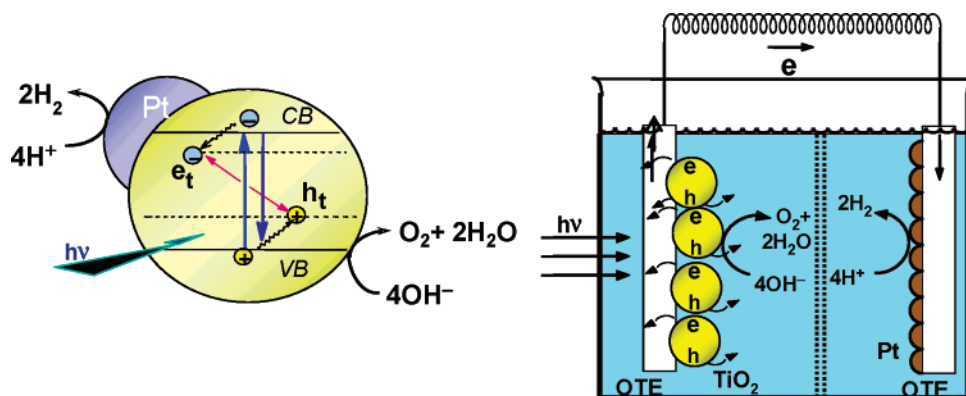


**Figure 8.** Photocatalytic splitting of water following the band gap excitation of the semiconductor nanoparticle (left) and a photoelectrolysis cell based on a nanostructured semiconductor film electrode (right).

**TABLE 1: Influence of Metal on the Hydrogen Evolution Rates in TiO<sub>2</sub> Assisted Water Splitting Reaction (from ref 121)**

catalyst	H <sub>2</sub> , μL/hr	catalyst	H <sub>2</sub> , μL/hr	catalyst	H <sub>2</sub> , μL/hr
Pt/TiO <sub>2</sub>	7.7	Ru/TiO <sub>2</sub>	0.2	Ni/TiO <sub>2</sub>	0.1
Pd/TiO <sub>2</sub>	6.7	Sn/TiO <sub>2</sub>	0.2	TiO <sub>2</sub>	<0.1
Rh/TiO <sub>2</sub>	2.8				

obtained using nanosecond laser flash experiments. Taking advantage of these properties of gold nanoparticles, a photoelectrochemical cell based on Chla and gold nanoparticles has been constructed.<sup>87</sup>

The examples discussed above show the ability of gold nanoparticles to accept electrons from excited chromophores. Such a photoinduced electron-transfer process occurs only with small size ( $\leq 5$  nm diameter) particles. The unique electron storage property of gold nanoparticles are yet to be explored fully for facilitating charge separation and charge transport in light harvesting systems.

## 2. Catalysis with Semiconductor/metal Nanocomposites

Semiconductor nanoparticles when subjected to band gap excitation undergo charge separation. Because of the small size of particles and high recombination rate, only a fraction ( $\sim 5\%$ ) of these charges can be utilized to induce redox processes at the interface. The photocatalytic processes using TiO<sub>2</sub> and other semiconductors have demonstrated the need to overcome the limitations in achieving higher photoconversion efficiencies. Of particular interest is the use of semiconductor nanostructures for solar hydrogen production by the photocatalytic splitting of water.<sup>47,107–110</sup> The principle of photocatalysis for producing solar hydrogen is presented in Figure 8.

Efforts to employ semiconductor–semiconductor or semiconductor–metal composite nanoparticles have been explored to facilitate charge rectification in the semiconductor nanostructures and improve the charge separation efficiency.<sup>111–119</sup> For example, the deposition of a noble metal on semiconductor nanoparticles is beneficial for maximizing the efficiency of photocatalytic reactions.<sup>47,120–125</sup>

During the early years of photocatalysis, it was shown that the photoinduced deposition of noble metals such as Pt, Pd, or Ir on semiconductor nanoclusters enhance their photocatalytic activity.<sup>121,125–131</sup> One of the early studies (Table 1) highlighted how different metals influence the semiconductor-assisted hydrogen production.<sup>121</sup> A basic understanding of the energetics and electron-transfer process at the semiconductor-metal interface is crucial to design new and efficient catalyst materials.

The noble metal (e.g., Pt), which acts as a reservoir for photogenerated electrons, promotes an interfacial charge-transfer process. A direct correlation between the work function of the

metal and the photocatalytic activity for the generation of NH<sub>3</sub> from azide ions has been made for metallized TiO<sub>2</sub> systems.<sup>132</sup> For more than two decades, a number of research groups are involved in modifying the photocatalytic properties of TiO<sub>2</sub> and other semiconductor materials using metal deposits.<sup>47,120,122,133–137</sup>

Doping of TiO<sub>2</sub> nanostructures with transition metal ions has been probed by several researchers to improve the photocatalytic properties of semiconductor nanoparticles (see for example refs 138 and 139). Effort was made to incorporate metal ions to extend the photoresponse of TiO<sub>2</sub> films into the visible.<sup>140,141</sup> Doping of TiO<sub>2</sub> with anions such as nitrogen and sulfur has been found to be effective in extending the photoresponse to the visible.<sup>142–151</sup> There has been significant activity in recent years to utilize new nanophotocatalysts that respond in the visible.<sup>141,152–155</sup> The splitting of water under visible light with a catalyst consisting of a solid solution of gallium and zinc nitrogen oxide (Ga<sub>1-x</sub>Zn<sub>x</sub>)(N<sub>1-x</sub>O<sub>x</sub>) has recently been reported using modifications with nanoparticles of a mixed oxide of rhodium and chromium.<sup>156</sup>

While investigating the effect of metal deposition on the photoelectrochemical properties, Nakato and Tsubumora observed unusually high open-circuit voltages for n-Si electrodes modified with metal islands.<sup>157,158</sup> Gold film deposition on a single-crystal TiO<sub>2</sub> electrode on the other hand led to a decrease in the photopotential.<sup>159,160</sup> An unusual photoelectrochemical effect has also been reported for Ni/TiO<sub>2</sub> nanocomposite films.<sup>161</sup> The photoelectrochemical performance of TiO<sub>2</sub> films is influenced by the adsorption of gold nanoparticles from a toluene solution.<sup>137,162–164</sup> Metal nanoparticle deposition was found to promote the interfacial charge-transfer process in these composite systems. A  $\sim 40\%$  enhancement in the hole transfer efficiency was confirmed in the laser flash photolysis study of gold capped TiO<sub>2</sub> nanoparticles. The size of nanoparticles as well as the mode of deposition of metal nanoparticles becomes crucial while tailoring the properties of semiconductor films.<sup>165</sup> Similarly, interfacial changes seen when subjected to UV irradiation also influence the overall photocatalytic activity of semiconductor–metal composites.<sup>166,167</sup>

Chemical, electrochemical, and photolytic methods are commonly used for the deposition of noble metals on semiconductor nanoparticles. One simple way to deposit metal on TiO<sub>2</sub> is to choose a metal ion that electrostatically binds to the oxide surface.<sup>137,168</sup> The gold capped TiO<sub>2</sub> nanoparticles for example can be prepared by first synthesizing a TiO<sub>2</sub> suspension in water (stabilized at pH 1.5) and then capping these particles with [AuCl<sub>4</sub>]<sup>-</sup>. The positively charged TiO<sub>2</sub> core acts as a support to bind [AuCl<sub>4</sub>]<sup>-</sup> ions that are subsequently reduced by chemical

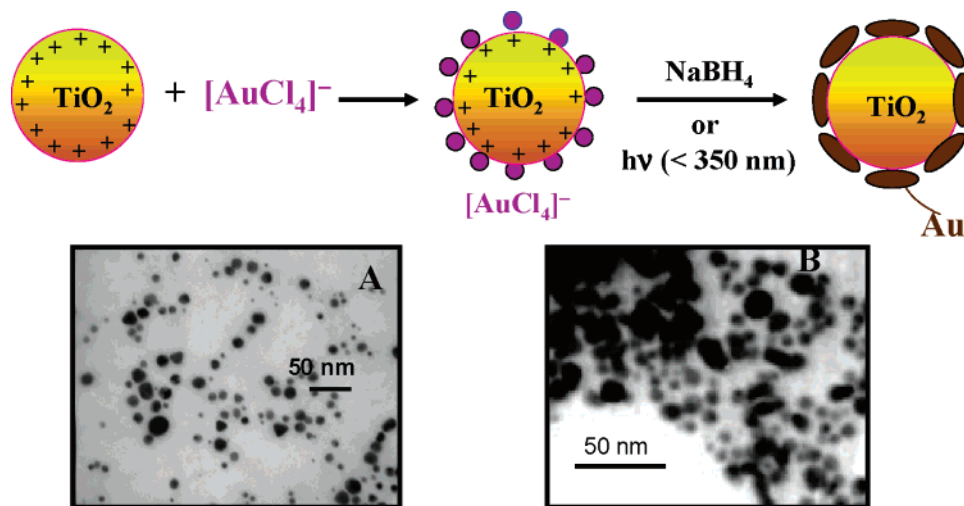


**Figure 9.** Synthetic strategy for preparing semiconductor-gold nanoparticles. TEM images of gold capped  $\text{TiO}_2$  particles prepared using (A) Chemical reduction and (B) UV-irradiation are shown. (From refs 168 and 169.)

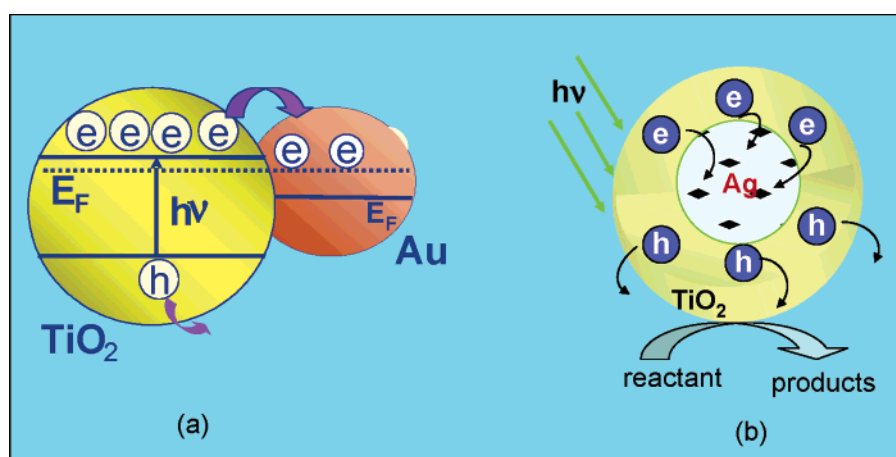


**Figure 10.** Design of semiconductor-metal nanocomposites using (a) coupled and (b) core-shell geometry.

reduction<sup>168</sup> or using UV irradiation.<sup>169</sup> The principle for preparing such metal-semiconductor nanocomposites is shown in Figure 9. Similar methodology has also been adopted to deposit silver clusters on anatase  $\text{TiO}_2$  nanorods.<sup>170,171</sup> These Ag- $\text{TiO}_2$  nanorods show the possibility of enhancing photocatalytic activities by way of morphology and the size of silver clusters.

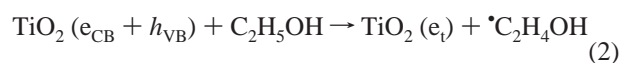
Fundamental understanding of the photoinduced interactions between a semiconductor and metal as well as the interfacial charge-transfer process in nanocomposites is important to elucidate the role of noble metals in semiconductor assisted photocatalysis. A better understanding of the energetics of such nanocomposite systems is important for tailoring the properties of next-generation nanodevices. The mediating role of noble metals in storing and shuttling photogenerated electrons from the semiconductor to an acceptor in a photocatalytic process can be understood by designing composite structures with coupled and core-shell geometry (Figure 10).

**a.  $\text{TiO}_2$ -Gold Composite Nanoparticles.** The realization of catalytic properties of ultrasmall gold nanoparticles has created a great deal of interest in its utilization and understanding of its size-dependent properties in photocatalytic reactions. Electrochemical,<sup>172-174</sup> photochemical,<sup>82,175</sup> and spectroelectrochemical<sup>83,176</sup> experiments have shown that the gold nanoparticles capped with organic molecules exhibit unusual redox activity by readily accepting electrons from a suitable donor or an electrode. If such metal particles come in contact with a

charged semiconductor nanostructure or nanoparticle, the Fermi levels of the two systems equilibrate.<sup>175,177-180</sup>

One factor that can potentially influence the electronic properties of the nanocomposite is the size of the metal particle. For example, Haruta and co-workers<sup>181,182</sup> demonstrated that gold nanoparticles in the 2-5 nm range show unusually high catalytic activities. Goodman and co-workers have demonstrated the influence of gold nanoparticle deposition on the overall energetics and catalytic activity of titania.<sup>183,184</sup> Similarly, size-dependent quantized conductance at metal nanocontacts has also been demonstrated.<sup>185</sup>

The Au-mediated electron transfer to an electron acceptor such as  $\text{C}_{60}$  can be followed by introducing Au nanoparticles to UV-irradiated  $\text{TiO}_2$  suspension.<sup>180,186</sup>



The spectra *a* and *b* in Figure 11 were recorded before and after the addition of Au nanoparticles to the UV-irradiated  $\text{TiO}_2$  suspension. The decreased blue coloration of the UV-irradiated  $\text{TiO}_2$  suspension shows the transfer of electrons to Au nanoparticles as the two particles undergo charge equilibration (reaction 3). Upon addition of  $\text{C}_{60}$  solution to the equilibrated  $\text{TiO}_2/\text{Au}(e)$  suspension (viz., the solution corresponding to

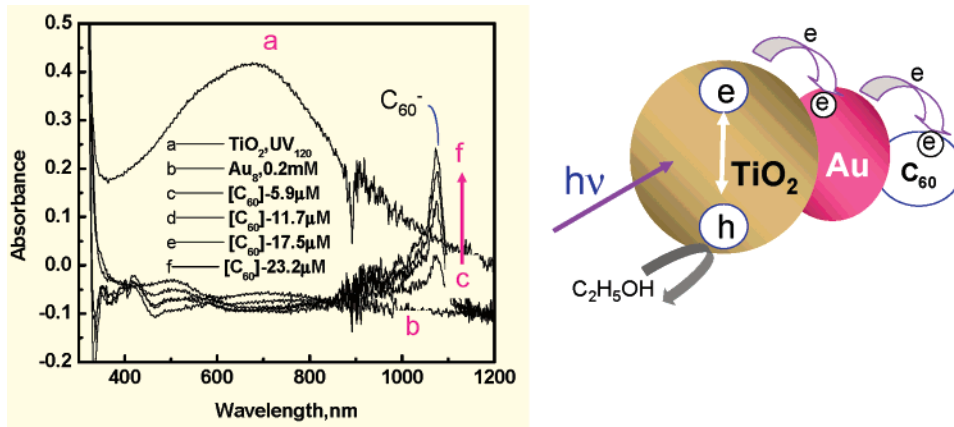
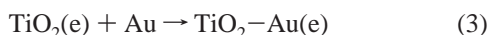


**Figure 11.** Absorption spectra of deaerated  $\text{TiO}_2$  (5.5 mM) suspension after UV irradiation ( $\lambda > 300$  nm) for 120 min: (a) before and (b) after addition of 0.6 mM Au nanoparticles (8 nm diameter). After equilibrating  $\text{TiO}_2$  and Au system, known amounts of  $\text{C}_{60}$  solution (deaerated) was syringed into the sample and reference cells. The concentrations of  $\text{C}_{60}$  in the sample cell were (c) 5.9, (d) 11.7, (e) 17.5, and (f) 23.2  $\mu\text{M}$ . (From ref 180.)

spectrum *b*) one can observe the formation of  $\text{C}_{60}^-$  from the absorption band at 1075 nm (spectra *c-f* in Figure 11). The increase in 1075 nm absorption quantitatively represents the formation of  $\text{C}_{60}^-$  as a result of electron transfer (reaction 4).



Noble metal mediated photocatalytic reduction reactions demonstrated in earlier studies (see for example, refs 20 and 187) can now be understood by isolating the individual electron-transfer steps (viz.,  $\text{TiO}_2(e) \rightarrow \text{Au}(e) \rightarrow \text{C}_{60}^-$ ). The ability to probe such individual electron-transfer steps is an important aspect toward understanding the factors that dictate the noble metal mediated catalytic reduction processes.

Murray and co-workers have demonstrated that Au nanoparticles possess the property of storing electrons in a quantized fashion.<sup>106,172</sup> The double-layer charging around the metal nanoparticle facilitates storage of the electrons within the gold nanoparticle. When the semiconductor and metal nanoparticles are in contact, the photogenerated electrons are distributed between  $\text{TiO}_2$  and Au nanoparticles (Fermi level of Au = +0.45 V versus NHE). The transfer of electrons from the excited  $\text{TiO}_2$  into Au continues until the two systems attain equilibration. Since the electron accumulation increases the Fermi level of Au to more negative potentials, the resultant Fermi level of the composite shifts closer to the conduction band of the semiconductor. This observed shift in the Fermi level of the composite system is in agreement with the observations made in the case of  $\text{ZnO-Au}$  systems.<sup>175,179</sup> The negative shift in the Fermi level is an indication of better charge separation and more reductive power for the composite system. Figure 12 illustrates the shift in the Fermi level of the composite as a result of charge equilibration between semiconductor and metal nanoparticles.

The particle size effect on the shift in apparent Fermi level was determined from the  $\text{C}_{60}^-$  yield using different size Au nanoparticles (Figure 13). The smaller Au particles induce greater shift in  $E_F^*$  than the larger particles. A -60 mV shift in the flat band potential was achieved using 3 nm diameter gold nanoparticles as compared to a -20 mV shift for 8 nm Au nanoparticles. This shows that we can tune the apparent Fermi level of the composite system by controlling the size of the metal nanoparticle. Since the energy levels in the gold nanoparticles are discrete, we expect a greater shift in the energy

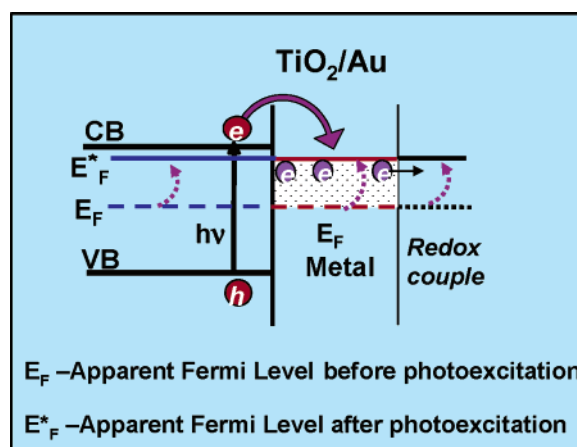


**Figure 12.** Schematic representation of shift in Fermi level of the composite as a result of electron storage. (From ref 180.)

level for each accumulated electron in smaller size Au nanoparticles than the larger ones. For example, a shift of 0.1 V/electron has been reported for  $\sim 2$  nm Au nanoparticles.<sup>172</sup> Thus, the composite catalyst with smaller Au nanoparticles is expected to be more active catalytically than that composed of larger Au particles. These observations parallel the size-dependent catalytic properties of gold nanoparticles deposited on titania in earlier studies.<sup>182</sup> By probing the photoinduced electron-transfer process in a stepwise manner, it is possible to demonstrate the effect of gold nanoparticle size on the overall energetics of the  $\text{TiO}_2\text{-Au}$  composite system.

If indeed, such a particle size effect influences the energetics by shifting the Fermi level to more negative potentials; it should be possible to translate this beneficial effect to the photoelectrochemistry of nanostructured semiconductor films. When  $\text{TiO}_2$  and  $\text{TiO}_2\text{-Au}$  films are deposited on conducting glass electrodes used as photoanode in a photoelectrochemical cell, they reflected the same trend. Photocurrents at different applied potentials recorded under UV illumination are presented in Figure 14.

The zero-current potential in these traces correspond to apparent flat band potential of the nanostructured semiconductor film. At this applied potential, all of the photogenerated electrons and holes recombine without producing any net current flow. From Figure 14, it is evident that the apparent flat band potential of nanostructured  $\text{TiO}_2$  in 0.05 M NaOH is at -0.98 V versus SCE (trace *a*). A shift in the flat band potential to negative potentials is seen for the  $\text{TiO}_2\text{-Au}$  composite system. The

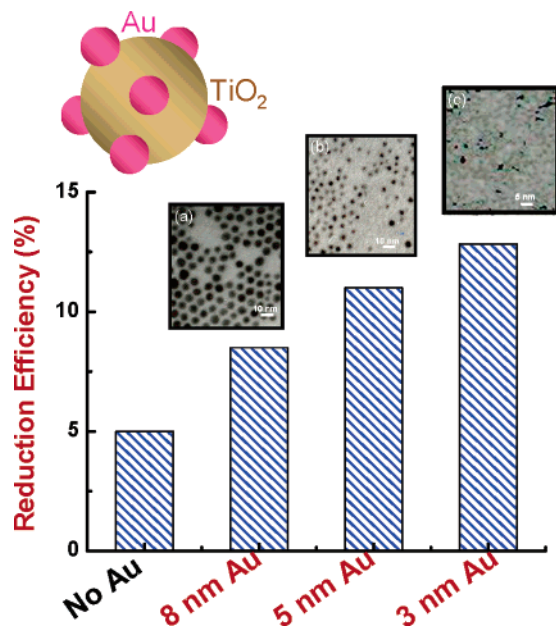


**Figure 13.** Effect of gold particle size on the photocatalytic reduction efficiency of  $\text{TiO}_2$  as monitored from  $\text{C}_{60}$  reduction. TEM images of corresponding gold nanoparticles are also shown. (Adapted from ref 180.)

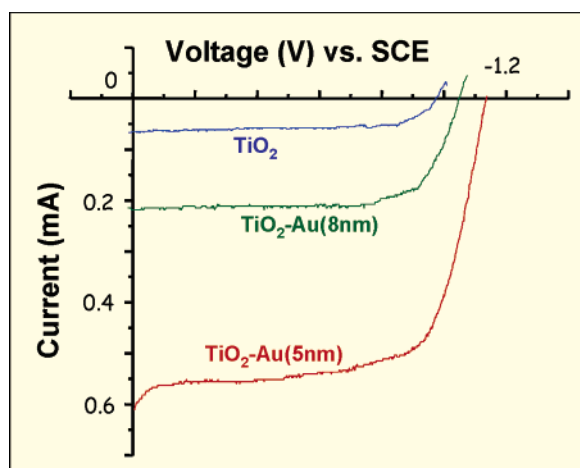


**Figure 14.** Shift in flat band potential of  $\text{TiO}_2$ -Au nanocomposite as monitored by I-V characteristics of  $\text{TiO}_2$  and  $\text{TiO}_2$ -Au electrode in a photoelectrochemical configuration. (From refs 163 and 180.)

shifted apparent flat band potential is observed at  $-1.04$  and  $-1.14$  V versus SCE for electrodes modified with 8 and 5 nm gold nanoparticles respectively. In other words, we can still draw a significant photocurrent using the  $\text{TiO}_2/\text{Au}$  system at potentials (e.g.,  $-0.98$  V vs SCE) that show complete recombination in pristine  $\text{TiO}_2$ . Obviously, the presence of Au facilitates charge separation and promotes interfacial electron transfer at the electrolyte interface. It is interesting to note that the trend of size-dependent shift of flat band potential is similar to that obtained in the particle suspension system (Table 1). The observed photocurrents at positive bias are significantly higher for the composite films involving Au nanoparticles. These photoelectrochemical measurements further confirm the effect of noble metal in improving the energetics of the semiconductor nanostructures.

The property of  $\text{TiO}_2$ -gold nanocomposites discussed in the above sections is an example to highlight the importance of nanostructured assemblies for modulating the energetics of photocatalysts. Such composites are yet to be explored fully

**TABLE 2: Apparent Fermi Level of  $\text{TiO}_2$  and  $\text{TiO}_2/\text{Au}$  Nanocomposite Systems<sup>180</sup>**

photocatalyst	diameter of Au particle (nm)	$[\text{C}_{60}]_0$ ( $\mu\text{M}$ )	$[\text{C}_{60}^-]^a$ ( $\mu\text{M}$ )	$E_F^{*b}$ (mV)
$\text{TiO}_2$	-	94	36.1	-230
$\text{TiO}_2$ -Au	8	94	50.9	-250
$\text{TiO}_2$ -Au	5	94	65.6	-270
$\text{TiO}_2$ -Au	3	94	76.8	-290

<sup>a</sup> A suspension containing 5.5 mM  $\text{TiO}_2$  and 0.06 mM Au in 1:1 toluene:ethanol mixture was irradiated with UV light for 30 min. Equilibrated concentration of  $\text{C}_{60}^-$  was determined spectrophotometrically after the addition of concentrated  $\text{C}_{60}$  solution to the preirradiated suspension. <sup>b</sup>  $E_F^* = E_{fb} = -0.25 + 0.059 \log [\text{C}_{60}]_{\text{eq}} / [\text{C}_{60}^-]$  where,  $[\text{C}_{60}]_{\text{eq}} = [\text{C}_{60}]_0 - [\text{C}_{60}^-]$ .

for energy viable photocatalytic conversion processes. Directing the future research efforts toward utilization of such less expensive noble metals as catalysts for the fuel production (e.g., solar hydrogen production) is important to design strategies for attaining higher photoconversion efficiencies.

**b. Ag Core- $\text{TiO}_2$  Shell Nanostructures for Storing Photogenerated Electrons.** Despite significant advance in designing metal core-semiconductor shell clusters,<sup>188-194</sup> the efforts to utilize such core-shell structures as photocatalysts in the light energy conversion systems (photoelectrochemical cells, hydrogen production, etc.) are limited. A coupled metal-semiconductor structure such as the one discussed in the previous section, though effective, results in exposing both metal and oxide surfaces to reactants, products, and the medium. Corrosion or dissolution of the noble metal particles during the operation of a photocatalytic reaction is likely to be problematic in using noble metals such as Ag and Au.<sup>163,169</sup> A better synthetic design would be to employ the metal as a core and the semiconductor photocatalyst as a shell. Silica has been employed as a shell to protect Ag and Au nanoparticles. Preparation and characterization of  $\text{Au}@SiO_2$  and  $\text{Ag}@SiO_2$  core-shell clusters have been reported for metal core-oxide shell clusters.<sup>188-190,195</sup>

By capping a noble metal with a semiconductor shell, one can design a new series of photocatalysts. For example, the  $\text{Ag}@TiO_2$  clusters are able to store electrons under UV irradiation and discharge them on demand in the dark.<sup>196,197</sup> When such metal core-semiconductor shell composite particles were subjected to UV irradiation, a blue shift in the plasmon absorption band from 480 to 420 nm was observed (Figure 15).

The shift of 60 nm in the plasmon absorption reflects increased electron density in the Ag core during photoirradiation. Since  $\text{TiO}_2$  undergoes charge separation under UV irradiation (similar to reactions 1 and 2), the photogenerated electrons are transferred quickly to Ag nanocore as the two systems undergo charge equilibration. Metal particles such as silver and gold with a favorable Fermi level ( $E_F = 0.4$  V) are good electron acceptors and facilitate quick electron transfer from excited  $\text{TiO}_2$ . The transfer of electrons from the excited semiconductor to the metal is an important aspect that dictates the overall energetics of the composite and hence the efficiency of photocatalytic reduction process.<sup>175,179,180,198</sup>

Figure 16 shows the reproducibility of the plasmon absorption peak response to the UV irradiation and air exposure in dark. The plasmon absorption band shifts from 470 to 420 nm during 1 min UV irradiation of deaerated  $\text{Ag}@TiO_2$  suspension. The plasmon absorption regains the original spectral features when the stored electrons are discharged in the dark by exposure to air. It is possible to repeat the photoinduced charging and dark

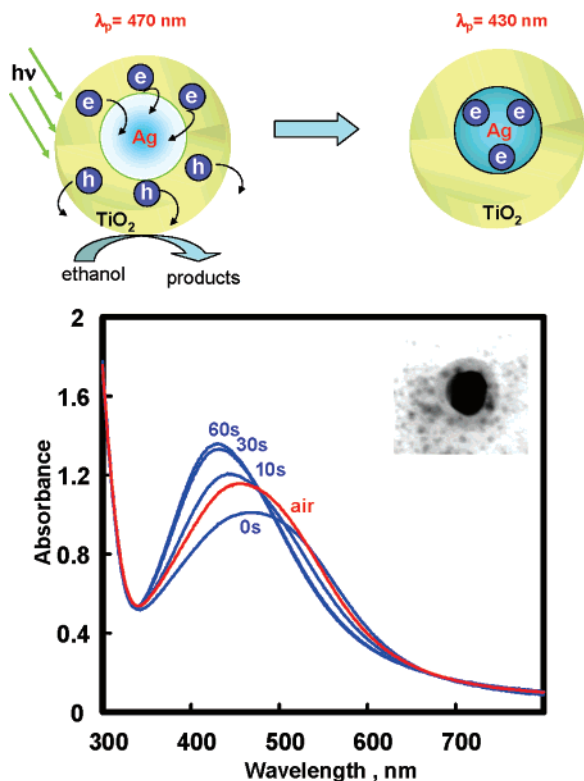


**Figure 15.** Photoinduced charge separation and storage in an Ag core-TiO<sub>2</sub> shell nanocomposite particles. A shift in the plasmon absorption can be seen upon excitation with UV light. (From ref 196.)

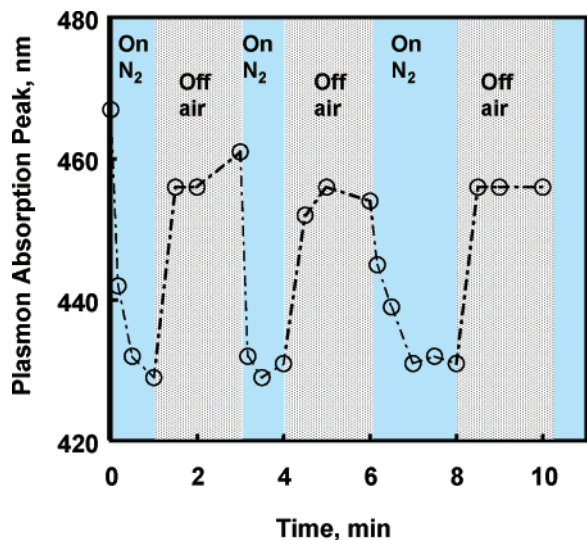


**Figure 16.** Response of plasmon absorbance peak to electron storage following the UV-irradiation of deaerated Ag@TiO<sub>2</sub> colloidal suspension in ethanol and dark discharge in air. (From refs 196 and 197.)

discharge cycles repeatedly and reproduce the plasmon absorption response to stored electrons (Figure 16).

A similar but less pronounced effect was noted for Au capped with SnO<sub>2</sub> particles.<sup>194</sup> The electrons were injected chemically using a reductant, NaBH<sub>4</sub>. Since the electrons stored in the Ag@TiO<sub>2</sub> colloids can equilibrate with the redox couple in solution, it is possible to carry out a redox titration and obtain quantitative information on the stored electrons. The stored electrons estimated by titration with thionine dye showed that one can store more than 50 electrons in the silver core and discharged on demand. In other words, stored electrons can be utilized to carry out catalytic reduction in dark. The formation of C<sub>60</sub><sup>•-</sup> with characteristic absorption in the IR region (1075

nm) is used to obtain quantitative information on the electron-transfer yield. These metal core–semiconductor shell composite clusters are photocatalytically active and are useful to promote light induced electron-transfer reactions. Exploring the catalytic activity of such composite structures could pave the way for designing novel light harvesting systems.

**c. Semiconductor–Semiconductor Composites.** Photoinduced charge separation in a semiconductor nanoparticle can be greatly improved by coupling it with another semiconductor particle having favorable energetics. By selecting a short band gap semiconductor, one can also harvest photons in the visible. Semiconductors such as CdS,<sup>111,199,200</sup> PbS,<sup>114,201</sup> Bi<sub>2</sub>S<sub>3</sub>,<sup>114,202</sup> CdSe,<sup>203</sup> and InP,<sup>117</sup> which absorb light in the visible, can serve as sensitizers as they are able to transfer electrons to large band gap semiconductors such as TiO<sub>2</sub> or SnO<sub>2</sub>. Improved charge separation and enhanced photocatalytic efficiency of such composite nanostructures have been extensively studied by our group<sup>115,118,204–207</sup> and other research groups.<sup>112,208–212</sup> Readers are referred to earlier reviews to obtain charge transfer and charge rectification in various semiconductor composite systems.<sup>134,178,213,214</sup>

By controlling the particle size of quantum dots, one can vary the energetics of the particles. Increased band energies of Q-dots can thus be utilized to promote,<sup>114</sup> suppress,<sup>207</sup> or rectify<sup>203,216</sup> the electron transfer between two semiconductor nanostructures. Such composite structures rectify the flow of charge carriers and improve the photocatalytic performance or photoelectrochemical performance of nanostructure semiconductor based systems. For example, nearly 10 times enhancement in the photocatalytic efficiency has been achieved by coupling TiO<sub>2</sub> and SnO<sub>2</sub> systems.<sup>118,206</sup> Similarly, composites of ZnO–CdS,<sup>113</sup> TiO<sub>2</sub>–SnO<sub>2</sub>,<sup>116</sup> SnO<sub>2</sub>–CdSe,<sup>217</sup> and SnO<sub>2</sub>–CdS<sup>115</sup> have been successfully used to promote efficient charge separation and charge propagation in dye-sensitized solar cells.

Our early study on the TiO<sub>2</sub>–CdSe system further highlights the importance of rectifying behavior of the composite system and their usefulness in improving the overall performance of nanostructured semiconductor systems.<sup>203,216</sup> Recently, we were able to establish the charge injection from excited CdSe quantum dots into TiO<sub>2</sub> particles using emission and transient absorption measurements.<sup>215</sup>

The transient absorption spectra representing the bleaching recovery of the CdSe quantum dots in the absence and presence of TiO<sub>2</sub> colloids are shown in Figure 17. In the absence of TiO<sub>2</sub>, the bleaching recovery of the 530 nm band occurs slowly, and only about 30% of the bleaching is recovered in 1.5 ns. On the other hand, the presence of TiO<sub>2</sub> in the suspension accelerates the recovery and nearly 75% of the recovery in 1.5 ns. The enhanced recovery of the 530 nm band reflects the influence of TiO<sub>2</sub> in accepting electrons from the relaxed <sup>1</sup>S<sub>3/2<sup>1</sup>S<sub>e</sub> state. Electron transfer from the thermally relaxed s-state occurs over a wide range of rate constant values between 0.073 and 1.95 × 10<sup>11</sup> s<sup>-1</sup>.<sup>215</sup> The injected charge carriers in a CdSe-modified TiO<sub>2</sub> film can be collected at a conducting electrode to generate a photocurrent. Another emerging area is the development of heterostructures synthesized from CdSe and CdTe which localizes carriers to different regions of the tetrahedral geometry.<sup>218</sup> The dynamics of carrier relaxation examined in this study showed heterostructures having rise times and biexponential decays longer than those of nanorods with similar dimensions. Opportunities exist to develop ordered assemblies of short and large band gap semiconductors and harvest photons over a wide spectral range of the visible and infrared light with better charge separation.</sub>

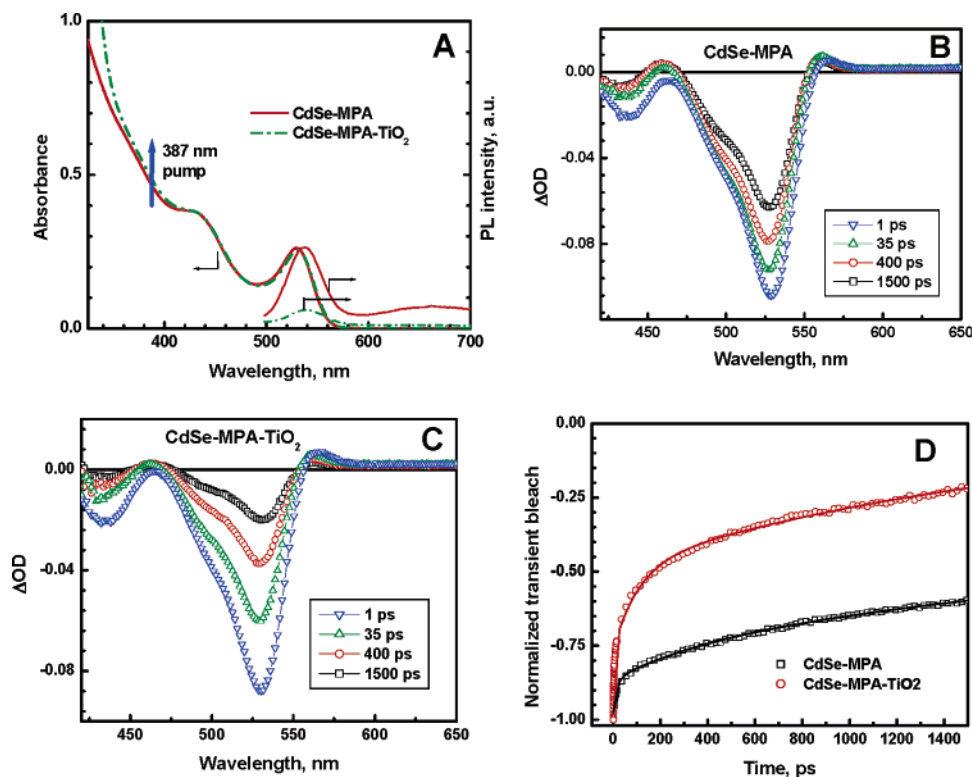


**Figure 17.** (A) Absorption and emission spectra of CdSe quantum dots before and after mixing with colloidal TiO<sub>2</sub> particles. (B) and (C) represent bleaching recovery of MPA capped CdSe quantum dots in the absence and presence of TiO<sub>2</sub> colloids respectively. Excitation was at 387 nm. (D) Absorption recovery profiles at 530 nm recorded following the 387 nm laser pulse excitation of CdSe and CdSe-TiO<sub>2</sub>. (From ref 215.)

### 3. Photochemical Solar Cells

Various strategies have been developed in recent years to construct photochemical solar cells using organized assemblies of nanostructure architectures. Some of the recent developments in the area of assembling nanostructures as organized assemblies on electrode surfaces and their role in improving the performance of solar cells are presented in this section. Many of these systems have the potential to develop third generation solar cells.<sup>16</sup> Four promising strategies will be discussed in detail here. These include (1) donor-acceptor based molecular clusters (2) dye sensitization of semiconductor nanostructures, (3) quantum dot solar cells, and (4) carbon nanostructure based solar cells. The illustration of these systems are given in Figure 18.

**a. Porphyrin-Fullerene Assemblies for Solar Cells.** Composites of donor and acceptor moieties (e.g., porphyrin and fullerene) in the form of clusters when assembled as a three-dimensional network on a conducting surface provide a means to achieve efficient photocurrent generation. The supramolecular chemistry approach as a means of assembling donor (porphyrin) and acceptor (C<sub>60</sub>) for light energy conversion has been extensively studied by us in recent papers.<sup>219-222</sup> This section represents an overview of utilizing organized assemblies of donor and acceptor moieties (viz., porphyrin and C<sub>60</sub>) for developing photochemical solar cells.

*Electrophoretic Deposition of Molecular Cluster Films.* Porphyrin and its derivatives (H<sub>2</sub>P-ref and porphyrin monolayer protected gold clusters -H<sub>2</sub>PC<sub>n</sub>MPC) and C<sub>60</sub> are soluble in nonpolar solvents such as toluene but sparingly soluble in polar solvents such as acetonitrile. When a concentrated solution of C<sub>60</sub> or porphyrin in toluene is mixed with acetonitrile by fast injection method, the molecules aggregate and form stable clusters of diameter 100-200 nm.<sup>223-225</sup> The same strategy can be extended to prepare mixed or composite molecular clusters consisting of H<sub>2</sub>P (or H<sub>2</sub>PC<sub>n</sub>MPC) and C<sub>60</sub> molecules. Mixed

cluster aggregates can be prepared by mixing an equimolar solution of porphyrin H<sub>2</sub>PC<sub>n</sub>MPC or H<sub>2</sub>P-ref and C<sub>60</sub> in toluene and then injecting it into a pool of acetonitrile.<sup>220</sup> These optically transparent composite clusters are stable at room temperature and they can be reverted back to their monomeric forms by diluting the solution with toluene.

The absorption spectra of H<sub>2</sub>PC<sub>11</sub>MPC and C<sub>60</sub> in neat toluene are compared with that of [(H<sub>2</sub>PC<sub>11</sub>MPC+C<sub>60</sub>)<sub>m</sub>] clusters in acetonitrile/toluene (3/1, v/v) in Figure 19A. The composite clusters [(H<sub>2</sub>PC<sub>11</sub>MPC+C<sub>60</sub>)<sub>m</sub>] in the mixed solvent (spectrum a) exhibit much broader and more intense absorption in the visible and near IR regions than those of parent H<sub>2</sub>PC<sub>11</sub>MPC (spectrum b) and C<sub>60</sub> (spectrum c) in toluene. The composite clusters absorb throughout the visible part of the solar spectrum. This demonstrates that the composite clusters of H<sub>2</sub>PC<sub>11</sub>MPC and C<sub>60</sub> are superior light absorbers as compared to the single component clusters of H<sub>2</sub>PC<sub>11</sub>MPC or C<sub>60</sub>. A similar trend is also observed for other chromophore functionalized metal particles, viz., H<sub>2</sub>PC<sub>5</sub>MPC and H<sub>2</sub>PC<sub>15</sub>MPC.<sup>221,226</sup>

These molecular clusters prepared in mixed solvents can be assembled on electrode surfaces using an electrophoretic deposition technique. In a typical deposition experiment, a known amount of porphyrin derivatives, C<sub>60</sub>, or mixed cluster solution in acetonitrile/toluene (3/1, v/v, 2 mL) is transferred to a 1 cm cuvette in which two optically transparent electrodes (viz., OTE/SnO<sub>2</sub> and OTE) are kept at a distance of 6 mm using a Teflon spacer. A DC voltage (200 V) is then applied between these two electrodes using a Fluke 415 power supply. The deposition of the film can be visibly seen as the solution becomes colorless with simultaneous brown coloration of the OTE/SnO<sub>2</sub> electrode. The OTE/SnO<sub>2</sub> electrode coated with mixed H<sub>2</sub>PC<sub>n</sub>MPC (porphyrin monolayer covered gold particles) and C<sub>60</sub> clusters is referred to OTE/SnO<sub>2</sub>/(H<sub>2</sub>PC<sub>n</sub>MPC + C<sub>60</sub>)<sub>m</sub>. A quaternary organization of donor-acceptor moieties on an electrode

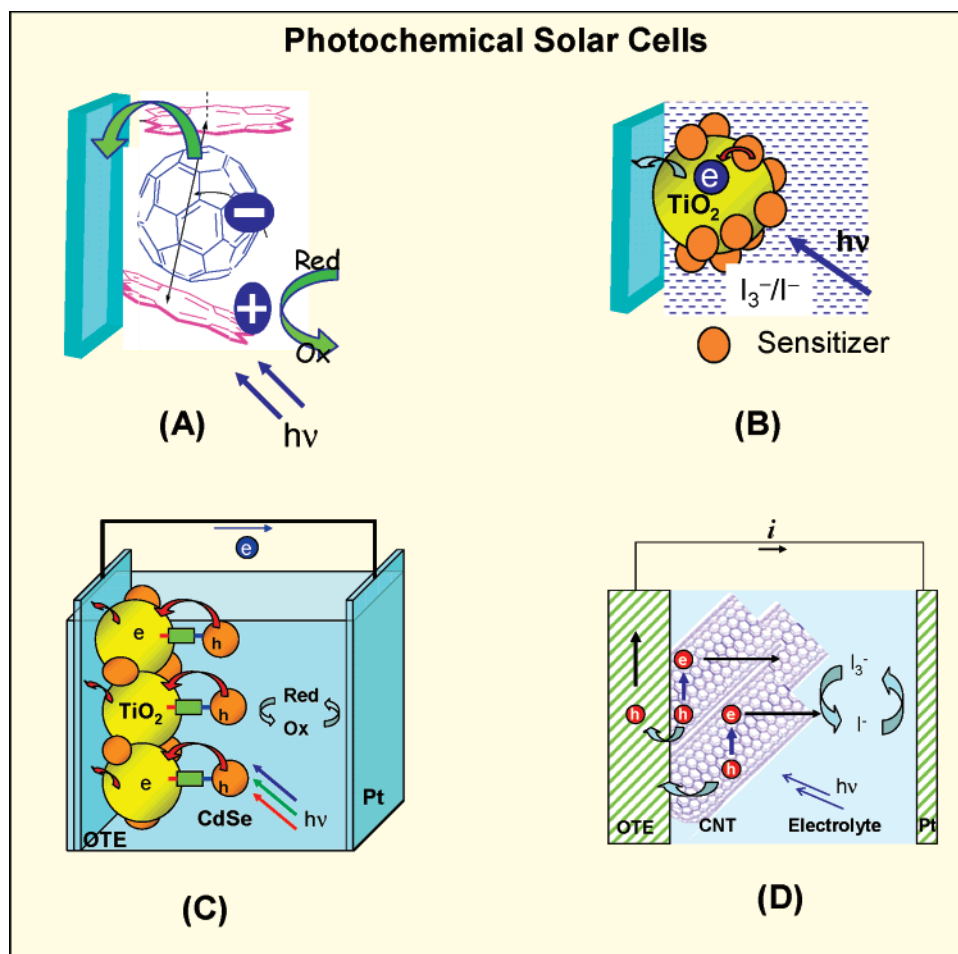


**Figure 18.** Strategies to utilize nanostructures in photochemical solar cells: (A) Photoinduced electron transfer in donor–acceptor assemblies; (B) Charge injection from excited dye into semiconductor particles; (C) Photoinduced electron–hole separation in CdSe quantum dot semiconductor assemblies; and (D) Carbon nanotube architectures on electrode surfaces.

surface<sup>226</sup> is shown in Figure 19B. The AFM image of the electrode consisting of donor acceptor ( $\text{H}_2\text{P}$  and  $\text{C}_{60}$ ) mixed clusters is also shown.

**Photoelectrochemical Performance.** The photoelectrochemical performance of the OTE/ $\text{SnO}_2$ / $(\text{H}_2\text{PCnMPC} + \text{C}_{60})_m$  electrode can be evaluated by employing it as a photoanode in a photoelectrochemical cell. Photocurrent measurements were performed in acetonitrile containing NaI (0.5 M) and  $\text{I}_2$  (0.01 M) as redox electrolyte using a Pt gauge counter electrode. Photocurrent action spectra of  $(\text{H}_2\text{PCnMPC} + \text{C}_{60})_m$  clusters were recorded by varying the excitation wavelength (Figure 21). The incident photon to charge carrier conversion efficiency (IPCE) values were calculated by normalizing the photocurrent values for incident light energy and intensity (expression 5)<sup>220,221,227</sup>

$$\text{IPCE (\%)} = 100 \times 1240 \times I_{\text{sc}} / (I_{\text{inc}} \times \lambda) \quad (5)$$

where  $I_{\text{sc}}$  is the short circuit photocurrent ( $\text{A}/\text{cm}^2$ ),  $I_{\text{inc}}$  is the incident light intensity ( $\text{W}/\text{cm}^2$ ), and  $\lambda$  is the wavelength (nm). The overall response of OTE/ $\text{SnO}_2$ / $(\text{H}_2\text{PCnMPC} + \text{C}_{60})_m$  parallels the broad absorption spectral features, indicating the involvement of both  $\text{H}_2\text{PCnMPC}$  and  $\text{C}_{60}$  in the photocurrent generation.

The photocurrent exhibits a clear dependence on the acceptor concentration. A maximum IPCE of 28% at 490 nm was attained with a relative ratio of  $[\text{H}_2\text{P}]:[\text{C}_{60}] = 38:62$ . Considering the well-established photodynamics of the porphyrin–fullerene

system, the porphyrin excited singlet state is expected to be quenched by  $\text{C}_{60}$  via electron transfer in the porphyrin– $\text{C}_{60}$  complex rather than by gold nanocluster via energy transfer. The length of the linker molecule also influenced the IPCE. Figure 20 shows the effect of the alkanethiolate chain length on the IPCE values.<sup>221</sup> Comparison of the photocurrent action spectra indicate that the higher IPCE and the broader photoresponse are attained with the longer chain length of  $\text{H}_2\text{PCnMPC}$ . In particular, OTE/ $\text{SnO}_2$ / $(\text{H}_2\text{PC15MPC} + \text{C}_{60})_m$  exhibits the maximum IPCE value (54%) and very broad photoresponse (up to  $\sim 1000$  nm), thus extending the response to the near IR region. In OTE/ $\text{SnO}_2$ / $(\text{H}_2\text{PC15MPC} + \text{C}_{60})_m$ , a long methylene spacer of  $\text{H}_2\text{PC15MPC}$  allows sufficient space for the insertion of fullerene molecules and interact with the neighboring two porphyrin moieties (See illustration of insertion of  $\text{C}_{60}$  between the porphyrin rings of  $\text{H}_2\text{PC15MPC}$  in Figure 20).<sup>221</sup>

The power conversion efficiency ( $\eta$ ) of the photochemical solar cell can be evaluated by varying the load resistance (Figure 21).<sup>221</sup> A drop in the photovoltage and an increase in the photocurrent are observed with decreasing load resistance. The OTE/ $\text{SnO}_2$ / $(\text{H}_2\text{PC15MPC} + \text{C}_{60})_m$  system has a much larger fill factor (FF) of 0.43, open circuit voltage ( $V_{\text{oc}}$ ) of 380 mV, short circuit current density ( $I_{\text{sc}}$ ) of  $1.0 \text{ mA cm}^{-2}$ , and the overall power conversion efficiency ( $\eta$ ) of 1.5% at input power ( $W_{\text{in}}$ ) of  $11.2 \text{ mW cm}^{-2}$ .

In the above example, the gold particle provides the necessary foundation to organize donor–acceptor moieties. Molecular architectures such as dendrimers and polypeptides can also be

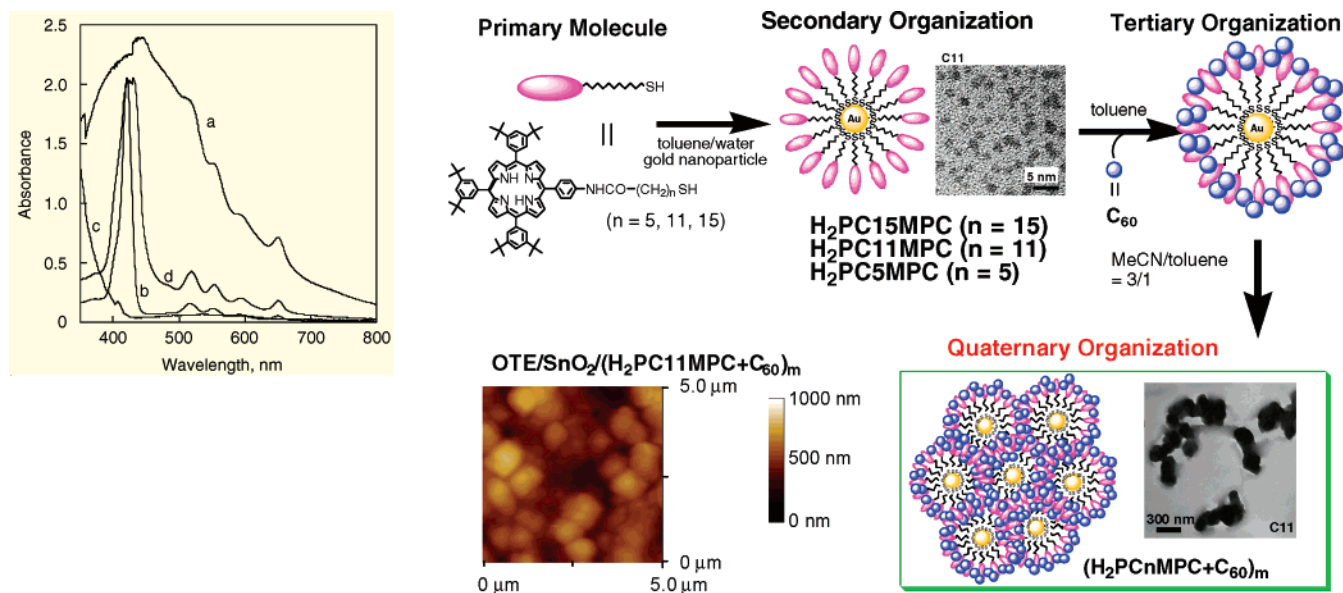


**Figure 19.** A. Left: Absorption spectra of (a)  $(\text{H}_2\text{PC11MPC} + \text{C}_{60})_m$  in acetonitrile/toluene (3/1, v/v);  $[\text{H}_2\text{P}] = 0.19 \text{ mM}$ ,  $[\text{C}_{60}] = 0.31 \text{ mM}$ , (b)  $\text{H}_2\text{PC11MPC}$  in toluene;  $[\text{H}_2\text{P}] = 18 \mu\text{M}$ , (c)  $\text{C}_{60}$  in toluene;  $[\text{C}_{60}] = 150 \mu\text{M}$  and (d)  $(\text{H}_2\text{PC11MPC})_m$  in acetonitrile/toluene (3/1, v/v);  $[\text{H}_2\text{P}] = 0.19 \text{ mM}$  (From ref 221). B. Illustration of high-order organization of porphyrin and  $\text{C}_{60}$  units with gold nanoparticles and their TEM image of (a)  $(\text{H}_2\text{PC11MPC} + \text{C}_{60})_m$  and (b)  $(\text{H}_2\text{PC11MPC})_m$ , AFM image of (c)  $\text{OTE}/\text{SnO}_2/(\text{H}_2\text{PC11MPC} + \text{C}_{60})_m$  and (d)  $\text{OTE}/\text{SnO}_2/(\text{H}_2\text{PC11MPC})_m$ . (From ref 226.)

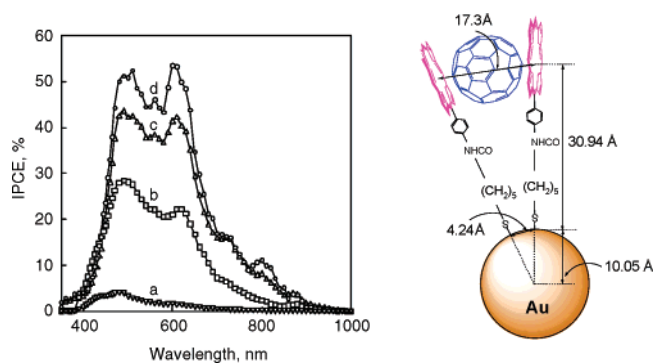


**Figure 20.** Photocurrent action spectra (presented in terms of IPCE)  $\text{OTE}/\text{SnO}_2/(\text{H}_2\text{PC}n\text{MPC} + \text{C}_{60})_m$  electrode ( $[\text{H}_2\text{P}] = 0.19 \text{ mM}$ ; (a)  $n = 5$ ,  $[\text{C}_{60}] = 0.31 \text{ mM}$ ; (b)  $n = 11$ ,  $[\text{C}_{60}] = 0.31 \text{ mM}$ ; (c)  $n = 15$ ,  $[\text{C}_{60}] = 0.31 \text{ mM}$ ; (d)  $n = 15$ ,  $[\text{C}_{60}] = 0.38 \text{ mM}$ . Electrolyte  $0.5 \text{ M NaI}$  and  $0.01 \text{ M I}_2$  in acetonitrile. The scheme (right) shows the organization of porphyrin and  $\text{C}_{60}$  on gold particle and the influence of the linker molecule chainlength in maximizing charge transfer interaction. (From ref 221.)

used to organize donor–acceptor molecules. An example of porphyrin octamer with a polypeptidic backbone ( $\text{P}(\text{H}_2\text{P})_8$ ) is shown in Figure 22. Such assemblies have been utilized to construct porphyrin–fullerene assemblies for solar cells.<sup>228</sup> The  $\text{OTE}/\text{SnO}_2/(\text{P}(\text{H}_2\text{P})_8 + \text{C}_{60})_m$  system has also a large fill factor (FF) of 0.47, open circuit voltage ( $V_{oc}$ ) of 300 mV, short circuit current density ( $I_{sc}$ ) of  $0.31 \text{ mA cm}^{-2}$ , and the overall power conversion efficiency ( $\eta$ ) of 1.3% at input power ( $W_{in}$ ) of  $3.4 \text{ mW cm}^{-2}$ .<sup>229</sup>

**Photocurrent Generation Mechanism.** The primary event responsible for photocurrent generation is the photoinduced charge separation between excited porphyrin ( ${}^1\text{H}_2\text{P}^*/\text{H}_2\text{P}^{*+} = -0.7 \text{ V vs NHE}$ ) and  $\text{C}_{60}$  ( $\text{C}_{60}/\text{C}_{60}^{*-} = -0.2 \text{ V vs NHE}$ ). The electron transfer from  ${}^1\text{H}_2\text{P}^*$  to  $\text{C}_{60}$  is completed in the subnanosecond time scale. The reduced  $\text{C}_{60}$  injects electrons into the  $\text{SnO}_2$  ( $E_{CB} = 0 \text{ V vs NHE}$ ) nanocrystallites and the oxidized porphyrin ( $\text{H}_2\text{P}/\text{H}_2\text{P}^{*+} = 1.2 \text{ V vs NHE}$ ) undergoes electron transfer with iodide ion ( $I_3^-/I^- = 0.5 \text{ V vs NHE}$ ).<sup>221</sup> The photocurrent mechanism is summarized in Figure 23. This

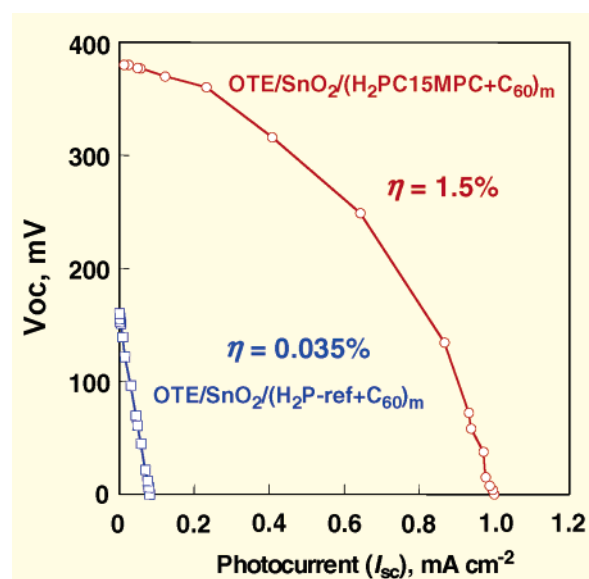


**Figure 21.** Current–voltage characteristics of (a)  $\text{OTE}/\text{SnO}_2/(\text{H}_2\text{PC15MPC} + \text{C}_{60})_m$  electrode and (b)  $\text{OTE}/\text{SnO}_2/(\text{H}_2\text{P-ref} + \text{C}_{60})_m$  electrode prepared from cluster solution of ( $[\text{H}_2\text{P}] = 0.19 \text{ mM}$ ;  $[\text{C}_{60}] = 0.38 \text{ mM}$ ) under visible light illumination ( $\lambda > 400 \text{ nm}$ ); electrolyte  $0.5 \text{ M NaI}$  and  $0.01 \text{ M I}_2$  in acetonitrile; input power:  $11.2 \text{ mW/cm}^2$ . (From ref 221.)

approach of photoinduced charge separation is similar to the photogalvanic mechanism proposed a few decades ago.<sup>230–233</sup> Because of the low dye concentration and mass transfer limitations, the efficiency of such cells remained quite low ( $<0.1\%$ ). As shown in this section, the ability to organize the donor–acceptor system is a key for achieving better charge separation and higher photoconversion efficiency. Many of the donor–acceptor assemblies synthesized during last two decades need to be explored for their application in solar cells.

**b. Dye Sensitized Solar Cells.** The process of utilizing subbandgap excitations with dyes is referred as photosensitization and is conveniently employed in silver halide photography and other imaging science applications. The dye-modified

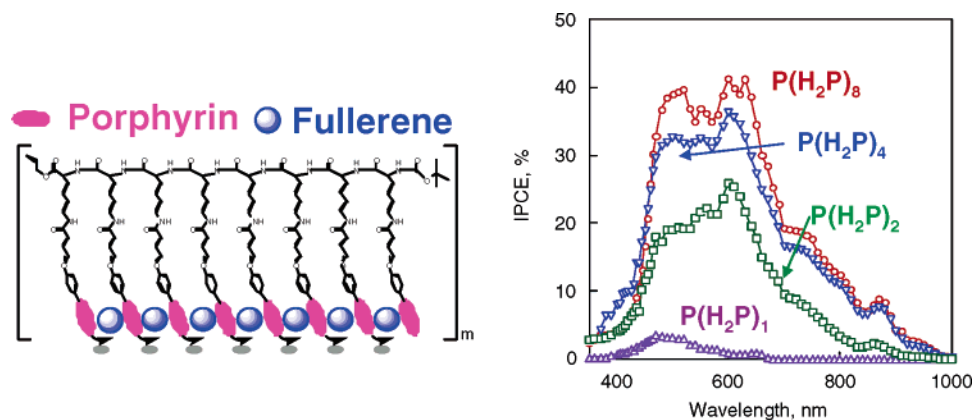


**Figure 22.** Organized assembly of porphyrin functionalized  $\alpha$ -polypeptides and fullerene clusters and photocurrent action spectra (IPCE vs wavelength) using different peptide units. OTE/SnO<sub>2</sub> electrodes were deposited with clusters from (a) [P(H<sub>2</sub>P)<sub>1</sub>] = 0.19 mM, (b) [P(H<sub>2</sub>P)<sub>2</sub>] = 0.10 mM, (c) [P(H<sub>2</sub>P)<sub>4</sub>] = 0.048 mM, and (d) [P(H<sub>2</sub>P)<sub>8</sub>] = 0.024 mM; [C<sub>60</sub>] = 0.31 mM in acetonitrile/toluene = 3/1. (From ref 229.)

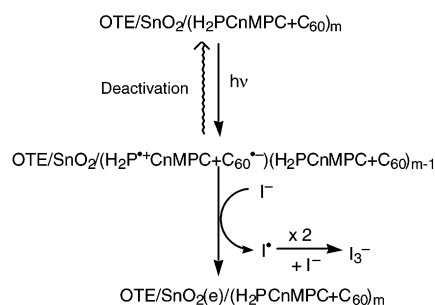


**Figure 23.** Mechanism of photocurrent generation at a OTE/SnO<sub>2</sub>/(P(H<sub>2</sub>P)<sub>8</sub> + C<sub>60</sub>)<sub>m</sub> electrode. (From ref 221.)

semiconductor films provide an efficient method to mimic the photosynthetic process. The charge separation in this case is facilitated by a semiconductor particle.

The high porosity of mesoscopic semiconductor films enables incorporation of sensitizing dyes in large concentrations. The nanostructured TiO<sub>2</sub> films modified with a ruthenium complex exhibit photoconversion efficiencies in the range of 11%, which is comparable to that of amorphous silicon-based photovoltaic cells.<sup>234–238</sup> Bignozzi et al. have presented a supramolecular approach for designing photosensitizers.<sup>239</sup> By optimizing the design of light harvesting molecules (sensitizers), it should be possible to suppress the interfacial charge recombination and improve the cross section for light absorption.

When the electrode is illuminated with visible light, the sensitizer molecules absorb light and inject electrons into the semiconductor particles (see for example some representative systems involving SnO<sub>2</sub>,<sup>240</sup> ZnO,<sup>241</sup> or TiO<sub>2</sub>.<sup>103,116,242–245</sup>). These electrons are then collected at the conducting glass surface to generate anodic photocurrent. The redox couple (e.g., I<sub>3</sub><sup>-</sup>/I<sup>-</sup>) present in the electrolyte quickly regenerates the sensitizer.<sup>246</sup> The quenching of the excited sensitizer by the redox couple can be readily suppressed by the use of C<sub>60</sub> clusters. These C<sub>60</sub> clusters act as a relay to shuttle electrons across the interface.<sup>247</sup> The charge injection between excited sensitizer and the semiconductor film can be readily modulated by applying an external bias.<sup>248–250</sup> Ru(II) trisbipyridyl-complex modified TiO<sub>2</sub> nanostructured films exhibit incident photon to charge carrier generation efficiency (IPCE) of nearly 90% under optimized light-harvesting conditions.<sup>234</sup> By choosing an appropriate sensitizer, it is possible to tune the photoresponse of these nanostructured semiconductor films. For example, sensitizing dyes such as chlorophyll analogues,<sup>251–254</sup> squaraines,<sup>255,256</sup> rhodamine,<sup>257</sup> and oxazines<sup>258</sup> can extend the photoresponse of SnO<sub>2</sub> films to the red-infrared region. Recently, excited-state

interaction between Ru(II) polypyridyl complex and CdSe has been investigated for the hole transfer process.<sup>259</sup>

The charge injection from excited sensitizer into semiconductor nanoparticles is an ultrafast process occurring on the time scale of femtoseconds to nanoseconds.<sup>242,244,260–272</sup> Electron-transfer kinetics in dye-sensitized SnO<sub>2</sub> and TiO<sub>2</sub> systems has been evaluated in terms of Marcus theory.<sup>273,274</sup> Hupp and co-workers<sup>275</sup> have successfully applied this theory to probe the recombination of conduction band electrons from SnO<sub>2</sub> to an oxidized sensitizer. Other research groups<sup>276,277</sup> have also employed this model to investigate the charge recombination kinetics. As the driving force,  $\Delta G$ , increases, the rate of ET increases, reaching a maximum when the driving force equals the reorganization energy.

Both experimental and theoretical evaluations of these cells have been carried out, and the efficiency limiting factors have been identified.<sup>278,279</sup> Recently, interest has been shown in developing ordered arrays of TiO<sub>2</sub> nanotubes either by electrochemical etching of Ti foil in a fluoride medium or depositing TiO<sub>2</sub> rods on a conducting surface.<sup>280–286</sup> Using this strategy, nanotube<sup>287</sup> and nanowire<sup>288</sup> based DSSC have also been reported. The dye-sensitized cell in which the traditional nanoparticle film is replaced by a dense array of oriented, crystalline ZnO nanowires ensures the rapid collection of carriers generated throughout the device.<sup>288</sup> Compared to mesoscopic semiconductor films, the ordered arrays of tubes, wires and rods provide a well defined architecture. An improvement in the electron transport observed in the ZnO array has been attributed to the decrease in the number of grain boundaries.<sup>289</sup> The ZnO rod array employed in one such investigation is shown in Figure 25.

Over the past decade, a number of research groups have worked toward fine-tuning the performance of electrode structure, pretreatment of TiO<sub>2</sub> surface, modification of ruthenium bipyridyl complex with a variety of functional groups, regenerative redox couples, and electrolyte medium. Despite this large body of work, the maximum attainable efficiency has remained in the range of 10–11%. A detailed discussion on various aspects of dye-sensitized solar cell is beyond the scope of the present review. Recent review articles provide more details on such dye-sensitized solar cells (DSSC) and their application in constructing solar panels.<sup>291–294</sup> Industrial interest in testing these systems for commercial solar panels is a bright spot in visualizing the potential application of dye sensitized solar cells.

**c. Quantum Dot Solar Cells.** Ordered assemblies of narrow band gap semiconductor nanostructures are convenient systems by which to harvest visible light energy if employed as

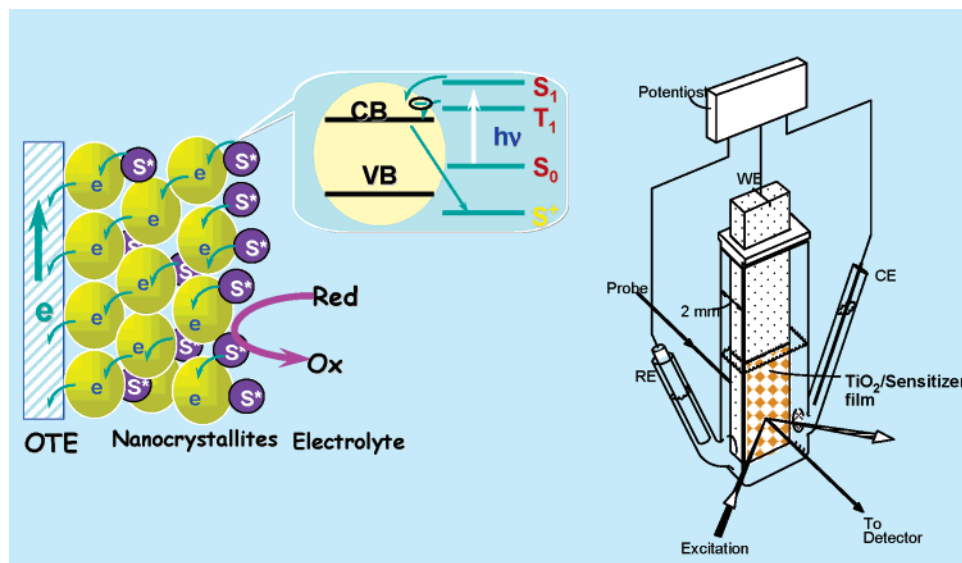


**Figure 24.** Principle of dye sensitized solar cell. The scheme shows charge injection from excited sensitizer ( $S^*$ ) into semiconductor electrolytes. The design on the right shows a versatile cell assembly that is useful for electrochemical, photoelectrochemical, spectroscopic, and spectroelectrochemical measurements.

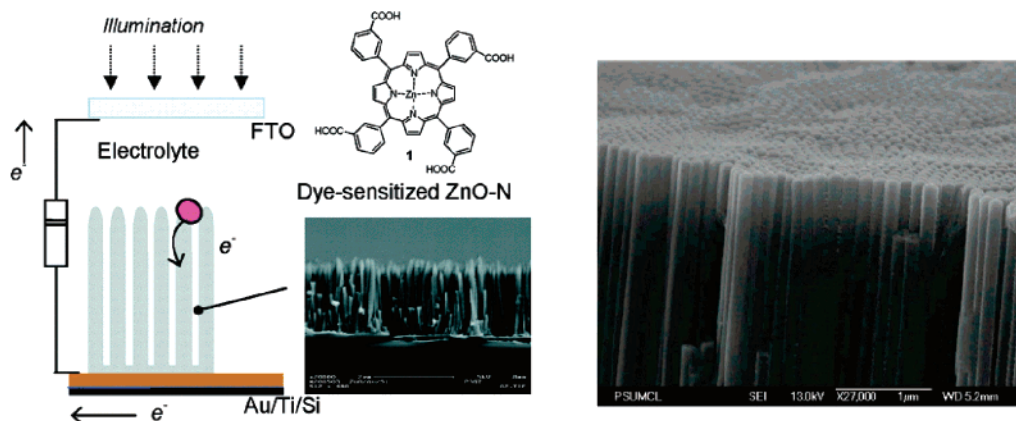


**Figure 25.** Left: Schematic representation of the ZnO-Nanorod array sensitized with Zinc porphyrin sensitizer. FESEM image of ZnO nanorod array prepared by MOCVD is also shown. (From ref 289.) Right: FESEM images of a nanotube-array sample grown by electrochemical etching. (From ref 290.)

electrodes in photoelectrochemical cells. The photocurrent obtained using such nanoparticle assemblies is often low as fast charge recombination limits photocurrent generation. By employing composite semiconductors, however, it has been possible to improve the efficiency of charge separation through charge rectification.<sup>216</sup> Chemically and electrochemically deposited CdS and CdSe nanocrystallites are capable of injecting electrons into wider gap materials such as  $\text{TiO}_2$ ,<sup>111,295,296</sup>  $\text{SnO}_2$ ,<sup>115, 217</sup> and  $\text{ZnO}$ ,<sup>113,254</sup> generating photocurrents under visible light irradiation. Size quantization often becomes an important factor to drive the energetics to more favorable levels as in the case of  $\text{TiO}_2/\text{PbS}$ ,<sup>114,201</sup>  $\text{TiO}_2/\text{InP}$ ,<sup>117</sup> and  $\text{TiO}_2/\text{InAs}$ .<sup>297</sup>

Semiconductor quantum dots (QDs) such as CdSe, InAs, PbS, and PbSe with its tunable band edge offer new opportunities for harvesting light energy in the visible region of the solar spectrum.<sup>201,297–299</sup> Most studies reported to date have been limited to explorations of quantum dot photophysical properties<sup>20,300–303</sup> or their use as biological probes.<sup>304–307</sup> Few recent studies report their use in organic photovoltaic cells.<sup>308–310</sup> The blend of PPV and CdSe quantum dots, for example, facilitates charge separation and the generation of photocurrents under visible light irradiation.

Specific advantages of using semiconductor quantum dots as light harvesting assemblies in solar cells exist.<sup>298</sup> First and

foremost, size quantization property allows one to tune the visible response and vary the band offsets to modulate the vectorial charge transfer across different sized particles. In addition, these quantum dots open up new ways to utilize hot electrons<sup>311</sup> or generate multiple charge carriers with a single photon.<sup>312,313</sup> Multiple carrier generation in PbSe nanocrystals have shown that two or more excitons can be generated with a single photon of energy greater than the band gap.<sup>312,314,315</sup> In order to explore the salient features of quantum dots, we have assembled  $\text{TiO}_2$  and CdSe nanoparticles using bifunctional surface modifiers of the type  $\text{HS-R-COOH}$  (Figure 26).

Bifunctional linker molecules ( $\text{HOOC-R-SH}$ ) with carboxylate and thiol functional groups facilitate binding CdSe quantum dots to  $\text{TiO}_2$ . Such an approach has been used to successfully link  $\text{TiO}_2$  nanoparticles to CdS<sup>316–318</sup> as well as to gold nanoparticles.<sup>83,319</sup> Modification of the  $\text{TiO}_2$  film with  $\text{HOOC-R-SH}$  can be carried out by immersing the OTE/ $\text{TiO}_2$  electrode in an acetonitrile-based  $\text{HOOC-R-SH}$  [viz., mercaptopropionic acid (MPA), thiolacetic acid (TAA) or mercaptohexadecanoic acid (MDA)] solution for 4 h.<sup>215</sup> The electrode after washing thoroughly with acetonitrile is then immersed in a toluene suspension of CdSe quantum dots.  $\text{TiO}_2$  has a strong affinity for the carboxylate group of the linker molecules, as demonstrated previously with a variety of sensitizing dyes.<sup>234,320</sup>

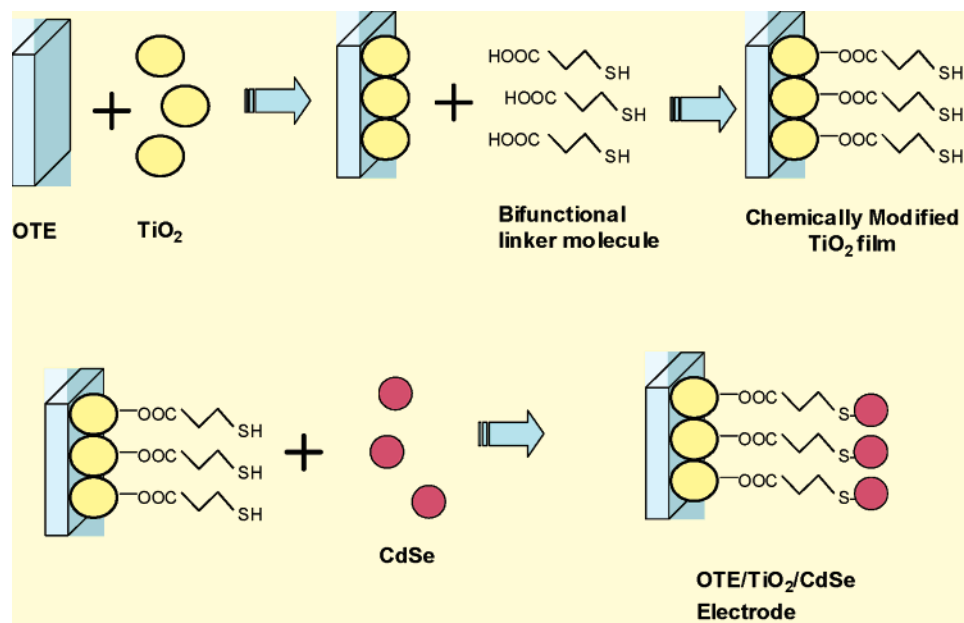


**Figure 26.** Linking CdSe QDs to TiO<sub>2</sub> surface with a bifunctional surface modifier. (From ref 215.)

Thiol and amine groups, on the other hand, bind strongly to CdSe nanoparticles.<sup>321–326</sup> Figure 26 illustrates the principle behind anchoring CdSe quantum dots onto a nanostructured TiO<sub>2</sub> film.

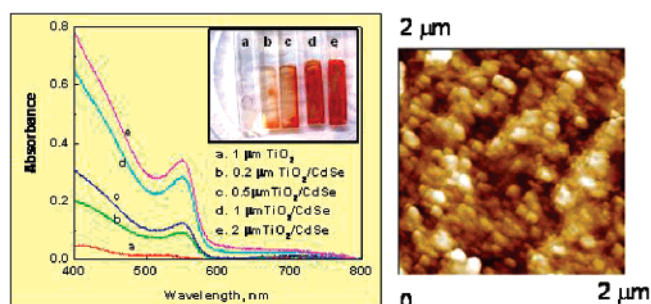
Absorption spectra, recorded after linking CdSe quantum dots to MPA-prefunctionalized TiO<sub>2</sub> films with different thicknesses are shown in Figure 27. Both the absorption onset and the band edge peak of the CdSe quantum dots are unaffected as a result of their binding to the mesoporous TiO<sub>2</sub>. The similarity of the resulting film's absorbance to that of 3 nm quantum dots in solution shows that the nanocrystals retain their optical properties when bound to TiO<sub>2</sub>. The dependence of the CdSe absorbance on the TiO<sub>2</sub> film thickness shows that 3 nm CdSe nanoparticles are capable of penetrating the porous network of TiO<sub>2</sub> film and provide a monolayer coverage, a phenomenon similar to the one observed for modification of TiO<sub>2</sub> films with dyes.

Figure 28 shows the photoresponse of the TiO<sub>2</sub> film before and after modification with CdSe quantum dots. Anodic current is generated upon illumination of the OTE/TiO<sub>2</sub>/CdSe film with visible light in a photoelectrochemical cell. A Na<sub>2</sub>S solution serves as the regenerative redox couple. An open circuit voltage of 0.5 V and short circuit current of 0.14 mA is also obtained. The photoelectrochemical response of the TiO<sub>2</sub>/CdSe films was further analyzed by measuring their action spectra. The incident photon to current conversion efficiency (IPCE) at different wavelengths was determined from the short circuit photocurrents ( $I_{sc}$ ) monitored at different excitation wavelengths ( $\lambda$ ) using the expression (6)

$$\text{IPCE}\% = \frac{[1240 \times I_{sc} (\text{A}/\text{cm}^2)]}{[\lambda (\text{nm}) \times I_{inc} (\text{W}/\text{cm}^2)]} \times 100 \quad (6)$$

where  $I_{inc}$  is the incident light power.

The spectral response of the IPCE spectrum of TiO<sub>2</sub>/CdSe films closely matches the absorption spectrum recorded in Figure 2. All three TiO<sub>2</sub>/CdSe films show photocurrent responses below 600 nm in contrast with the TiO<sub>2</sub> film that responds only in the UV (<380 nm). A maximum IPCE value of 12% was observed for TiO<sub>2</sub> films modified with CdSe quantum dots using MDA and MPA as linker molecules. IPCE values of CdSe/TiO<sub>2</sub> films



**Figure 27.** Absorption spectra of the OTE/TiO<sub>2</sub> films linked with CdSe quantum dots using MPA as a linker. The spectrum a corresponds to blank TiO<sub>2</sub> film before modification. Spectra b–e correspond to the OTE/TiO<sub>2</sub>/MPA/CdSe electrodes after modification with CdSe QDs. The TiO<sub>2</sub> film thickness was varied. (b) 0.2 μm, (c) 0.5 μm, (d) 1 μm, and (e) 2 μm. The photograph of these films is shown in the inset. The AFM image of the CdSe modified TiO<sub>2</sub> film is shown on the right. (From ref 215.)

prepared using TAA linker molecules show slightly lower efficiencies with a maximum IPCE of 9%. These lower IPCE values indicate that a larger fraction of carriers is lost to charge recombination within the particle or at the CdSe/TiO<sub>2</sub> interface. Comparison of the three traces (b, c, and d in Figure 28) indicates that MPA and MDA are better than TAA as linkers for anchoring CdSe quantum dots to TiO<sub>2</sub>.

The photoelectrochemical behavior of CdSe quantum dot-based solar cell demonstrates the feasibility of employing semiconductor nanocrystals for harvesting light energy. Injection of both hot and thermalized electrons from excited CdSe quantum dots into TiO<sub>2</sub> nanoparticles is the primary step in the photocurrent generation. Charge recombination and scattering at the CdSe/TiO<sub>2</sub> heterointerface and grain boundaries within the TiO<sub>2</sub> network limit the photoconversion efficiency of these solar cells.

**d. Carbon Nanostructure Based Photochemical Solar Cells.** Unique electrical and electronic properties, a wide electrochemical stability window, and a high surface area have prompted many researchers to employ carbon nanostructures such as single wall carbon nanotubes (SWCNT) assemblies for energy conversion devices.<sup>327–329</sup> Fullerenes for example exhibit rich photochemistry and act as an electron shuttle in photo-

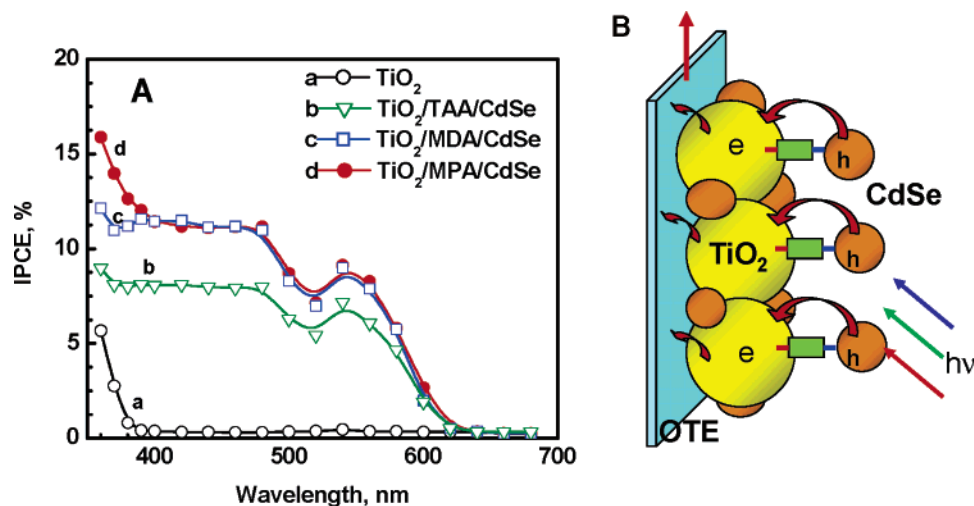


**Figure 28.** (A) Photocurrent action spectra of  $\text{TiO}_2$  (a), and OTE/ $\text{TiO}_2$ /L/ $\text{CdSe}$  films where L = (b) TAA, (c) MDA, and (d) MPA. Electrolyte 0.1 M  $\text{Na}_2\text{S}$  and Pt counter electrode. (B) Photocurrent versus time profiles of (a) OTE/ $\text{TiO}_2$  (b) OTE/ $\text{TiO}_2$ / $\text{CdSe}$  films using MPA as a linker molecule. (0.2 M  $\text{Na}_2\text{S}$  electrolyte and illumination intensity =  $120\text{mW}/\text{cm}^2$ ). (From ref 215.)

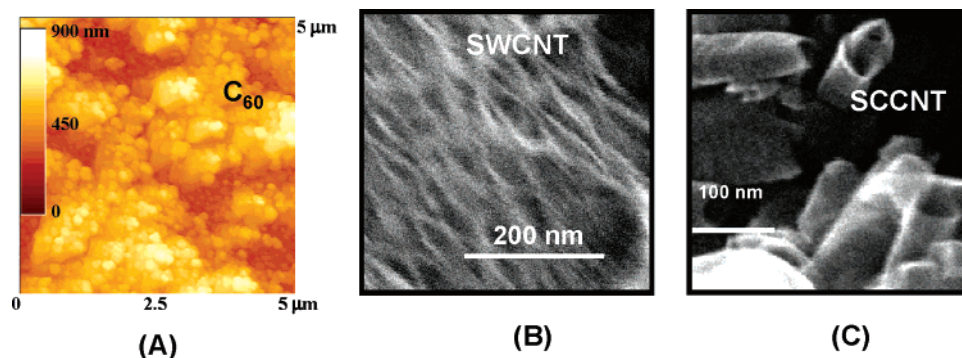


**Figure 29.** Carbon nanostructured films cast on conducting glass electrodes. (A) AFM image of  $\text{C}_{60}$  cluster film; (B) single wall carbon nanotube film, and (C) stacked cup carbon nanotube film. (From refs 219, 332, and 333. Reprinted with permission from Wiley Science and the American Chemical Society.)

chemical solar cells.<sup>247</sup> They also play an important role in improving the performance of organic photovoltaic cells. On the other hand, the semiconducting carbon nanotubes undergo charge separation when subjected to band gap excitation. The exciton annihilation and charge separation processes have been characterized by transient absorption and emission measurements. Another new class of carbon nanostructures are stacked-cup carbon nanotubes (SCCNT). The photon harvesting properties of carbon nanotubes have been discussed in detail in recent review articles.<sup>330,331</sup>

Fullerene clusters, SWCNTs, and SCCNTs can be conveniently deposited as thin films on optically transparent glass electrodes. The clusters of fullerenes or nanotubes suspended in a nonpolar solvent are readily driven to an electrode surface by the application of an electric field. The AFM and TEM images of different types of carbon nanostructure films are shown in Figure 29. These films are electrochemically active and exhibit electrocatalytic<sup>334</sup> and photoelectrochemical effects.<sup>219,225,333,335</sup> The SWCNT films cast on optically transparent electrodes respond to visible light excitation. These electrodes when used in a photoelectrochemical cell containing  $\text{I}_3^-/\text{I}^-$  as redox couple exhibit photocurrent generation.

Figure 30 compares the photocurrent action spectra of electrodes prepared with fullerenes, SWCNT, and SCCNT. On the basis of the electronic properties of the carbon nanostructure employed, we observe different mechanism operative for the photocurrent generation. The low photocurrent generation efficiency in SWCNT films is attributed to ultrafast recombi-

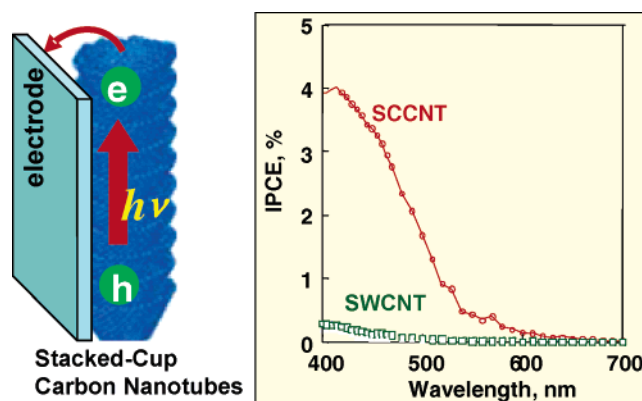


**Figure 30.** Photocurrent action spectra (IPCE vs wavelength) of (a) OTE/ $\text{SnO}_2$ /SCCNT, and (b) OTE/ $\text{SnO}_2$ /SWCNT. Electrolyte: 0.5 M  $\text{NaI}$  and 0.01 M  $\text{I}_2$  in acetonitrile. (From ref 333. Reprinted with permission from Wiley Science.)

tion of photogenerated charge carriers. SCCNT films on the other hand exhibit relatively high IPCE.

#### 4. Hybrid Architectures

A combination of two or more nanostructure architectures provides a new way to modulate the performance of light harvesting devices. New concepts are being attempted by various research groups to explore both combinative and synergetic properties of such hybrid systems. An area that can significantly benefit from such a hybrid architecture is the nanostructure based

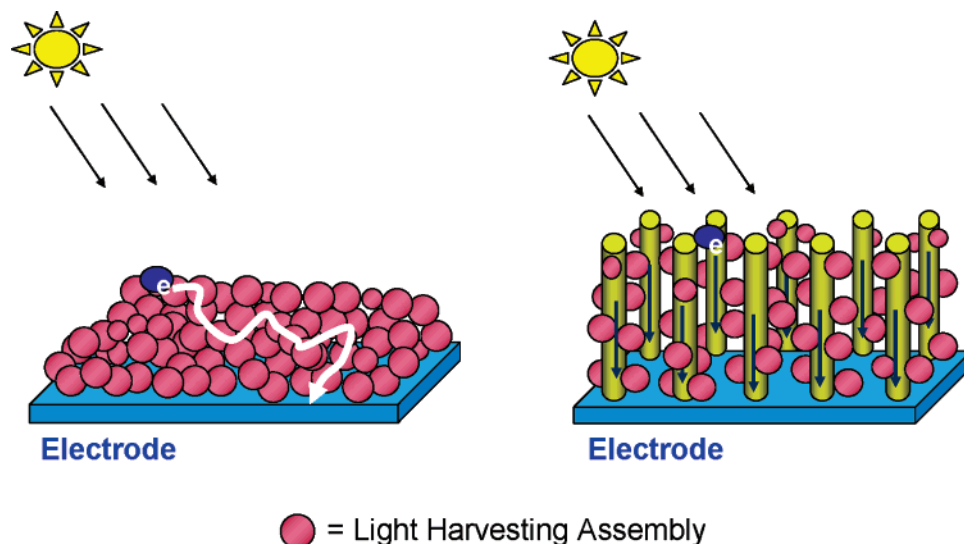


**Figure 31.** Collection of photogenerated charges at the electrode surface: Left: Mesoscopic film. Right: Hybrid assemblies of nanotubes and light harvesting assemblies.

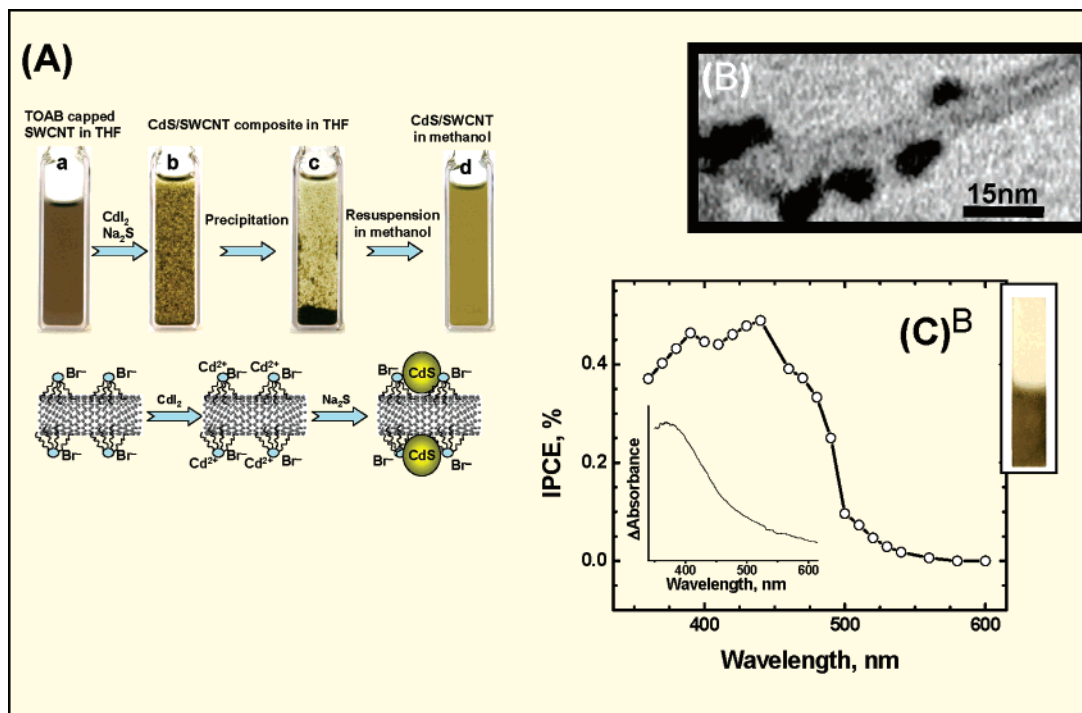


**Figure 32.** (A) Synthetic steps involved in the preparation of SWCNT–CdS composite. (B) TEM image of the CdS bound SWCNT. (C) Photocurrent response and absorbance of SWCNT–CdS composite film in a photoelectrochemical cell. (From ref 347.)

photoelectrochemical cells. For example, in nanostructured semiconductor films prepared from particles, the electron transport across particles is susceptible for recombination loss at the grain boundaries. The use of nanotube support to anchor light harvesting assemblies (e.g., semiconductor particles) provides a convenient way to capture photogenerated charge and transport them to the electrode surface. The illustration of these two scenarios can be seen in Figure 31.

#### a. Carbon Nanotubes as Conduits for Charge Transport.

A single wall carbon nanotube (SWCNT) is an ideal candidate as a conduit for collecting and transporting charges across light harvesting assemblies. Efforts to synthesize semiconductor–CNT composite films has shown significant progress in recent years.<sup>336–343</sup> These early studies have mainly focused on establishing synthetic strategies and characterization of the

composite systems. These include carbon nanotubes in contact with TiO<sub>2</sub>,<sup>344</sup> SnO<sub>2</sub>,<sup>345</sup> CdSe,<sup>340,342</sup> and CdS.<sup>346</sup>

Of particular interest is the CdS–CNT composite that is capable of generating photocurrent from visible light with unusually high efficiency.<sup>337,347</sup> The luminescence of CdS is quenched by SWCNT. Transient absorption experiments have confirmed the quick deactivation of excited CdS on the SWCNT surface as the transient bleaching recovers in about 200 ps. Excitation of CdS deposited on SWCNT films produces photocurrent with a maximum incident photon to current generation efficiency of 0.5% and thus provides evidence for the electron-transfer pathway in the composite. The ability of the CdS–SWCNT nanocomposite system to undergo photoinduced charge separation opens up new ways to design light harvesting assemblies.

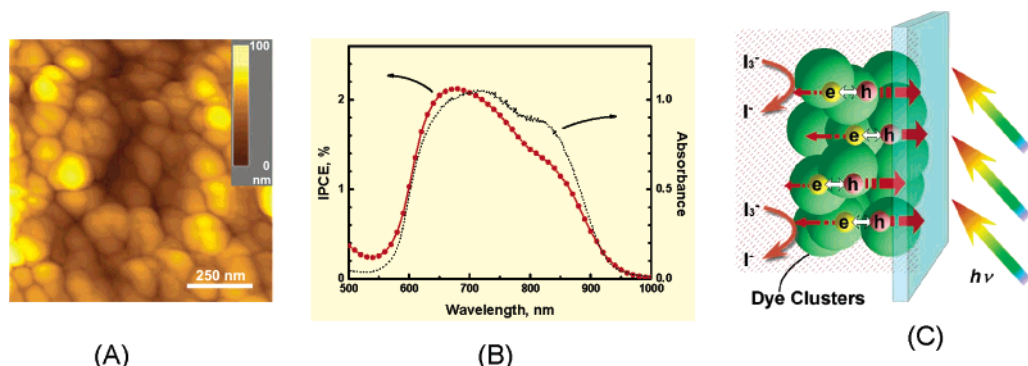


**Figure 33.** (A) AFM image of IR 125 dye clusters deposited on a conducting glass electrode. (B) Photocurrent action spectrum and absorption spectrum of the cluster film and (C) mechanism of photocurrent generation. (From ref 348.)

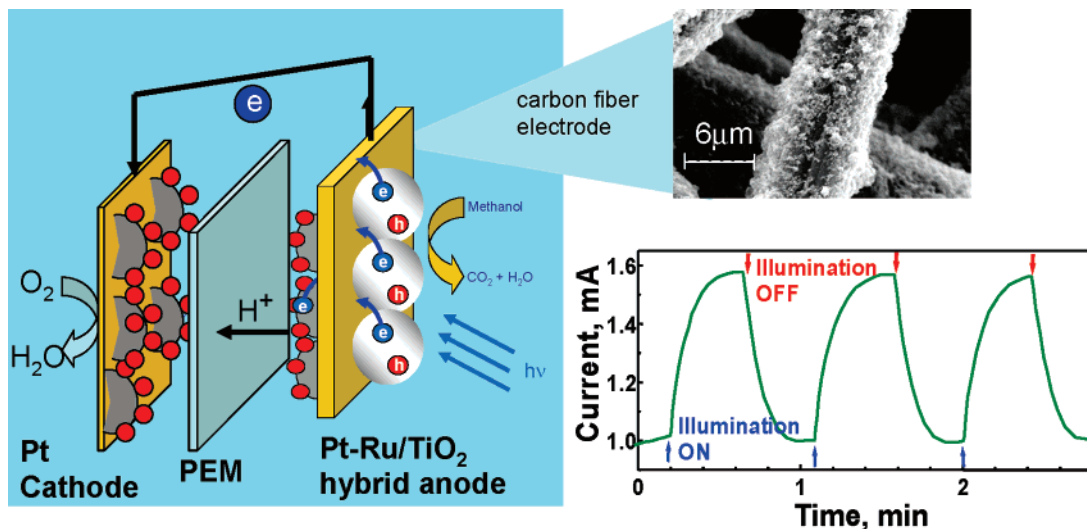


**Figure 34.** Schematic diagram illustrating the operation of a hybrid cell incorporating the principle of electrocatalysis and photocatalysis (left). The boost in the current is seen when the cell is illuminated with UV light (right). A magnified view of the carbon fiber electrode shows the deposition of Pt–Ru and TiO<sub>2</sub> particles is also shown. (From ref 361.)

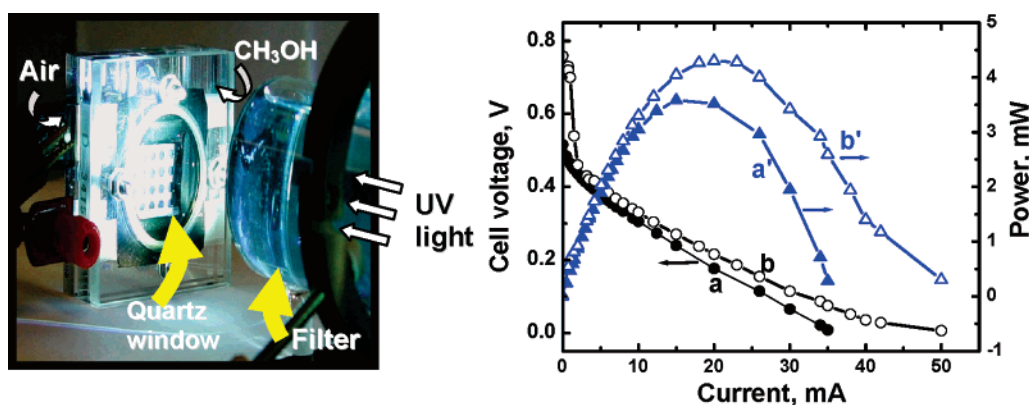


**Figure 35.** Left: Air breathing direct methanol fuel cell (DMFC) cell equipped with quartz window for UV excitation. Right: Galvanostatic polarization and power output data at 295 K using TiO<sub>2</sub>/CFE/Pt–Ru anode and CFE/Pt black cathode. Traces were recorded (a) and (a') in the absence and (b) and (b') in the presence of UV illumination. The Pt loadings for both cathode and anode were maintained at 0.15 mg/cm<sup>2</sup> and TiO<sub>2</sub> loading of 0.4 mg/cm<sup>2</sup>. The electrolyte was aqueous 1 M CH<sub>3</sub>OH (electrode surface area 5 cm<sup>2</sup>). (From ref 361.)

**b. Organic Polymer Hybrid Photovoltaic Cells.** The solution processibility and attractive photoconversion efficiency has drawn significant attention of organic semiconductor materials for constructing solar cells. Up to 2.5% power conversion efficiencies have been attained.<sup>349–355</sup>

Figure 33 shows the response of tricarbocyanine dye clusters to infrared excitation. Molecular clusters of this dye show broad absorption in the 550–950 nm region compared to the sharp monomer absorption band at 800 nm. The molecular clusters of the dye are readily deposited as a thin film on optically

transparent electrodes under the application of a dc field.<sup>348</sup> These electrodes are photoactive in the infrared region and produce a cathodic current when employed in a photoelectrochemical cell. Inability of these dye clusters to undergo efficient charge separation and low mobility of charge carriers limits the efficiency of photocurrent generation.

Whereas free electron–hole pairs are formed in inorganic semiconductors, excitons or bound electron–hole pairs are formed in organic materials upon photoexcitation. By introducing an interface using second material (e.g., C<sub>60</sub>), one can drive

away one of the charge carriers and increase the probability of collecting the charges at the collecting electrode surface. Semiconductor nanostructures provide an attractive alternative to introduce charge-transfer junctions. Blends of conjugated polymers and semiconductor nanoparticles have been probed to investigate the charge-transfer properties.<sup>310,356</sup> Alivisatos and co-workers have shown that CdSe nanorods when combined with poly(3-hexylthiophene) create charge-transfer junctions with high interfacial area.<sup>309</sup> By tuning the band gap, these researchers succeeded in optimizing the overlap between the cell absorption and solar spectrum. A monochromatic efficiency of 6.9% was reported. By improving the polymer–semiconductor interface, it should be possible to increase the carrier mobilities and hence the overall photoconversion efficiency. The details on the mechanism of photocurrent generation and recent advances in organic solar cells can be found in recent reviews.<sup>351,352,354,357–360</sup>

**c. Photocatalyst Based Hybrid Methanol Fuel Cells.** For more than two decades, the electrode assembly employed in the operation of a direct methanol fuel cell (DMFC) relies on the Pt–Ru catalyst anchored on a carbon support.<sup>362–365</sup> A proton exchange membrane (PEM) separates the C/Pt–Ru anode and C/Pt cathode and allows ion transport between the two cell compartments. In a recent study,<sup>361</sup> we have shown that TiO<sub>2</sub> photocatalyst particles can be incorporated in the anode along with the Pt–Ru catalyst and carry out methanol oxidation both electrocatalytically and photocatalytically in a synergetic way. We made use of the photocatalytic properties of TiO<sub>2</sub> to boost the traditionally attained current from the oxidation of methanol in the Pt–Ru catalyst system. Figure 34 illustrates the principle of methanol oxidation at this hybrid electrode and the response of the hybrid fuel cell to UV excitation. An increase in the current during UV excitation represents the contribution from the photocatalytic oxidation at the TiO<sub>2</sub> surface. The power characteristics of the hybrid cell shown in Figure 35 shows an overall improvement in the deliverable power when exposed to UV light.

Though use of a photocatalyst is likely to have limited applications, such simple approaches can greatly minimize the use of precious metals, yet deliver higher output. In addition, the presence of oxides can also minimize the poisoning effect. Possible application of such photocatalyst based hybrid cells can be visualized in outdoor fixtures where single stack fuel cells can be spread out to capture sunlight. The rising clean energy demand will compel us in the near future to find hybrid devices that are tailored to applications.

### Concluding Remarks

During the past decade, new synthetic strategies have been developed to design nanostructure architectures of semiconductors, metals, polymers and light harvesting assemblies. Despite the vast array of literature on such materials their optical and light harvesting properties are yet to be understood fully. A concerted effort is needed to screen potentially useful systems and find ways to design solar energy conversion devices. The examples discussed in this article provide unique optical, photocatalytic, and photoelectrochemical properties of various nanostructures that could aid in the development of the next generation light harvesting devices. Developing strategies to organize ordered assemblies of two or more components on electrode surfaces will be the key for improving the performance of photochemical solar cells. In addition, new sensitizer or semiconductor systems that can harvest infrared photons are necessary to broaden the photoresponse in the solar spectrum.

Q-dot and carbon nanostructure based solar cells are still in their infancy. Harvesting multiple charge carriers generated in semiconductor Q-dots will be a major challenge for the researchers working in this area.

Hybrids of solar and conventional devices may provide an interim benefit in seeking economically viable devices. However, commercialization of large scale solar cells based on nanostructure architecture is yet to be a reality. With the increasing demand for clean energy alternatives, the orphan status of solar energy is expected to change. Increasing interest from the private sector and venture capitalist investment should bring in major breakthroughs in developing economically viable solar energy conversion devices.

**Acknowledgment.** The research at Notre Dame Radiation Laboratory is supported by the Office of Basic Energy Sciences of the U.S. Department of Energy. Thanks are due to the students, postdoctoral associates, visiting scientists, and collaborators who have actively contributed to the significant advance of our solar energy research (see <http://www.nd.edu/~pkamat> for further details). Individual contributions are recognized in the cited work. I also acknowledge helpful discussions with my colleagues, peers, and fellow scientists at the annual DOE Solar Photochemistry Research Conference and other scientific meetings. I thank Mr. Ian Duncanson and Mr. James Strobe for their assistance in designing and constructing various experimental set up used in our investigations. This is contribution NDRL 4697 from the Notre Dame Radiation Laboratory.

### References and Notes

- (1) Weisz, P. B. Basic choices and constraints on long-term energy supplies. *Phys. Today* **2004**.
- (2) Bartlett, A. A. Sustained availability: A management program for nonrenewable resources. *Am. J. Phys.* **1986**, *54*, 398–402.
- (3) Myers, N.; Kent, J. New consumers: The influence of affluence on the environment. *Proc. Natl. Acad. Sci. U.S.A.* **2003**, *100*, 4963–4968.
- (4) Campbell, C. J. Petroleum and People. *Popul. Environ.* **2002**, *24*, 193–207.
- (5) Hubbert, M. K. Energy from Fossil Fuels. *Science* **1949**, *109*, 103–109.
- (6) Hubbert, M. K. The world's evolving energy system. *Am. J. Phys.* **1981**, *49*, 1007–1029.
- (7) Hubbert, M. K.; Grathwohl, M. World-Energy Supply Resources, Technologies, Perspectives. *Am. Sci.* **1984**, *72*, 293–293.
- (8) Campbell, C. J. Industry urged to watch for regular oil production peaks, depletion signals. *Oil Gas J. Tulsa* **2003**, *101*, 38–44.
- (9) Campbell, C. J.; Laherrere, J. H. The end of cheap oil. *Sci. Am.* **1998**, *278*, 60–65.
- (10) Deffeyes, K. S. *Hubbert's Peak: The Impending World Oil Shortage*. Princeton University Press: Princeton, NJ, 2001.
- (11) Dresselhaus, M. S.; Thomas, I. L. Alternative energy technologies. *Nature* **2001**, *414*, 332–337.
- (12) Ragauskas, A. J.; Williams, C. K.; Davison, B. H.; Britovsek, G.; Cairney, J.; Eckert, C. A.; William J. Frederick, J.; Hallett, J. P.; Leak, D. J.; Liotta, C. L.; Mielenz, J. R.; Murphy, R.; Templer, R.; Tschaplinski, T. The Path Forward for Biofuels and Biomaterials. *Science* **2006**, *484*–489.
- (13) Mann, M. E.; Bradley, R. S.; Hughes, M. K. Global-scale temperature patterns and climate forcing over the past six centuries. *Nature* **1998**, *392*, 779–787.
- (14) Hoffert, M. I.; Caldeira, K.; Jain, A. K.; Haites, E. F.; Harveyk, L. D. D.; Potter, S. D.; Schlesinger, M. E.; Schneider, S. H.; G. Watts, I. R.; Wigley, T. L.; J. Wuebbles, D. Energy implications of future stabilization of atmospheric CO<sub>2</sub> content. *Nature* **1998**, *395*, 881–884.
- (15) Hoffert, M. I.; Caldeira, K.; Benford, G.; Criswell, D. R.; Green, C.; Herzog, H.; Jain, A. K.; Kheshgi, H. S.; Lackner, K. S.; Lewis, J. S.; Lightfoot, H. D.; Manheimer, W.; Mankins, J. C.; Mauel, M. E.; Perkins, L. J.; Schlesinger, M. E.; Volk, T.; Wigley, T. M. L. Advanced Technology Paths to Global Climate Stability: Energy for a Greenhouse Planet. *Science* **2002**, *298*, 981–987.
- (16) Lewis, N. S.; Crabtree, G. W.; Nozik, A. J.; Wasielewski, M. R.; Alivisatos, A. P., *Basic Energy Sciences Report on Basic Research Needs*

for Solar Energy Utilization. Office of Science, U.S. Department of Energy: Washington, DC, 2005; [http://www.sc.doe.gov/bes/reports/files/SEU\\_rpt.pdf](http://www.sc.doe.gov/bes/reports/files/SEU_rpt.pdf).

(17) Crabtree, G. W.; Dresselhaus, M. S.; Buchanan, M. V. The hydrogen economy. *Phys. Today* **2004**, *57*, 39–44.

(18) Green, M. A. *Third Generation Photovoltaics: Advanced Solar Energy Conversion*; Springer-Verlag: Berlin, Germany, 2004.

(19) Barnham, K. W. J.; Mazzer, M.; Clive, B. Resolving the energy crisis: nuclear or photovoltaics? *Nat. Mater.* **2006**, *5*, 161–164.

(20) Henglein, A. Small-particle research: Physicochemical properties of extremely small colloidal metal and semiconductor particles. *Chem. Rev.* **1989**, *89*, 1861–73.

(21) Steigerwald, M. L.; Brus, L. E. Semiconductor crystallites: A class of large molecules. *Acc. Chem. Res.* **1990**, *23*, 183–8.

(22) Brus, L. Electronic wave functions in semiconductor clusters: Experiment and theory. *J. Phys. Chem.* **1986**, *90*, 2555–60.

(23) Weller, H. Quantized semiconductor particles: A novel state of matter for materials science. *Adv. Mater.* **1993**, *5*, 88–95.

(24) Banyai, L.; Koch, S. W. *Semiconductor quantum Dots*; World Scientific Publishing Co.: River Edge, NJ, 1993.

(25) Kamat, P. V. *Native and surface modified semiconductor nanoclusters*, in *Molecular level artificial photosynthetic materials. Progress in Inorganic Chemistry Series*; Meyer, J., Ed.; John Wiley & Sons, Inc.: New York, 1997; pp 273–243.

(26) Alivisatos, P. Perspectives on the physical chemistry of semiconductor nanocrystals. *J. Phys. Chem.* **1996**, *100*, 13226–13239.

(27) Kamat, P. V. Photophysical, photochemical and photocatalytic aspects of metal nanoparticles. *J. Phys. Chem. B* **2002**, *106*, 7729–7744.

(28) Adams, D.; Brus, L.; Chidsey, C. E. D.; Creager, S.; Cruetz, C.; Kagan, C. R.; Kamat, P. V.; Lieberman, M.; Lindsay, S.; Marcus, R. A.; Metzger, R. M.; Michel-Beyerle, M. E.; Miller, J. R.; Newton, M. D.; Rolison, D. R.; Sankey, O.; Schanze, K. S.; Yardley, J.; Zhu, X. Charge Transfer on the Nanoscale. *J. Phys. Chem. B* **2003**, *107*, 6668–6697.

(29) George Thomas, K.; Kamat, P. V. Chromophore Functionalized Gold Nanoparticles. *Acc. Chem. Res.* **2003**, *36*, 888–898.

(30) Shipway, A. N.; Katz, E.; Willner, I. Nanoparticle arrays on surfaces for electronic, optical, and sensor applications. *Chem. Phys. Chem.* **2000**, *1*, 18–52.

(31) Willner, I.; Kaganer, E.; Joselevich, E.; Durr, H.; David, E.; Gunter, M. J.; Johnston, M. R. Photoinduced electron transfer in supramolecular assemblies of transition metal complexes. *Coord. Chem. Rev.* **1998**, *171*, 261–285.

(32) Ward, M. D. Photo-induced electron and energy transfer in non-covalently bonded supramolecular assemblies. *Chem. Soc. Rev.* **1999**, 365–375.

(33) Ouyang, M.; Huang, J. L.; Lieber, C. M. Fundamental electronic properties and applications of single-walled carbon nanotubes. *Acc. Chem. Res.* **2002**, *35*, 1018–1025.

(34) Xia, Y. N.; Yang, P. D.; Sun, Y. G.; Wu, Y. Y.; Mayers, B.; Gates, B.; Yin, Y. D.; Kim, F.; Yan, Y. Q. One-dimensional nanostructures: Synthesis, characterization, and applications. *Adv. Mater.* **2003**, *15*, 353–389.

(35) El-Sayed, M. A. Some interesting properties of metals confined in time and nanometer space of different shapes. *Acc. Chem. Res.* **2001**, *34*, 257–264.

(36) Burda, C.; Chen, X. B.; Narayanan, R.; El-Sayed, M. A. Chemistry and properties of nanocrystals of different shapes. *Chem. Rev.* **2005**, *105*, 1025–1102.

(37) Sirbully, D. J.; Law, M.; Yan, H.; Yang, P. Semiconductor Nanowires for Subwavelength Photonics Integration. *J. Phys. Chem. B* **2005**, *109*, 15190–15213.

(38) Cao, G. Web release, Growth of Oxide Nanorod Arrays through Sol Electrophoretic Deposition. *J. Phys. Chem. B* **2005**, *109*.

(39) Kelly, K. L.; Coronado, E.; Zhao, L. L.; Schatz, G. C. The Optical Properties of Metal Nanoparticles: The Influence of Size, Shape, and Dielectric Environment. *J. Phys. Chem. B* **2003**, *107*, 668–677.

(40) Jin, R.; Cao, Y. C.; Hao, E.; Me'traux, G. S.; Schatz, G. C.; Mirkin, C. A. Controlling anisotropic nanoparticle growth through plasmon excitation. *Nature* **2003**, *425*, 487.

(41) Henzie, J.; Shuford, K. L.; Kwak, E. S.; Schatz, G. C.; Odom, T. W. Manipulating the Optical Properties of Pyramidal Nanoparticle Arrays. *J. Phys. Chem. B* **2006**, *110*, 14028–14031.

(42) Murphy, C. J.; Gole, A. M.; Hunyadi, S. E.; Orendorff, C. J. One-Dimensional Colloidal Gold and Silver Nanostructures. *Inorg. Chem.* **2006**, *45*, 7544–7554.

(43) Wang, F.; Dong, A.; Sun, J.; Tang, R.; Yu, H.; Bhuro, W. E. Solution-Liquid-Solid Growth of Semiconductor Nanowires. *Inorg. Chem.* **2006**, *45*, 7511–7521.

(44) Greene, L. E.; Yuhas, B. D.; Law, M.; Zitoun, D.; Yang, P. Solution-Grown Zinc Oxide Nanowires. *Inorg. Chem.* **2006**, *45*, 7535–7543.

(45) Kline, T. R.; Tian, M.; Wang, J.; Sen, A.; Chan, M. W. H.; Mallouk, T. E. Template-Grown Metal Nanowires. *Inorg. Chem.* **2006**, *45*, 7555–7565.

(46) Grätzel, M. Artificial photosynthesis: Water cleavage into hydrogen and oxygen by visible light. *Acc. Chem. Res.* **1981**, *14*, 376–84.

(47) Bard, A. J.; Fox, M. A. Artificial photosynthesis: Solar splitting of water to hydrogen and oxygen. *Acc. Chem. Res.* **1995**, *28*, 141–5.

(48) Gust, D.; Moore, T. A.; Moore, A. L. Mimicking photosynthetic solar energy transduction. *Acc. Chem. Res.* **2001**, *34*, 40–48.

(49) Brune, A.; Jeong, G.; Liddell, P. A.; Sotomura, T.; Moore, T. A.; Moore, A. L.; Gust, D. Porphyrin-Sensitized Nanoparticulate TiO<sub>2</sub> as the Photoanode of a Hybrid Photoelectrochemical Biofuel Cell. *Langmuir* **2004**, *20*, 8366–8371.

(50) Imahori, H.; Kashiwagi, Y.; Hanada, T.; Endo, Y.; Nishimura, Y.; Yamazaki, I.; Fukuzumi, S. Metal and size effects on structures and photophysical properties of porphyrin-modified metal nanoclusters. *J. Mater. Chem.* **2003**, *13*, 2890–2898.

(51) Campbell, W. M.; Burrell, A. K.; Officer, D. L.; Jolley, K. W. Porphyrins as light harvesters in the dye-sensitized TiO<sub>2</sub> solar cell. *Coord. Chem. Rev.* **2004**, *248* 1363–1379.

(52) Thomas, K. G.; George, M. V.; Kamat, P. V. Photoinduced Electron Transfer Processes in Fullerene-Based Donor-Acceptor Systems. *Helv. Chim. Acta.* **2005**, *88*, 1291–1308.

(53) D'Souza, F.; Ito, O. Photoinduced electron transfer in supramolecular systems of fullerenes functionalized with ligands capable of binding to zinc porphyrins and zinc phthalocyanines. *Coord. Chem. Rev.* **2005**, *249*, 1410–1422.

(54) Guldi, D. M. Biomimetic assemblies of carbon nanostructures for photochemical energy conversion. *J. Phys. Chem. B* **2005**, *109*, 11432–11441.

(55) Wasielewski, M. R. Energy, charge, and spin transport in molecules and self-assembled nanostructures inspired by photosynthesis. *J. Org. Chem.* **2006**, *71*, 5051–5066.

(56) Gust, D.; Moore, T. A.; Moore, A. L. Photochemistry of supramolecular systems containing C-60. *J. Photochem. Photobiol. B-Biol.* **2000**, *58*, 63–71.

(57) Alstrum-Acevedo, J. H.; Brennaman, M. K.; Meyer, T. J. Chemical Approaches to Artificial Photosynthesis. 2. *Inorg. Chem.* **2005**, *44*, 6802–6827.

(58) Oelhafen, P.; Schuler, A. Nanostructured materials for solar energy conversion. *Solar Energy* **2005**, *79*, 110–121.

(59) Templeton, A. C.; Wuelfing, W. P.; Murray, R. W. Monolayer protected cluster molecules. *Acc. Chem. Res.* **2000**, *33*, 27–36.

(60) Whetten, R. L.; Shafiqullin, M. N.; Khoury, J. T.; Schaaff, T. G.; Vezmar, I.; Alvarez, M. M.; A. W. Crystal Structures of Molecular Gold Nanocrystal Arrays. *Acc. Chem. Res.* **1999**, *32*, 397–406.

(61) Hassenkam, T.; Nørgaard, K.; Iversen, L.; Kiely, C. J.; Brust, M.; Bjørnholm, T. Fabrication of 2D Gold Nanowires by Self-Assembly of Gold Nanoparticles on Water Surfaces in the Presence of Surfactants. *Adv. Mater.* **2002**, *14*, 1126–1130.

(62) Sastry, M.; Rao, M.; Ganesh, K. N. Electrostatic assembly of nanoparticles and biomacromolecules. *Acc. Chem. Res.* **2002**, *35*, 847–855.

(63) Brust, M.; Bethell, D.; Schiffrin, D. J.; Kiely, C. J. Novel Gold-Dithiol Nano-Networks With Nonmetallic Electronic-Properties. *Adv. Mater.* **1995**, *7*, 795.

(64) Brust, M.; Kiely, C. Some recent advances in nanostructure preparation from gold and silver particles: a short topical review. *Colloid Surf. A* **2002**, *202*, 175–186.

(65) Brust, M.; Bethell, D.; Kiely, C. J.; Schiffrin, D. J. Self-assembled gold nanoparticle thin films with nonmetallic optical and electronic properties. *Langmuir* **1998**, *14*, 5425–5429.

(66) Willner, I.; Willner, B. Molecular and biomolecular optoelectronics. *Pure Appl. Chem.* **2001**, *73*, 535–542.

(67) Lahav, M.; Shipway, A. N.; Willner, I. Au-nanoparticle-bis-bipyridinium cyclophane superstructures: assembly, characterization and sensoric applications. *J. Chem. Soc., Perkin Trans. 2* **1999**, 1925–1931.

(68) Lioubashevski, O.; Chegel, V. I.; Patolsky, F.; Katz, E.; Willner, I. Enzyme-catalyzed bio-pumping of electrons into Au-nanoparticles: A surface plasmon resonance and electrochemical study. *J. Am. Chem. Soc.* **2004**, *126*, 7133–7143.

(69) Correa-Duarte, M. A.; Sobal, N.; Liz-Marzan, L. M.; Giersig, M. Linear assemblies of silica-coated gold nanoparticles using carbon nanotubes as templates. *Adv. Mater.* **2004**, *16* 2179–+.

(70) Ribrioux, S.; Kleymann, G.; Haase, W.; Heitmann, K.; Ostermeier, C.; Michel, H. Use of Nanogold- and Fluorescent-labeled Antibody Fv Fragments in Immunocytochemistry. *J. Histochem. Cytochem.* **1996**, *44*, 207–213.

(71) Elghanian, R.; Storhoff, J. J.; Mucic, R. C.; Letsinger, R. L.; Mirkin, C. A. Selective Colorimetric Detection of Polynucleotides Based on the Distance-Dependent Optical Properties of Gold Nanoparticles. *Science* **1997**, *277*, 1078–1081.

- (72) Schmid, G.; Corain, B. Nanoparticulated Gold: Syntheses, Structures, Electronics, and Reactivities. *Eur. J. Inorg. Chem.* **2003**, 3081–3098.
- (73) Brust, M.; Walker, M.; Bethell, D.; Schiffrin, D. J.; Whyman, R. Synthesis of thiol-derivatized gold nanoparticles in a two-phase liquid-liquid system. *J. Chem. Soc. Chem. Commun.* **1994**, 801–802.
- (74) Brust, M.; Fink, J.; Bethell, D.; Schiffrin, D. J.; Kiely, C. Synthesis and reactions of functionalized gold nanoparticles. *J. Chem. Soc. Chem. Commun.* **1995**, 1655–1656.
- (75) Hostetler, M. J.; Templeton, A. C.; Murray, R. W. Dynamics of Place-Exchange Reactions on Monolayer-Protected Gold Cluster Molecules. *Langmuir* **1998**, *15*, 3782–3789.
- (76) Montalti, M.; Prodi, L.; Zaccaroni, N.; Baxter, R.; Teobaldi, G.; Zerbetto, F. Kinetics of Place-Exchange Reactions of Thiols on Gold Nanoparticles. *Langmuir* **2003**, *19*, 5172–5174.
- (77) Shaffer, A. W.; Worden, J. G.; Huo, Q. Comparison Study of the Solution Phase versus Solid Phase Place Exchange Reactions in the Controlled Functionalization of Gold Nanoparticles. *Langmuir* **2004**, *20*, 8343–8351.
- (78) Drexhage, K. H.; Kuhn, H.; Shafer, F. P. Variation of the fluorescence decay time of a molecule in front of a mirror, metal, energy transfer. *Ber. Bunsen-Ges. Phys. Chem.* **1968**, *72*, 329.
- (79) Ishida, A.; Sakata, Y.; Majima, T. Surface plasmon excitation of a porphyrin covalently linked to a gold surface. *J. Chem. Soc. Chem. Commun.* **1998**, 57–58.
- (80) Saito, K. Quenching of excited J aggregates on metals by surface plasmon excitations. *J. Phys. Chem. B* **1999**, *103*, 6579–6583.
- (81) Pagnot, T.; Barchiesi, D.; Tribillon, G. Energy transfer from fluorescent thin films to metals in near-field optical microscopy: Comparison between time-resolved and intensity measurements. *Appl. Phys. Lett.* **1999**, *75*, 4207–4209.
- (82) Ipe, B. I.; George Thomas, K.; Barazzouk, S.; Hotchandani, S.; Kamat, P. V. Photoinduced Charge Separation in a Fluorophore-Gold Nanoassembly. *J. Phys. Chem. B* **2002**, *106*, 18–21.
- (83) Kamat, P. V.; Barazzouk, S.; Hotchandani, S. Electrochemical Modulation of Fluorophore Emission at a Nanostructured Gold Film. *Angew. Chem., Int. Ed.* **2002**, *41*, 2764–2767.
- (84) George Thomas, K.; Kamat, P. V. Making Gold Nanoparticles Glow. Enhanced emission from a Surface Bound Probe. *J. Am. Chem. Soc.* **2000**, *122*, 2655–2656.
- (85) George Thomas, K.; Ipe, B. I.; Sudeep, P. K. Photochemistry of chromophore-functionalized gold nanoparticles. *Pure Appl. Chem.* **2002**, *74*, 1731–1738.
- (86) Ipe, B. I.; George Thomas, K. Investigations on nanoparticle-chromophore and interchromophore interactions in pyrene-capped gold nanoparticles. *J. Phys. Chem. B* **2004**, *108*, 13265–13272.
- (87) Barazzouk, S.; Kamat, P. V.; Hotchandani, S. Photoinduced Electron Transfer between Chlorophyll a and Gold Nanoparticles. *J. Phys. Chem. B* **2005**, *109*, 7116–723.
- (88) Stellacci, F.; Bauer, C. A.; Meyer-Friedrichsen, T.; Wenseleers, W.; Marder, S. R.; Perry, J. W. Ultrabright supramolecular beacons based on the self-assembly of two-photon chromophores on metal nanoparticles. *J. Am. Chem. Soc.* **2003**, *125*, 328–329.
- (89) Imahori, H.; Arimura, M.; Hanada, T.; Nishimura, Y.; Yamazaki, I.; Sakata, Y.; Fukuzumi, S. Photoactive three-dimensional monolayers: Porphyrin-alkanethiolate-stabilized gold clusters. *J. Am. Chem. Soc.* **2001**, *123*, 335–336.
- (90) Templeton, A. C.; Cliffler, D. E.; Murray, R. W. Redox and fluorophore functionalization of water soluble, tioponin-protected gold clusters. *J. Am. Chem. Soc.* **1999**, *121*, 7081–7089.
- (91) Hranisavljevic, J.; Dimitrijevic, N. M.; Wurtz, G. A.; Wiederrecht, G. P. Photoinduced Charge Separation Reactions of J-Aggregates Coated on Silver Nanoparticles. *J. Am. Chem. Soc.* **2001**, *124*, 4536–4537.
- (92) Hu, J.; Zhang, J.; Liu, F.; Kittredge, K.; Whitesell, J. K.; Fox, M. A. Competitive photochemical reactivity in a self-assembled monolayer on a colloidal gold cluster. *J. Am. Chem. Soc.* **2001**, *123*, 1464–1470.
- (93) Chen, M. M. Y.; Katz, A. Steady-State Fluorescence-Based Investigation of the Interaction between Protected Thiols and Gold Nanoparticles. *Langmuir* **2002**, *18*, 2413–2420.
- (94) Wang, T. X.; Zhang, D. Q.; Xu, W.; Yang, J. L.; Han, R.; Zhu, D. B. Preparation, characterization, and photophysical properties of alkanethiols with pyrene units-capped gold nanoparticles: Unusual fluorescence enhancement for the aged solutions of these gold nanoparticles. *Langmuir* **2002**, *18*, 1840–1848.
- (95) Dulkeith, E.; Morteani, A. C.; Niedereichholz, T.; Klar, T. A.; Feldmann, J.; Levi, S. A.; van Veggel, F. C. J. M.; Reinhoudt, D. N.; Moller, M.; Gittins, D. I. Fluorescence quenching of dye molecules near gold nanoparticles: Radiative and nonradiative effects. *Phys. Rev. Lett.* **2002**, *89*, art. no. 203002.
- (96) Sudeep, P. K.; Ipe, B. I.; George Thomas, K.; George, M. V.; Barazzouk, S.; Hotchandani, S.; Kamat, P. V. Fullerene Functionalized Gold Nanoparticles. A self assembled Photoactive Antenna-Metal Nanocore Assembly. *Nano Lett.* **2002**, *2*, 29–35.
- (97) Wiederrecht, G. P.; Wurtz, G. A.; Hranisavljevic, J. Coherent coupling of molecular excitons to electronic polarizations of noble metal nanoparticles. *Nano Lett.* **2004**, *4*, 2121–2125.
- (98) Wiederrecht, G. P. Near-field optical imaging of noble metal nanoparticles. *Euro. Phys. J. Appl. Phys.* **2004**, *28*, 3–18.
- (99) Wurtz, G. A.; Hranisavljevic, J.; Wiederrecht, G. P. Photo-initiated energy transfer in nanostructured complexes observed by near-field optical microscopy. *J. Microsc.-Oxford* **2003**, *210*, 340–343.
- (100) Fan, C. H.; Wang, S.; Hong, J. W.; Bazan, G. C.; Plaxco, K. W.; Heeger, A. J. Beyond superquenching: Hyper-efficient energy transfer from conjugated polymers to gold nanoparticles. *Proc. Nat. Acad. Sci. U.S.A.* **2003**, *100*, 6297–6301.
- (101) Maxwell, D. J.; Taylor, J. R.; Nie, S. M. Self-assembled nanoparticle probes for recognition and detection of biomolecules. *J. Am. Chem. Soc.* **2002**, *124*, 9606–9612.
- (102) Wang, G. L.; Zhang, J.; Murray, R. W. DNA binding of an ethidium intercalator attached to a monolayer-protected gold cluster. *Anal. Chem.* **2002**, *74*, 4320–4327.
- (103) Kamat, P. V. Photoelectrochemistry in particulate systems. 9. Photosensitized reduction in a colloidal TiO<sub>2</sub> system using anthracene-9-carboxylic acid as the sensitizer. *J. Phys. Chem.* **1989**, *93*, 859–64.
- (104) Liu, D.; Hug, G. L.; Kamat, P. V. Photochemistry on Surfaces. Intermolecular energy and electron transfer processes between excited Ru-(bpy)<sub>3</sub><sup>2+</sup> and H-aggregates of Cresyl Violet on SiO<sub>2</sub> and SnO<sub>2</sub> colloids. *J. Phys. Chem.* **1995**, *99*, 16768–16775.
- (105) Liu, D.; Kamat, P. V. Picosecond dynamics of Cresyl violet H-aggregates adsorbed on SiO<sub>2</sub> and SnO<sub>2</sub> nanocrystallites. *J. Chem. Phys.* **1996**, *105*, 965–970.
- (106) Chen, S.; Murray, R. W. Electrochemical Quantized Capacitance Charging of Surface Ensembles of Gold Nanoparticles. *J. Phys. Chem. B* **1999**, *103*, 9996–10000.
- (107) Amouyal, E. Photochemical production of hydrogen and oxygen from water: A review and state of the art. *Sol. Energy Mater. Sol. Cells* **1995**, *38*, 249–76.
- (108) Parmon, V. N. Photoproduction of hydrogen (an overview of modern trends). *Adv. Hydrogen Energy (Hydrogen Energy Prog.)* **1990**, *8*, 801–13.
- (109) Tanaka, A.; Kondo, J. N.; Domen, K. Photocatalytic properties of ion-exchangeable layered oxides. *Crit. Rev. Surface Chem.* **1995**, *5*, 305–326.
- (110) Turner, J. A. Sustainable hydrogen production. *Science* **2004**, *305*, 972–974.
- (111) Gerischer, H.; Luebke, M. A particle size effect in the sensitization of TiO<sub>2</sub> electrodes by a CdS deposit. *J. Electroanal. Chem.* **1986**, *204*, 225–7.
- (112) Spanhel, L.; Weller, H.; Henglein, A. Photochemistry of semiconductor colloids. 22. Electron injection from illuminated CdS into attached TiO<sub>2</sub> and ZnO particles. *J. Am. Chem. Soc.* **1987**, *109*, 6632–5.
- (113) Hotchandani, S.; Kamat, P. V. Charge-transfer processes in coupled semiconductor systems. Photochemistry and photoelectrochemistry of the colloidal CdS-ZnO system. *J. Phys. Chem.* **1992**, *96*, 6834–9.
- (114) Vogel, R.; Hoyer, P.; Weller, H. Quantum-sized PbS, CdS, Ag<sub>2</sub>S, Sb<sub>2</sub>S<sub>3</sub> and Bi<sub>2</sub>S<sub>3</sub> particles as sensitizers for various nanoporous wide-bandgap semiconductors. *J. Phys. Chem.* **1994**, *98*, 3183–3188.
- (115) Nasr, C.; Hotchandani, S.; Kim, W. Y.; Schmehl, R. H.; Kamat, P. V. Photoelectrochemistry of composite semiconductor thin films. Photosensitization of SnO<sub>2</sub>/CdS coupled nanocrystallites with a Ruthenium complex. *J. Phys. Chem. B* **1997**, *101*, 7480–7487.
- (116) Nasr, C.; Hotchandani, S.; Kamat, P. V. Photoelectrochemistry of composite semiconductor thin films. II. Photosensitization of SnO<sub>2</sub>/TiO<sub>2</sub> coupled system with a ruthenium polypyridyl complex. *J. Phys. Chem. B* **1998**, *102*, 10047–10056.
- (117) Zaban, A.; Micic, O. I.; Gregg, B. A.; Nozik, A. J. Photosensitization of Nanoporous TiO<sub>2</sub> Electrodes with InP Quantum Dots. *Langmuir* **1998**, *14*, 3153–3156.
- (118) Vinodgopal, K.; Kamat, P. V. Enhanced rates of photocatalytic degradation of an azo dye using SnO<sub>2</sub>/TiO<sub>2</sub> coupled semiconductor thin films. *Environ. Sci. Technol.* **1995**, *29*, 841–845.
- (119) Tada, H.; Teranishi, T. K.; Yo-ichi, I.; Ito, S. Ag Nanocluster Loading Effect on TiO<sub>2</sub> Photocatalytic Reduction of Bis(2-dipyridyl)-disulfide to 2-Mercaptopyridine by H<sub>2</sub>O Hiroaki. *Langmuir* **2000**, *16*, 3304–3309.
- (120) Bard, A. J. Design of semiconductor photoelectrochemical systems for solar energy conversion. *J. Phys. Chem.* **1982**, *86*, 172–7.
- (121) Baba, R.; Nakabayashi, S.; Fujishima, A.; Honda, K. Investigation of the mechanism of hydrogen evolution during photocatalytic water decomposition on metal-loaded semiconductor powders. *J. Phys. Chem.* **1985**, *89*, 1902–5.
- (122) Heller, A. Optically transparent metallic catalysts on semiconductors. *Pure Appl. Chem.* **1986**, *58*, 1189–92.
- (123) Heller, A. Metallic catalysts on semiconductors: Transparency and electrical contact properties. *Nato Asi Ser. Ser. C* **1986**, *15*.

- (124) Domen, K.; Sakata, Y.; Kudo, A.; Maruya, K.; Onishi, T. The photocatalytic activity of a platinumized titanium dioxide catalyst supported over silica. *Bull. Chem. Soc. Jpn.* **1988**, *61*, 359–62.
- (125) Anpo, M.; Chiba, K.; Tomonari, M.; Coluccia, S.; Che, M.; Fox, M. A. Photocatalysis on native and platinum-loaded TiO<sub>2</sub> and ZnO catalysts. Origin of different reactivities on wet and dry metal oxides. *Bull. Chem. Soc. Jpn.* **1991**, *64*, 543–51.
- (126) Kraeutler, B.; Bard, A. J. Heterogeneous photocatalytic preparation of supported catalysts. Photodeposition of platinum on TiO<sub>2</sub> powder and other substrates. *J. Am. Chem. Soc.* **1978**, *100*, 4317–8.
- (127) Heller, A.; Aharon, S. E.; Bonner, W. A.; Miller, B. Hydrogen-evolving semiconductor photocathodes. Nature of the junction and function of the platinum group metal catalyst. *J. Am. Chem. Soc.* **1982**, *104*, 6942–8.
- (128) Aspnes, D. E.; Heller, A. Photoelectrochemical hydrogen evolution and water-photolyzing semiconductor suspensions: Properties of platinum group metal catalyst-semiconductor contacts in air and in hydrogen. *J. Phys. Chem.* **1983**, *87*, 4919–29.
- (129) Borgarello, E.; Harris, R.; Serpone, N. Photochemical deposition and photorecovery of gold using semiconductor dispersions. A practical application of photocatalysis. *Nouv. J. Chim.* **1985**, *9*, 743–7.
- (130) Mills, A.; Williams, G. Photosensitized oxidation of water by CdS-based suspensions. *J. Chem. Soc. Faraday Trans. 1* **1989**, *85*, 503–19.
- (131) Amouyal, E.; Koffi, P. Photochemical production of hydrogen from water. *J. Photochem.* **1985**, *29*, 227–42.
- (132) Nosaka, Y.; Norimatsu, K.; Miyama, H. The function of metals in metal-compounded semiconductor photocatalysts. *Chem. Phys. Lett.* **1984**, *106*, 128–31.
- (133) Wang, C. M.; Heller, A.; Gerischer, H. Palladium catalysis of O<sub>2</sub> reduction by electrons accumulated on TiO<sub>2</sub> particles during photoassisted oxidation of organic compounds. *J. Am. Chem. Soc.* **1992**, *114*, 5230–4.
- (134) Henglein, A. Photochemical properties of small metal particles in solution: “Microelectrode” reactions, chemisorption, composite metal particles, and the atom-to-metal transition. *J. Phys. Chem.* **1993**, *97*, 5457–71.
- (135) Kamat, P. V. Photochemistry on nonreactive and reactive (semiconductor) surfaces. *Chem. Rev.* **1993**, *93*, 267–300.
- (136) Mulvaney, P. Spectroscopy of metal colloids. Some comparisons with semiconductor colloids. In *Semiconductor Nanoclusters - Physical, Chemical and Catalytic Aspects*; Kamat, P. V., Meisel, D., Eds.; Elsevier Science: Amsterdam, 1997; pp 99–123.
- (137) Kamat, P. V.; Flumiani, M.; Dawson, A. Metal-metal and metal-semiconductor composite nanoclusters. *Colloids Surf. A* **2002**, *202*, 269–279.
- (138) Martin, S. C.; Morrison, C. L.; Hoffmann, M. R. Photochemical mechanism of size-quantized vanadium-doped TiO<sub>2</sub> particles. *J. Phys. Chem.* **1994**, *98*, 13695–13704.
- (139) Choi, W.; Termin, A.; Hoffmann, M. R. The role of metal ion dopants in quantum-sized TiO<sub>2</sub>: Correlation between photoreactivity and charge carrier recombination dynamics. *J. Phys. Chem.* **1994**, *98*, 13669–13679.
- (140) Zang, L.; Macyk, W.; Lange, C.; Maier, W. F.; Antonius, C.; Meissner, D.; Kisch, H. Visible-Light Detoxification and Charge Generation by Transition Metal Chloride Modified Titania. *Chem. Eur. J.* **2000**, *6*, 379–384.
- (141) Kato, H.; Kudo, A. Visible-light-response and photocatalytic activities of TiO<sub>2</sub> and SrTiO<sub>3</sub> photocatalysts codoped with antimony and chromium. *J. Phys. Chem. B* **2002**, *106*, 5029–5034.
- (142) Morikawa, T.; Asahi, R.; Ohwaki, T.; Aoki, K.; Taga, Y. Band-gap narrowing of titanium dioxide by nitrogen doping. *Jpn. J. Appl. Phys. Part 2-Lett.* **2001**, *40*, L561–L563.
- (143) Ihara, T.; Miyoshi, M.; Iriyama, Y.; Matsumoto, O.; Sugihara, S. Visible-light-active titanium oxide photocatalyst realized by an oxygen-deficient structure and by nitrogen doping. *Appl. Catal. B-Environ.* **2003**, *42*, 403–409.
- (144) Chiaramonte, T.; Cardoso, L. P.; Gelamo, R. V.; Fabreguette, F.; Sacilotti, M.; de Lucas, M. C. M.; Imhoff, L.; Bourgeois, S.; Kihn, Y.; Casanove, M. J. Structural characterization of TiO<sub>2</sub>/TiN<sub>x</sub>O<sub>y</sub> (delta-doping) heterostructures on (110)TiO= substrates. *Appl. Surf. Sci.* **2003**, *212*, 661–666.
- (145) Burda, C.; Lou, Y. B.; Chen, X. B.; Samia, A. C. S.; Stout, J.; Gole, J. L. Enhanced nitrogen doping in TiO<sub>2</sub> nanoparticles. *Nano Lett.* **2003**, *3*, 1049–1051.
- (146) Wang, H.; Lewis, J. P. Second-generation photocatalytic materials: anion-doped TiO<sub>2</sub>. *J. Phys.-C* **2006**, *18*, 421–434.
- (147) Batzill, M.; Morales, E. H.; Diebold, U. Influence of nitrogen doping on the defect formation and surface properties of TiO<sub>2</sub> rutile and anatase. *Phys. Rev. Lett.* **2006**, *96*.
- (148) Ghicov, A.; Macak, J. M.; Tsuchiya, H.; Kunze, J.; Haeublein, V.; Frey, L.; Schmuki, P. Ion implantation and annealing for an efficient N-doping of TiO<sub>2</sub> nanotubes. *Nano Lett.* **2006**, *6*, 1080–1082.
- (149) Sakthivel, S.; Janczarek, M.; Kisch, H. Visible light activity and photoelectrochemical properties of nitrogen-doped TiO<sub>2</sub>. *J. Phys. Chem. B* **2004**, *108*, 19384–19387.
- (150) Thompson, T. L.; Yates, J. T. TiO<sub>2</sub>-based photocatalysis: Surface defects, oxygen and charge transfer. *Top. Catal.* **2005**, *35*, 197–210.
- (151) Park, J. H.; Kim, S.; Bard, A. J. Novel carbon-doped TiO<sub>2</sub> nanotube arrays with high aspect ratios for efficient solar water splitting. *Nano Lett.* **2006**, *6*, 24–28.
- (152) Maeda, K.; Takata, T.; Hara, M.; Saito, N.; Inoue, Y.; Kobayashi, H.; Domen, K. GaN:ZnO solid solution as a photocatalyst for visible-light-driven overall water splitting. *J. Am. Chem. Soc.* **2005**, *127*, 8286–8287.
- (153) Teramura, K.; Maeda, K.; Saito, T.; Takata, T.; Saito, N.; Inoue, Y.; Domen, K. Characterization of ruthenium oxide nanocluster as a cocatalyst with (Ga<sub>1-x</sub>Zn<sub>x</sub>)(N<sub>1-x</sub>O<sub>x</sub>) for photocatalytic overall water splitting. *J. Phys. Chem. B* **2005**, *109*, 21915–21921.
- (154) Kitano, M.; Takeuchi, M.; Matsuoka, M.; Thomas, J. M.; Anpo, M. Preparation of Visible Light-Responsive TiO<sub>2</sub> Thin Film Photocatalysts by an RF Magnetron Sputtering Deposition Method and Their Photocatalytic Reactivity. *Chem. Lett.* **2005**, *34*, 616–617.
- (155) Kikuchi, H.; Kitano, M.; Takeuchi, M.; Matsuoka, M.; Anpo, M.; Kamat, P. V. Extending the Photoresponse of TiO<sub>2</sub> to the Visible Light Region: Photoelectrochemical Behavior of TiO<sub>2</sub> Thin Films Prepared by RF-Magnetron Sputtering Deposition Method. *J. Phys. Chem. B* **2006**, *110*, 5537–5541.
- (156) Maeda, K.; Teramura, K.; Lu, D.; Takata, T.; Saito, N.; Inoue, Y.; Domen, K. Photocatalyst releasing hydrogen from water. *Nature* **2006**, *295*.
- (157) Nakato, Y.; Tsubomura, H. Structures and functions of thin metal layers on semiconductor electrodes. *J. Photochem.* **1985**, *29*, 257–66.
- (158) Nakato, Y.; Ueda, K.; Yano, H.; Tsubomura, H. Effect of microscopic discontinuity of metal overlayers on the photovoltages in metal-coated semiconductor-liquid junction photoelectrochemical cells for efficient solar energy conversion. *J. Phys. Chem.* **1988**, *92*, 2316–2324.
- (159) Nakato, Y.; Tsubomura, H. The photoelectrochemical behavior of an n-TiO<sub>2</sub> electrode coated with a thin metal film, as revealed by measurements of the potential of the metal film. *Isr. J. Chem.* **1982**, *22*, 180–3.
- (160) Nakato, Y.; Shioji, M.; Tsubomura, H. Photoeffects on the potentials of thin metal films on a n-TiO<sub>2</sub> crystal wafer. The mechanism of semiconductor photocatalysts. *Chem. Phys. Lett.* **1982**, *90*, 453–6.
- (161) de Tacconi, N. R.; Carmona, J.; Rajeshwar, K. Chemically modified Ni/TiO<sub>2</sub> nanocomposite films. Charge transfer from photoexcited TiO<sub>2</sub> particles to hexacyanoferrate redox centers within the film and unusual photoelectrochemical behavior. *J. Phys. Chem. B* **1997**, *101*, 10151–4.
- (162) Chandrasekharan, N.; Kamat, P. V. Improving the Photoelectrochemical Performance of Nanostructured TiO<sub>2</sub> Films by Adsorption of Gold Nanoparticles. *J. Phys. Chem. B* **2000**, *104*, 10851–10857.
- (163) Subramanian, V.; Wolf, E.; Kamat, P. V. Semiconductor-Metal Composite Nanostructures. To What Extent Metal Nanoparticles (Au, Pt, Ir) Improve the Photocatalytic Activity of TiO<sub>2</sub> Films? *J. Phys. Chem. B* **2001**, *105*, 11439–11446.
- (164) Chen, M. S.; Goodman, D. W. The structure of catalytically active gold on titania. *Science* **2004**, *306*, 252–255.
- (165) Hiesgen, R.; Meissner, D. Nanoscale photocurrent variations at metal-modified semiconductor surfaces. *J. Phys. Chem. B* **1998**, *102*, 6549–6557.
- (166) Subramanian, V.; Kamat, P. V.; Wolf, E. E. Mass-Transfer and Kinetic Studies during the Photocatalytic Degradation of an Azo Dye on Optically Transparent Electrode Thin Film. *Ind. Eng. Chem. Res.* **2003**, *42*, 2131–2138.
- (167) Lahiri, D.; Subramanian, V.; Bunker, B. A.; Kamat, P. V. Probing photochemical transformations at TiO<sub>2</sub>/Pt and TiO<sub>2</sub>/Ir interfaces using x-ray absorption spectroscopy. *J. Chem. Phys.* **2006**, *124*, 204720.
- (168) Dawson, A.; Kamat, P. V. Semiconductor-metal nanocomposites. Photoinduced fusion and photocatalysis of gold-capped TiO<sub>2</sub> (TiO<sub>2</sub>/Au) nanoparticles. *J. Phys. Chem. B* **2001**, *105*, 960–966.
- (169) Subramanian, V.; Wolf, E. E.; Kamat, P. V. Influence of Metal/Ion Concentration on the Photocatalytic Activity of TiO<sub>2</sub>-Au Composite Nanoparticles. *Langmuir* **2003**, *19*, 469–474.
- (170) Cozzoli, P. D.; Comparelli, R.; Fanizza, E.; Curri, M. L.; Agostiano, A.; Laub, D. Photocatalytic synthesis of silver nanoparticles stabilized by TiO<sub>2</sub> nanorods: A semiconductor/metal nanocomposite in homogeneous nonpolar solution. *J. Am. Chem. Soc.* **2004**, *126*, 3868–3879.
- (171) Cozzoli, P. D.; Fanizza, E.; Comparelli, R.; Curri, M. L.; Agostiano, A.; Laub, D. Role of metal nanoparticles in TiO<sub>2</sub>/Ag nanocomposite-based microheterogeneous photocatalysis. *J. Phys. Chem. B* **2004**, *108*, 9623–9630.
- (172) Chen, S.; Ingram, R. S.; Hostetler, M. J.; Pietron, J. J.; Murray, R. W.; Schaaff, T. G.; Khoury, J. T.; Alvarez, M. M.; Whetten, R. L. Gold Nanoelectrodes of Varied Size: Transition to Molecule-Like Charging. *Science* **1998**, *280*, 2098–2101.
- (173) Hicks, J. F.; Templeton, A. C.; Chen, S.; Sheran, K. M.; Jasti, R.; Murray, R. W.; Debord, J.; Schaaff, T. G.; Whetten, R. L. The Monolayer

Thickness Dependence of Quantized Double-Layer Capacitances of Monolayer-Protected Gold Clusters. *Anal. Chem.* **1999**, *71*, 3703–3711.

(174) Hostetler, M. J.; Green, S. J.; Stokes, J. J.; Murray, R. W. Monolayers in Three Dimensions: Synthesis and Electrochemistry of -Functionalized Alkanethiolate-Stabilized Gold Cluster Compounds. *J. Am. Chem. Soc.* **1999**, *118*, 4212–4213.

(175) Wood, A.; Giersig, M.; Mulvaney, P. Fermi Level Equilibration in Quantum Dot-Metal Nanojunctions. *J. Phys. Chem. B* **2001**, *105*, 8810–8815.

(176) Ung, T.; Dunstan, D.; Giersig, M.; Mulvaney, P. Spectroelectrochemistry of colloidal silver. *Langmuir* **1997**, *13*, 1773–1782.

(177) Henglein, A.; Holzwarth, A.; Mulvaney, P. Fermi level equilibration between colloidal lead and silver particles in aqueous solution. *J. Phys. Chem.* **1992**, *96*, 8700–2.

(178) Kamat, P. V. Photoinduced Transformations in Semiconductor-Metal Nanocomposite Assemblies. *Pure Appl. Chem.* **2002**, *74*, 1693–1706.

(179) Subramanian, V.; Wolf, E. E.; Kamat, P. V. Green Emission to Probe Photoinduced Charging Events in ZnO-Au Nanoparticles. Charge Distribution and Fermi-Level Equilibration. *J. Phys. Chem. B* **2003**, *107*, 7479–7485.

(180) Subramanian, V.; Wolf, E. E.; Kamat, P. V. Catalysis with TiO<sub>2</sub>/Au Nanocomposites. Effect of Metal Particle Size on the Fermi Level Equilibration. *J. Am. Chem. Soc.* **2004**, *126*, 4943–4950.

(181) Bamwenda, G. R.; Tsubota, S.; Kobayashi, T.; Haruta, M. Photoinduced hydrogen production from an aqueous solution of ethylene glycol over ultrafine gold supported on TiO<sub>2</sub>. *J. Photochem. Photobiol. A* **1994**, *77*, 59–67.

(182) Haruta, M. Size- and support-dependency in the catalysis of gold. *Catal. Today* **1997**, *36*, 153–166.

(183) Valden, M.; Lai, X.; Goodman, D. W. Onset of catalytic activity of gold clusters on titania with the appearance of nonmetallic properties. *Science* **1998**, *281*, 1647–1650.

(184) Yang, Z. X.; Wu, R. Q.; Goodman, D. W. Structural and electronic properties of Au on TiO<sub>2</sub>(110). *Phys. Rev. B* **2000**, *6*, 14066–14071.

(185) Li, J.; Yamada, Y.; Murakoshi, K.; Nakato, Y. Sustainable metal nano-contacts showing quantized conductance prepared at a gap of thin metal wires in solution. *Chem. Commun.* **2001**, 2170–2171.

(186) Kamat, P. V.; Bedja, I.; Hotchandani, S. Photoinduced charge transfer between carbon and semiconductor clusters. One-electron reduction of C<sub>60</sub> in colloidal TiO<sub>2</sub> Semiconductor suspensions. *J. Phys. Chem.* **1994**, *98*, 9137–9142.

(187) Kalyanasundaram, K.; Grätzel, M.; Pelizzetti, E. Interfacial electron transfer in colloidal metal and semiconductor dispersions and photodecomposition of water. *Coord. Chem. Rev.* **1986**, *69*, 57–125.

(188) Liz-Marzan, L. M.; Mulvaney, P. The assembly of coated nanocrystal. *J. Phys. Chem. B* **2003**, *107*, 7312–7326.

(189) Caruso, F.; Spasova, M.; Saigueirino-Maceira, V.; Liz-Marzan, L. M. Multilayer assemblies of silica-encapsulated gold nanoparticles on decomposable colloid templates. *Adv. Mater.* **2001**, *13*, 1090.

(190) Ung, T.; Liz-Marzan, L. M.; Mulvaney, P. Controlled method for silica coating of silver colloids. Influence of coating on the rate of chemical reactions. *Langmuir* **1998**, *14*, 3740–3748.

(191) Zhong, C. J.; Maye, M. M. Core-Shell Assembled Nanoparticles as Catalysts. *Adv. Mater.* **2001**, *13*, 1507–1511.

(192) Hardikar, V.; Matijevic, E. Coating of nanosize silver particles with silica. *J. Colloid Interface Sci.* **2000**, *221*, 133–136.

(193) Oldenburg, S. J.; Averitt, R. D.; Westcott, S. L.; Halas, N. J. Nanoengineering of optical resonances. *Chem. Phys. Lett.* **1998**, *288*, 243–47.

(194) Oldfield, G.; Ung, T.; Mulvaney, P. Au@SnO<sub>2</sub> core-shell nanocapacitors. *Adv. Mater.* **2000**, *12*, 1519–1522.

(195) Mulvaney, P.; Liz-Marzan, L. M.; Giersig, M.; Ung, T. Silica encapsulation of quantum dots and metal clusters. *J. Mater. Chem.* **2000**, *10*, 1259–1270.

(196) Hirakawa, T.; Kamat, P. V. Electron Storage and Surface Plasmon Modulation in Ag@TiO<sub>2</sub> Clusters. *Langmuir* **2004**, *20*, 5645–5647.

(197) Hirakawa, T.; Kamat, P. V. Charge Separation and Catalytic Activity of Ag@TiO<sub>2</sub> Core-Shell Composite Clusters under UV-Irradiation. *J. Am. Chem. Soc.* **2005**, *127*, 3928–3934.

(198) Shanghavi, B.; Kamat, P. V. Interparticle electron transfer in metal/semiconductor composites. Picosecond dynamics of CdS capped gold nanoclusters. *J. Phys. Chem. B* **1997**, *101*, 7675–7679.

(199) Vogel, R.; Pohl, K.; Weller, H. Sensitization of highly porous, polycrystalline TiO<sub>2</sub> electrodes by quantum sized CdS. *Chem. Phys. Lett.* **1990**, *174*, 241–6.

(200) Kohtani, S.; Kudo, A.; Sakata, T. Spectral sensitization of a TiO<sub>2</sub> semiconductor electrode by CdS microcrystals and its photoelectrochemical properties. *Chem. Phys. Lett.* **1993**, *206*, 166–70.

(201) Plass, R.; Pelet, S.; Krueger, J.; Grätzel, M.; Bach, U. Quantum dot sensitization of organic-inorganic hybrid solar cells. *J. Phys. Chem. B* **2002**, *106*, 7578–7580.

(202) Peter, L. M.; Wijayantha, K. G. U.; Riley, D. J.; Waggett, J. P. Band-edge tuning in self-assembled layers of Bi<sub>2</sub>S<sub>3</sub> nanoparticles used to photosensitize nanocrystalline TiO<sub>2</sub>. *J. Phys. Chem. B* **2003**, *107*, 8378–8381.

(203) Liu, D.; Kamat, P. V. Photoelectrochemical behavior of thin CdSe and coupled TiO<sub>2</sub>/CdSe semiconductor films. *J. Phys. Chem.* **1993**, *97*, 10769–73.

(204) Gopidas, K. R.; Bohorquez, M.; Kamat, P. V. Photoelectrochemistry in semiconductor particulate systems. 16. Photophysical and photochemical aspects of coupled semiconductors. Charge-transfer processes in colloidal CdS-TiO<sub>2</sub> and CdS-AgI systems. *J. Phys. Chem.* **1990**, *94*, 6435–40.

(205) Bedja, I.; Kamat, P. V. Capped semiconductor colloids. Synthesis and Photoelectrochemical properties of TiO<sub>2</sub> capped SnO<sub>2</sub> surfaces. *J. Phys. Chem.* **1995**, *99*, 9182–9188.

(206) Vinodgopal, K.; Bedja, I.; Kamat, P. V. Nanostructured semiconductor films for photocatalysis. Photoelectrochemical behavior of SnO<sub>2</sub>/TiO<sub>2</sub> coupled systems and its role in photocatalytic degradation of a textile azo dye. *Chem. Mater.* **1996**, *8*, 2180–2187.

(207) Sant, P. A.; Kamat, P. V. Inter-Particle Electron Transfer between Size-Quantized CdS and TiO<sub>2</sub> Semiconductor Nanoclusters. *Phys. Chem. Chem. Phys.* **2002**, *4*, 198–203.

(208) Spanhel, L.; Henglein, A.; Weller, H. Photochemistry of colloidal semiconductors. 24. Interparticle electron transfer in Cd<sub>3</sub>P<sub>2</sub>-TiO<sub>2</sub> and Cd<sub>3</sub>P<sub>2</sub>-ZnO sandwich structures. *Ber. Bunsen-Ges. Phys. Chem.* **1987**, *91*, 1359–63.

(209) Dabbousi, B. O.; Rodriguez-Viejo, J.; Mikulec, F. V.; Heine, J. R.; Mattoussi, H.; Ober, R.; Jensen, K. F.; Bawendi, M. G. (CdSe)ZnS core-shell quantum dots: Synthesis and characterization of a size series of highly luminescent nanocrystallites. *J. Phys. Chem. B* **1997**, *101*, 9463–9475.

(210) Tian, Y.; Newton, T.; Kotov, N. A.; Guldi, D. M.; Fendler, J. H. Coupled Composite CdS-CdSe and Core-Shell Types of (CdS)CdSe and (CdSe)CdS Nanoparticles. *J. Phys. Chem.* **1996**, *100*, 8927–8939.

(211) Mews, A.; Kadavanich, A. V.; Banin, U.; Alivisatos, A. P. Structural and spectroscopic characterization of the CdS/HgS/CdS quantum dot quantum wells. *Phys. Rev. B* **1996**, *53*, 13242–13245.

(212) Micic, O. I.; Smith, B. B.; Nozik, A. J. Core-Shell Quantum Dots of Lattice-Matched ZnCdSe<sub>2</sub> Shells on InP Cores: Experiment and Theory. *J. Phys. Chem. B* **2000**, *104*, 12149–12156.

(213) Kamat, P. V. Composite Semiconductor Nanoclusters. In *Semiconductor Nanoclusters - Physical, Chemical and Catalytic Aspects*; Kamat, P. V., Meisel, D., Eds.; Elsevier Science: Amsterdam, 1997; pp 237–259.

(214) Rajeshwar, K.; de Tacconi, N. R.; Chenthamarakshan, C. R. Semiconductor-Based Composite Materials: Preparation, Properties, and Performance. *Chem. Mater.* **2001**, *13*, 2765–2782.

(215) Robel, I.; Subramanian, V.; Kuno, M.; Kamat, P. V. Quantum Dot Solar Cells. Harvesting Light Energy with CdSe Nanocrystals Molecularly Linked to Mesoscopic TiO<sub>2</sub> Films. *J. Am. Chem. Soc.* **2006**, *128*, 2385–2393.

(216) Liu, D.; Kamat, P. V. Electrochemical rectification in CdSe + TiO<sub>2</sub> coupled semiconductor films. *J. Electroanal. Chem. Interfacial Electrochem* **1993**, *347*, 451–6.

(217) Nasr, C.; Kamat, P. V.; Hotchandani, S. Photoelectrochemical behavior of coupled SnO<sub>2</sub>/CdSe nanocrystalline semiconductor films. *J. Electroanal. Chem.* **1997**, *420*, 201–207.

(218) Peng, P.; Milliron, D. J.; Hughes, S. M.; Johnson, J. C.; Alivisatos, A. P.; Saykally, R. J. Femtosecond spectroscopy of carrier relaxation dynamics in type II CdSe/CdTe tetrapod heterostructures. *Nano Lett.* **2005**, *5*, 1809–1813.

(219) Kamat, P. V.; Barazzouk, S.; Hotchandani, S. Nanostructured Fullerene Films. *Adv. Mater.* **2001**, *13*, 1614–1617.

(220) Hasobe, T.; Imahori, H.; Fukuzumi, S.; Kamat, P. V. Light Energy Harvesting Using Mixed Molecular Nanoclusters. Porphyrin and C<sub>60</sub> Cluster Films for Efficient Photocurrent Generation. *J. Phys. Chem. B* **2003**, *107*, 12105–12112.

(221) Hasobe, T.; Imahori, H.; Kamat, P. V.; Fukuzumi, S. Photovoltaic Cells using composite nanoclusters of porphyrins and fullerenes with gold nanoparticles. *J. Am. Chem. Soc.* **2005**, *127*, 1216–1228.

(222) Hasobe, T.; Kamat, P. V.; Absalom, M. A.; Kashiwagi, Y.; Sly, J.; Crossley, M. J.; Hosomizu, K.; Imahori, H.; Fukuzumi, S. Supramolecular Photovoltaic Cells Based on Composite Molecular Nanoclusters: Dendritic Porphyrin and C<sub>60</sub>, Porphyrin Dimer and C<sub>60</sub>, and Porphyrin-C<sub>60</sub> Dyad. *J. Phys. Chem. B* **2004**, *108*, 12865–12872.

(223) George Thomas, K.; Biju, V.; George, M. V.; Guldi, D. M.; Kamat, P. V. Photoinduced Charge Separation and Stabilization in Clusters of a Fullerene-Aniline Dyad. *J. Phys. Chem. B* **1999**, *103*, 8864–8869.

(224) Nath, S.; Pal, H.; Palit, D. K.; Sapre, A. V.; Mittal, J. P. Aggregation of fullerene, C-60, in benzonitrile. *J. Phys. Chem. B* **1998**, *102*, 10158–10164.

(225) Kamat, P. V.; Barazzouk, S.; Hotchandani, S.; George Thomas, K. Nanostructured Thin Films of C<sub>60</sub>-Aniline Dyad Clusters. Electrodepo-

- tion. Charge Separation and Photoelectrochemistry. *Chem. Euro. J.* **2000**, *6*, 3914–3921.
- (226) Hasobe, T.; Imahori, H.; Fukuzumi, S.; Kamat, P. V. Quaternary Self-Organization of Porphyrin and Fullerene Units by Clusterization with Gold Nanoparticles on SnO<sub>2</sub> Electrodes for Organic Solar Cells. *J. Am. Chem. Soc.* **2003**, *125*, 14962–14963.
- (227) Hasobe, T.; Imahori, H.; Fukuzumi, S.; Kamat, P. V. Nanostructured assembly of porphyrin clusters for light energy conversion. *J. Mater. Chem.* **2003**, *13*, 2515–2520.
- (228) Solladié, N.; Hamel, A.; Gross, M. *Tetrahedron Lett.* **2000**, *41*, 6075.
- (229) Hasobe, T.; Kamat, P. V.; Troiani, V.; Solladié, N.; Ahn, T. K.; Kim, S. K.; Kim, D.; Kongkanand, A.; Kuwabata, S.; Fukuzumi, S. Enhancement of Light-Energy Conversion Efficiency by Multi-Porphyrin Arrays of Porphyrin-Peptide Oligomers with Fullerene Clusters. *J. Phys. Chem. B* **2005**, *109*, 19–23.
- (230) Kamat, P. V.; Fox, M. A. Dye loaded polymer electrodes. III. Generation of photogalvanic effects at n-SnO<sub>2</sub> electrodes coated with poly-(4-vinyl pyridine) films containing rose bengal. *J. Electrochem. Soc.* **1984**, *131*, 1032–7.
- (231) Albery, W. J. Development of photogalvanic cells for solar energy conversion. *Acc. Chem. Res.* **1982**, *15*, 142–8.
- (232) Albery, W. J.; Archer, M. D. Optimum efficiency of photogalvanic cells for solar energy conversion. *Nature* **1977**, *270*, 399–402.
- (233) Wildes, P. D.; Lichtin, N. N. Correlation of Open-Circuit Voltage and Short-Circuit Current of Totally Illuminated, Thin-Layer Iron-Thionine Photogalvanic Cell with Photostationary Composition. *J. Am. Chem. Soc.* **1978**, *100*, 6568–6572.
- (234) Nazeeruddin, M. K.; Kay, A.; Rodicio, I.; Humphry, B. R.; Mueller, E.; Liska, P.; Vlachopoulos, N.; Grätzel, M. Conversion of light to electricity by cis-X<sub>2</sub>bis(2,2'-bipyridyl-4,4'-dicarboxylate)ruthenium(II) charge-transfer sensitizers (X = Cl<sup>-</sup>, Br<sup>-</sup>, I<sup>-</sup>, CN<sup>-</sup>, and SCN<sup>-</sup>) on nanocrystalline TiO<sub>2</sub> electrodes. *J. Am. Chem. Soc.* **1993**, *115*, 6382–90.
- (235) Cahen, D.; Hodes, G.; Grätzel, M.; Guillemoles, J. F.; Riess, I. Nature of photovoltaic action in dye-sensitized solar cells. *J. Phys. Chem. B* **2000**, *104*, 2053–2059.
- (236) Grätzel, M. Photoelectrochemical cells. *Nature* **2001**, *414*, 338.
- (237) Grätzel, M. Nanocrystalline electronic junctions. In *Semiconductor Nanoclusters - Physical, Chemical and Catalytic Aspects*; Kamat, P. V., Meisel, D., Eds.; Elsevier Science: Amsterdam, 1997; pp 353–375.
- (238) Sauvé, G.; Cass, M. E.; Doig, S. J.; Lauermann, I.; Pomykal, K. S. L. N. High Quantum Yield Sensitization of Nanocrystalline Titanium Dioxide Photoelectrodes with cis-Dicyanobis(4,4'-dicarboxy-2,2'-bipyridine)osmium(II) or Tris(4,4'-dicarboxy-2,2'-bipyridine)osmium(II) Complexes. *J. Phys. Chem. B* **2000**, *104*, 3488–3491.
- (239) Bignozzi, C. A.; Argazzi, R.; Indelli, T.; Scandola, F. Design of Supramolecular systems for spectral sensitization of semiconductors. *Solar Energy Mater.* **1994**, *32*, 229–244.
- (240) Bedja, I.; Hotchandani, S.; Kamat, P. V. Preparation and characterization of thin SnO<sub>2</sub> nanocrystalline semiconductor films and their sensitization with bis(2,2'-bipyridine)(2,2'-bipyridine-4,4'-dicarboxylic acid)-ruthenium complex. *J. Phys. Chem.* **1994**, *98*, 4133–4140.
- (241) Bedja, I.; Kamat, P. V.; Hua, X.; Lappin, A. G.; Hotchandani, S. Photosensitization of Nanocrystalline ZnO Films by Bis(2,2'-bipyridine)-(2,2'-bipyridine-4,4'-dicarboxylic acid)ruthenium(II). *Langmuir* **1997**, *13*, 2398–2403.
- (242) Fessenden, R. W.; Kamat, P. V. Rate constants for charge injection from excited sensitizer into SnO<sub>2</sub>, ZnO, and TiO<sub>2</sub> semiconductor nanocrystallites. *J. Phys. Chem.* **1995**, *99*, 12902–12906.
- (243) Vinodgopal, K.; Hua, X.; Dahlgren, R. L.; Lappin, A. G.; Patterson, L. K.; Kamat, P. V. Photochemistry of Ru(bpy)<sub>2</sub>(dcbpy)<sup>2+</sup> on Al<sub>2</sub>O<sub>3</sub> and TiO<sub>2</sub> surfaces. An insight into the mechanism of photosensitization. *J. Phys. Chem.* **1995**, *99*, 10883–10889.
- (244) Martini, I.; Hodak, J.; Hartland, G.; Kamat, P. V. Ultrafast study of interfacial electron transfer between 9-anthracene-carboxylate and TiO<sub>2</sub> semiconductor particles. *J. Chem. Phys.* **1997**, *107*, 8064–8072.
- (245) Khazraji, A. C.; Hotchandani, S.; Das, S.; Kamat, P. V. Controlling Dye (Merocyanine-540) Aggregation on nanostructured TiO<sub>2</sub> Films. An Organized Assembly Approach for Enhancing the Efficiency of Photosensitization. *J. Phys. Chem. B* **1999**, *103*, 4693–4700.
- (246) Nasr, C.; Hotchandani, S.; Kamat, P. V. Role of Iodide in Photoelectrochemical Solar Cells. Electron Transfer between Iodide Ions and Ruthenium Polypyridyl Complex Anchored on Nanocrystalline SiO<sub>2</sub> and SnO<sub>2</sub> Films. *J. Phys. Chem. B* **1998**, *102*, 4944–4951.
- (247) Kamat, P. V.; Hara, M.; Hotchandani, S. C<sub>60</sub> Cluster as an Electron Shuttle in a Ru(II)-Polypyridyl Sensitizer Based Photochemical Solar Cell. *J. Phys. Chem. B* **2004**, *108*, 5166–5170.
- (248) Kamat, P. V.; Bedja, I.; Hotchandani, S.; Patterson, L. K. Photosensitization of nanocrystalline semiconductor films. Modulation of electron transfer between excited ruthenium complex and SnO<sub>2</sub> nanocrystallites with an externally applied bias. *J. Phys. Chem.* **1996**, *100*, 4900–4908.
- (249) Tachibana, Y.; Haque, S. A.; Mercer, I. P.; Moser, J. E.; Klug, D. R.; Durrant, J. R. Modulation of the Rate of Electron Injection in Dye-Sensitized Nanocrystalline TiO<sub>2</sub> Films by Externally Applied Bias. *J. Phys. Chem. B* **2001**, *105*, 7424–7431.
- (250) Sauvé, G.; Cass, M. E.; Coia, G.; Doig, S. J.; Lauermann, I.; Pomykal, K. E.; Lewis, N. S. Dye Sensitization of Nanocrystalline Titanium Dioxide with Osmium and Ruthenium Polypyridyl Complexes. *J. Phys. Chem. B* **2000**, *104*, 6821–6836.
- (251) Kamat, P. V.; Chauvet, J. P.; Fessenden, R. W. Photoelectrochemistry in particulate systems. 4. Photosensitization of a TiO<sub>2</sub> semiconductor with a chlorophyll analogue. *J. Phys. Chem.* **1986**, *90*, 1389–94.
- (252) Bedja, I.; Kamat, P. V.; Hotchandani, S. Fluorescence and photoelectrochemical behavior of chlorophyll a adsorbed on a nanocrystalline SnO<sub>2</sub> film. *J. Appl. Phys.* **1996**, *80*, 4637–4643.
- (253) Bedja, I.; Hotchandani, S.; Carpentier, R.; Fessenden, R. W.; Kamat, P. V. Chlorophyll b modified nanocrystalline SnO<sub>2</sub> semiconductor thin film as a photosensitive electrode. *J. Appl. Phys.* **1994**, *75*, 5444–5456.
- (254) Hotchandani, S.; Kamat, P. V. Modification of electrode surface with semiconductor colloids and its sensitization with chlorophyll a. *Chem. Phys. Lett.* **1992**, *191*, 320–6.
- (255) Hotchandani, S.; Das, S.; George Thomas, K.; George, M. V.; Kamat, P. V. Interaction of semiconductor colloids with J-aggregates of squaraine dye and its role in sensitizing nanocrystalline semiconductor films. *Res. Chem. Intermed.* **1994**, *20*, 927–938.
- (256) Kim, Y.-S.; Liang, K.; Law, K.-Y.; Whitten, D. G. An investigation of photocurrent generation by squaraine aggregates in monolayer-modified SnO<sub>2</sub> electrodes. *J. Phys. Chem.* **1994**, *98*, 984–988.
- (257) Nasr, C.; Liu, D.; Hotchandani, S.; Kamat, P. V. Dye capped semiconductor colloids. Excited state and photosensitization aspects of Rhodamine 6G-H aggregates electrostatically bound to SiO<sub>2</sub> and SnO<sub>2</sub> Colloids. *J. Phys. Chem.* **1996**, *100*, 11054–11061.
- (258) Liu, D.; Kamat, P. V. Electrochemically active nanocrystalline SnO<sub>2</sub> films. Surface modification with thiazine and oxazine dye aggregates. *J. Electrochem. Soc.* **1995**, *142*, 835–839.
- (259) Sykora, M.; Petruska, M. A.; Alstrum-Acevedo, J.; Bezel, I.; Meyer, T. J.; Klimov, V. I. Photoinduced Charge Transfer between CdSe Nanocrystal Quantum Dots and Ru-Polypyridine Complexes. *J. Am. Chem. Soc.* **2006**, *128*, 9984–9985.
- (260) Rehm, J. M.; McLendon, G. L.; Nagasawa, Y.; Yoshihara, K.; Moser, J.; Grätzel, M. Femtosecond Electron-Transfer Dynamics at a Sensitizing Dye-Semiconductor (TiO<sub>2</sub>) Interface. *J. Phys. Chem.* **1996**, *100*, 9577–9578.
- (261) Burfeindt, B.; Hannappel, T.; Storck, W.; Willig, F. Measurement of Temperature-Independent Femtosecond Interfacial Electron Transfer from an Anchored Molecular Electron Donor to a Semiconductor as Acceptor. *J. Phys. Chem.* **1996**, *100*, 16463–16465.
- (262) Martini, I.; Hartland, G.; Kamat, P. V. Ultrafast Investigation of the Photophysics of Cresyl Violet adsorbed onto Nanometer Sized Particles of SnO<sub>2</sub> and SiO<sub>2</sub>. *J. Phys. Chem. B* **1997**, *101*, 4826–4830.
- (263) Tachibana, Y.; Moser, J. E.; Grätzel, M.; Klug, D. R.; Durrant, J. R. Subpicosecond interfacial charge separation in dye-sensitized nanocrystalline titanium dioxide films. *J. Phys. Chem.* **1996**, *100*, 20056–20062.
- (264) Hannappel, T.; Burfeindt, B.; Storck, W.; Willig, F. Measurement of ultrafast photoinduced electron transfer from chemically anchored Ru-dye molecules into empty electronic states in a colloidal anatase TiO<sub>2</sub> film. *J. Phys. Chem. B* **1997**, *101*, 6799–6802.
- (265) Randy, J.; Ellingson, R. J.; Asbury, J. B.; Ferrere, S.; Ghosh, H. N.; Sprague, J. R.; Lian, T.; Nozik, A. J. Dynamics of Electron Injection in Nanocrystalline Titanium Dioxide Films Sensitized with [Ru(4,4'-dicarboxy-2,2'-bipyridine)<sub>2</sub>(NCS)<sub>2</sub>] by Infrared Transient Absorption. *J. Phys. Chem. B* **1998**, *102*, 6455–6458.
- (266) Asbury, J. B.; Wang, Y. Q.; Lian, T. Multiple-Exponential Electron Injection in Ru(dcbpy)<sub>2</sub>(SCN)<sub>2</sub> Sensitized ZnO Nanocrystalline Thin Films. *J. Phys. Chem. B* **1999**, *103*, 6643–6647.
- (267) Asbury, J. B.; Randy, J.; Ellingson, R. J.; Ghosh, H. N.; Ferrere, S.; Nozik, A. J.; Lian, T. Femtosecond IR Study of Excited-State Relaxation and Electron-Injection Dynamics of Ru(dcbpy)<sub>2</sub>(NCS)<sub>2</sub> in Solution and on Nanocrystalline TiO<sub>2</sub> and Al<sub>2</sub>O<sub>3</sub>. *J. Phys. Chem. B* **1999**, *103*, 3110–3119.
- (268) Asbury, J. B.; Hao, E.; Wang, Y.; Lian, T. Bridge Length-Dependent Ultrafast Electron Transfer from Ru Polypyridyl Complexes to Nanocrystalline TiO<sub>2</sub> Thin Films Studied by Femtosecond Infrared Spectroscopy. *J. Phys. Chem. B* **2000**, *104*, 11957–11964.
- (269) Bauer, C.; Boschloo, G.; Mukhtar, E.; Hagfeldt, A. Electron Injection and Recombination in Ru(dcbpy)<sub>2</sub>(NCS)<sub>2</sub> Sensitized Nanostructured ZnO. *J. Phys. Chem. B* **2001**, *105*, 5585–5588.
- (270) Kallioinen, J.; Benkö, G.; Sundström, V.; Korppi-Tommola, J. E. I.; Yartsev, A. P. Electron transfer from the singlet and triplet excited states of Ru(dcbpy)<sub>2</sub>(NCS)<sub>2</sub> into nanocrystalline TiO<sub>2</sub> thin films. *J. Phys. Chem. B* **2002**, *106*, 4396–4404.
- (271) Furube, A.; Katoh, R.; Hara, K.; Murata, S.; Arakawa, H.; Tachiya, M. Ultrafast Stepwise Electron Injection from Photoexcited Ru-Complex

- into Nanocrystalline ZnO Film via Intermediates at the Surface. *J. Phys. Chem. B* **2003**, *107*, 4162–4166.
- (272) Horiuchi, H.; Katoh, R.; Hara, K.; Yanagida, M.; Murata, S.; Arakawa, H.; Tachiya, M. Electron injection efficiency from excited  $N_3$  into nanocrystalline ZnO films: Effect of ( $N_3$ -Zn $^{2+}$ ) aggregate formation. *J. Phys. Chem. B* **2003**, *107*, 2570–2574.
- (273) Marcus, R. A.; Sutin, N. Electron transfers in chemistry and biology. *Biochim. Biophys. Acta.* **1985**, *811*, 265.
- (274) Marcus, R. A. On theory of electron-transfer reactions .6. Unified treatment for homogeneous and electrode reactions. *J. Chem. Phys.* **1965**, *43*, 679–701.
- (275) Gaal, D. A.; Hupp, J. T. Thermally activated, inverted interfacial electron transfer kinetics: High driving force reactions between tin oxide nanoparticles and electrostatically-bound molecular reactants. *J. Am. Chem. Soc.* **2000**, *122*, 10956–10963.
- (276) Kuciauskas, D.; Freund, M. S.; Gray, H. B.; Winkler, J. R.; Lewis, N. S. Electron Transfer Dynamics in Nanocrystalline Titanium Dioxide Solar Cells Sensitized with Ruthenium or Osmium Polypyridyl Complexes. *J. Phys. Chem. B* **2001**, *105*, 392–403.
- (277) Clifford, J. N.; Palomares, E.; Nazeeruddin, M. K.; Grätzel, M.; Nelson, J.; Li, X.; Long, N. J.; Durrant, J. R. Molecular Control of Recombination Dynamics in Dye-Sensitized Nanocrystalline TiO $_2$  Films: Free Energy vs Distance Dependence. *J. Am. Chem. Soc.* **2004**, *126*, 5225–5233.
- (278) Smestad, G.; Bignozzi, C.; Argazzi, R. A. Testing of dye sensitized TiO $_2$  solar cells I: Experimental photocurrent output and conversion efficiencies. *Solar Energy Mater.* **1994**, *32*, 259–272.
- (279) Smestad, G. Testing of dye sensitized TiO $_2$  solar cells I: Theoretical voltage output and photoluminescence efficiencies. *Solar Energy Mater.* **1994**, *32*, 273–288.
- (280) Imai, H.; Takei, Y.; Shimizu, K.; Matsuda, M.; Hirashima, H. Direct preparation of anatase TiO $_2$  nanotubes in porous alumina membranes. *J. Mater. Chem.* **1999**, *9*, 2971–2972.
- (281) Tian, Z. R. R.; Voigt, J. A.; Liu, J.; McKenzie, B.; Xu, H. F. Large oriented arrays and continuous films of TiO $_2$ -based nanotubes. *J. Am. Chem. Soc.* **2003**, *125*, 12384–12385.
- (282) Wu, J. J.; Yu, C. C. Aligned TiO $_2$  nanorods and nanowalls. *J. Phys. Chem. B* **2004**, *108*, 3377–3379.
- (283) Ruan, C.; Paulose, M.; Varghese, O. K.; Mor, G. K.; Grimes, C. A. Fabrication of Highly Ordered TiO $_2$  Nanotube Arrays Using an Organic Electrolyte. *J. Phys. Chem. B* **2005**, *109*, 15754–15759.
- (284) Mor, G. K.; Varghese, O. K.; Paulose, M.; Shankar, K.; Grimes, C. A. A review on highly ordered, vertically oriented TiO $_2$  nanotube arrays: Fabrication, material properties, and solar energy applications. *Sol. Energy Mater. Solar Cells.* **2006**, *90*, 2011–2075.
- (285) Paulose, M.; Shankar, K.; Varghese, O. K.; Mor, G. K.; Grimes, C. A. Application of highly-ordered TiO $_2$  nanotube-arrays in heterojunction dye-sensitized solar cells. *J. Phys. D-Appl. Phys.* **2006**, *39*, 2498–2503.
- (286) Adachi, M.; Murata, Y.; Okada, I.; Yoshikawa, S. Formation of titania nanotubes and applications for dye-sensitized solar cells. *J. Electrochem. Soc.* **2003**, *150*, G488–G493.
- (287) Macak, J. M.; Tsuchiya, H.; Ghicov, A.; Schmuki, P. Dye-sensitized anodic TiO $_2$  nanotubes. *Electrochem. Commun.* **2005**, *7*, 1133–1137.
- (288) Law, M.; Greene, L. E.; Johnson, J. C.; Saykally, R.; Yang, P. Nanowire dye-sensitized solar cells. *Nat. Mater.* **2005**, *4*, 455–459.
- (289) Galoppini, E.; Rochford, J.; Chen, H.; Saraf, G.; Lu, Y.; Hagfeldt, A.; Boschloo, G. Fast Electron Transport in Metal Organic Vapor Deposition Grown Dye-sensitized ZnO Nanorod Solar Cells. *J. Phys. Chem. B* **2006**, *110*, 16159–16161.
- (290) Paulose, M.; Shankar, K.; Yoriya, S.; Prakasam, H. E.; Varghese, O. K.; Mor, G. K.; Latempa, T. A.; Fitzgerald, A.; Grimes, C. A. Anodic Growth of Highly Ordered TiO $_2$  Nanotube Arrays to 134 mm in length. *J. Phys. Chem. B* **2006**, *110*, 16179–16184.
- (291) Galoppini, E. Linkers for anchoring sensitizers to semiconductor nanoparticles. *Coord. Chem. Rev.* **2004**, *248*, 1283–1297.
- (292) Grätzel, M. Solar Energy Conversion by Dye-Sensitized Photovoltaic Cells. *Inorg. Chem.* **2005**, *44*, 6841–6851.
- (293) Bisquert, J.; Cahen, D.; Hodes, G.; Rühle, S.; Zaban, A. Physical Chemical Principles of Photovoltaic Conversion with Nanoparticulate, Mesoporous Dye-Sensitized Solar Cells. *J. Phys. Chem. B* **2004**, *108*, 8106–8118.
- (294) Meyer, G. J. Molecular Approaches to Solar Energy Conversion with Coordination Compounds Anchored to Semiconductor Surfaces. *Inorg. Chem.* **2005**, *44*, 6852–6864.
- (295) Hao, E.; Yang, B.; Zhang, J.; Zhang, X.; Sun, J.; Shen, J. Assembly of alternating TiO $_2$ /CdS nanoparticle composite films. *J. Mater. Chem.* **1999**, *8*, 1327–1328.
- (296) Fang, J. J.; Wu, J. X.; Lu, X.; Shen, Y.; Lu, Z. Sensitization of nanocrystalline TiO $_2$  electrode with quantum sized CdSe and ZnTCPC molecules. *Chem. Phys. Lett.* **1997**, *270*, 145.
- (297) Yu, P.; Zhu, K.; Norman, A. G.; Ferrere, S.; Frank, A. J.; Nozik, A. J. Nanocrystalline TiO $_2$  Solar Cells Sensitized with InAs Quantum Dots. *J. Phys. Chem. B* **2006**, *110*, 25455–25461.
- (298) Nozik, A. J. Quantum dot solar cells. *Physica E* **2002**, *14*, 115–120.
- (299) Wang, Z. L. Transmission Electron Microscopy of Shape-Controlled Nanocrystals and Their Assemblies. *J. Phys. Chem. B* **2000**, *104*, 1153–1175.
- (300) Nirmal, M.; Brus, L. Luminescence photophysics in semiconductor nanocrystals. *Acc. Chem. Res.* **1999**, *32*, 407–414.
- (301) Empedocles, S.; Bawendi, M. Spectroscopy of Single CdSe Nanocrystallites. *Acc. Chem. Res.* **1999**, *32*, 389–396.
- (302) Kuno, M.; Fromm, D. P.; Hamann, H. F.; Gallagher, A.; Nesbitt, D. J. Nonexponential “blinking” kinetics of single CdSe quantum dots: A universal power law behavior. *J. Chem. Phys.* **2000**, *112*, 3117–3120.
- (303) Halpernt, J. E.; Porter, V. J.; Zimmer, J. P.; Bawendi, M. G. Synthesis of CdSe/CdTe Nanobarbells. *J. Am. Chem. Soc.* **2006**, *128*, 12590–12591.
- (304) Chan, W. C. W.; Nie, S. Quantum Dot Bioconjugates for Ultrasensitive Nonisotopic Detection. *Science* **1998**, *281*, 2016–2018.
- (305) Mattoussi, H.; Mauro, J. M.; Goldman, E. R.; Anderson, G. P.; Sundar, V. C.; Mikulec, F. V.; Bawendi, M. G. Self-assembly of CdSe-ZnS quantum dot bioconjugates using an engineered recombinant protein. *J. Am. Chem. Soc.* **2000**, *122*, 12142–12150.
- (306) Niemeyer, C. M. Nanoparticles, Proteins, and Nucleic Acids: Biotechnology Meets Materials Science. *Angew. Chem. (Int. Ed.)* **2001**, *40*, 4128–4158.
- (307) Bruchez, M.; Moronne, M.; Gin, P.; Weiss, S.; Alivisatos, A. P. Semiconductor nanocrystals as fluorescent biological labels. *Science* **1998**, *281*, 2013–2016.
- (308) Mattoussi, H.; Radzilowski, L. H.; Dabbousi, B. O.; Thomas, E. L.; Bawendi, M. G.; Rubner, M. F. Electroluminescence from heterostructures of poly(phenylene vinylene) and inorganic CdSe nanocrystals. *J. Appl. Phys.* **1998**, *83*, 7965–7974.
- (309) Huynh, W. U.; Dittmer, J. J.; Alivisatos, A. P. Hybrid Nanorod-Polymer Solar Cells. *Science* **2002**, *295*, 2425–2427.
- (310) Pientka, M.; Wisch, J.; Boger, S.; Parisi, J.; Dyakonov, V.; Rogach, A.; Talapin, D.; Weller, H. Photogeneration of charge carriers in blends of conjugated polymers and semiconducting nanoparticles. *Thin Solid Films* **2004**, *451–52*, 48–53.
- (311) Ross, R. T.; Nozik, A. J. Efficiency of hot-carrier solar energy converters. *J. Appl. Phys.* **1982**, *53*, 3813–8.
- (312) Schaller, R. D.; Klimov, V. I. High Efficiency Carrier Multiplication in PbSe Nanocrystals: Implications for Solar Energy Conversion. *Phys. Rev. Lett.* **2004**, *92*, 186601.
- (313) Schaller, R. D.; Agranovich, V. M.; Klimov, V. C. High-efficiency carrier multiplication through direct photogeneration of multi-excitons via virtual single-exciton states. *Nat. Phys.* **2005**, *1*, 189–195.
- (314) Ellingson, R. J.; Beard, M. C.; Johnson, J. C.; Yu, P. R.; Micic, O. I.; Nozik, A. J.; Shabaev, A.; Efros, A. L. Highly efficient multiple exciton generation in colloidal PbSe and PbS quantum dots. *Nano Lett.* **2005**, *5*, 865–871.
- (315) Califano, M.; Zunger, A.; Franceschetti, A. Efficient inverse Auger recombination at threshold in CdSe nanocrystals. *Nano Lett.* **2004**, *4*, 525–531.
- (316) Lawless, D.; Kapoor, S.; Meisel, D. Bifunctional capping of CdS nanoparticles and bridging to TiO $_2$ . *J. Phys. Chem.* **1995**, *99*, 10329–10335.
- (317) Granot, E.; Patolsky, F.; Willner, I. Electrochemical assembly of a CdS semiconductor nanoparticle monolayer on surfaces: Structural properties and photoelectrochemical applications. *J. Phys. Chem. B* **2004**, *108*, 5875–5881.
- (318) Baron, R.; Huang, C. H.; Bassani, D. M.; Onopriyenko, A.; Zayats, M.; Willner, I. Hydrogen-bonded CdS nanoparticle assemblies on electrodes for photoelectrochemical applications. *Angew. Chem., Int. Ed.* **2005**, *44*, 4010–4015.
- (319) Zayats, M.; Kharitonov, A. B.; Pogorelova, S. P.; Lioubashevski, O.; Katz, E.; Willner, I. Web release, Probing Photoelectrochemical Processes in Au-CdS Nanoparticle Arrays by Surface Plasmon Resonance: Application for the Detection of Acetylcholine Esterase Inhibitors. *J. Am. Chem. Soc.* **2003**, *125*, 16006–16014.
- (320) Meyer, T. J.; Meyer, G. J.; Pfennig, B. W.; Schoonover, J. R.; Timpson, C. J.; Wall, J. F.; Kobusch, C.; Chen, X. H.; Peek, B. M.; Wall, C. G.; Ou, W.; Erickson, B. W.; Bignozzi, C. A. Molecular-Level Electron-Transfer and Excited-State Assemblies on Surfaces of Metal-Oxides and Glass. *Inorg. Chem.* **1994**, *33*, 3952–3964.
- (321) Rogach, A. L.; Kornowski, A.; Gao, M.; Eychmüller, A.; Weller, H. Synthesis and Characterization of a Size Series of Extremely Small Thiol-Stabilized CdSe Nanocrystals. *J. Phys. Chem. B* **1999**, *103*, 3065–3069.
- (322) Hens, Z.; Tallapin, D. V.; Weller, H. Breaking and restoring a molecularly bridged metal|quantum dot junction. *Appl. Phys. Lett.* **2002**, *81*, 4245–4247.

- (323) Cassagneau, T.; Mallouk, T. E.; Fendler, J. H. Layer-by-layer assembly of thin film zener diodes from conducting polymers and CdSe nanoparticles. *J. Am. Chem. Soc.* **1998**, *120*, 7848–7859.
- (324) Landes, C.; Burda, C.; Braun, M.; El-Sayed, M. A. Photoluminescence of CdSe nanoparticles in the presence of a hole acceptor: *n*-butylamine. *J. Phys. Chem. B* **2001**, *105*, 2981–2986.
- (325) Landes, C. F.; Braun, M.; El-Sayed, M. A. On the nanoparticle to molecular size transition: Fluorescence quenching studies. *J. Phys. Chem. B* **2001**, *105*, 10554–10558.
- (326) Sharma, S.; Pillai, Z. S.; Kamat, P. V. Photoinduced charge transfer between CdSe nanocrystals and *p*-phenylenediamine. *J. Phys. Chem. B* **2003**, *107*, 10088–10093.
- (327) Hammel, E.; Tang, X.; Trampert, M.; Schmitt, T.; Mauthner, K.; Eder, A.; Potschke, P. Carbon nanofibers for composite applications. *Carbon* **2004**, *42*, 1153–1158.
- (328) Wang, J.; Deo, R. P.; Poulin, P.; Mangey, M. Carbon nanotube fiber microelectrodes. *J. Am. Chem. Soc.* **2003**, *125*, 14706–14707.
- (329) Rajesh, B.; Thampi, K. R.; Bonard, J. M.; Mathieu, H. J.; Xanthopoulos, N.; Viswanathan, B. Conducting polymeric nanotubules as high performance methanol oxidation catalyst support. *Chem. Commun.* **2003**, 2022–2023.
- (330) Kamat, P. V. Carbon Nanomaterials: Building Blocks in Energy Conversion Devices. *Interface* **2006**, *15*, 45–47.
- (331) Kamat, P. V. Harvesting photons with carbon nanotubes. *Nanotoday* **2006**, *1*, 20–27.
- (332) Girishkumar, G.; Hall, T. D.; Vinodgopal, K.; Kamat, P. V. Single Wall Carbon Nanotube Supports for Portable Direct Methanol Fuel Cells. *J. Phys. Chem. B* **2006**, *110*, 107–114.
- (333) Hasobe, T.; Fukuzumi, S.; Kamat, P. V. Stacked-Cup Carbon Nanotubes for Photoelectrochemical Solar Cells. *Angew. Chem., Int. Ed.* **2006**, *45*, 755–759.
- (334) Barazzouk, S.; Hotchandani, S.; Kamat, P. V. Unusual Electrocatalytic Behavior of Ferrocene Bound Fullerene Cluster Films. *J. Mater. Chem.* **2002**, *12*, 2021–2025.
- (335) Barazzouk, S.; Hotchandani, S.; Vinodgopal, K.; Kamat, P. V. Single wall carbon nanotube films for photocurrent generation. A prompt response to visible light irradiation. *J. Phys. Chem. B* **2004**, *108*, 17015–17018.
- (336) Baughman, R. H.; Zakhidov, A. A.; de Heer, W. A. Carbon nanotubes - the route toward applications. *Science* **2002**, *297*, 787–792.
- (337) Sheeney-Haj-Khia, L.; Basnar, B.; Willner, I. Efficient generation of photocurrents by using CdS/Carbon nanotube assemblies on electrodes. *Angew. Chem., Int. Ed.* **2005**, *44*, 78–83.
- (338) Huang, Q.; Gao, L. Synthesis and characterization of CdS/multiwalled carbon nanotube heterojunctions. *Nanotechnology* **2004**, *15*, 1855–1860.
- (339) Banerjee, S.; Wong, S. S. In situ quantum dot growth on multiwalled carbon nanotubes. *J. Am. Chem. Soc.* **2003**, *125*, 10342–10350.
- (340) Banerjee, S.; Wong, S. S. Formation of CdSe nanocrystals onto oxidized, ozonized single-walled carbon nanotube surfaces. *Chem. Commun.* **2004**, 1866–1867.
- (341) Chaudhary, S.; Kim, J. H.; Singh, K. V.; Ozkan, M. Fluorescence microscopy visualization of single-walled carbon nanotubes using semiconductor nanocrystals. *Nano Lett.* **2004**, *4*, 2415–2419.
- (342) Haremza, J. M.; Hahn, M. A.; Krauss, T. D. Attachment of single CdSe nanocrystals to individual single-walled carbon nanotubes. *Nano Lett.* **2002**, *2*, 1253–1258.
- (343) Ravindran, S.; Chaudhary, S.; Colburn, B.; Ozkan, M.; Ozkan, C. S. Covalent coupling of quantum dots to multiwalled carbon nanotubes for electronic device applications. *Nano Lett.* **2003**, *3*, 447–453.
- (344) Banerjee, S.; Wong, S. S. Synthesis and characterization of carbon nanotube-nanocrystal heterostructures. *Nano Lett.* **2002**, *2*, 195–200.
- (345) Han, W. Q.; Zettl, A. Coating single-walled carbon nanotubes with tin oxide. *Nano Lett.* **2003**, *3*, 681–683.
- (346) Shi, J.; Qin, Y.; Wu, W.; Li, X.; Guo, Z.-X.; Zhu, D. In situ synthesis of CdS nanoparticles on multi-walled carbon nanotubes. *Carbon* **2004**, *42*, 455–458.
- (347) Robel, I.; Bunker, B.; Kamat, P. V. SWCNT-CdS nanocomposite as light harvesting assembly. Photoinduced charge transfer interactions. *Adv. Mater.* **2005**, *17*, 2458–2463.
- (348) Takechi, K.; Sudeep, S.; Kamat, P. V. Harvesting Infrared Photons with Tricarbocyanine Dye Clusters. *J. Phys. Chem. B* **2006**, *110*, 16169–16173.
- (349) Tang, C. W. 2-Layer Organic Photovoltaic Cell. *Appl. Phys. Lett.* **1986**, *48*, 183–185.
- (350) Shaheen, S. E.; Brabec, C. J.; Sariciftci, N. S.; Padinger, F.; Fromherz, T.; Hummelen, J. C. 2.5% efficient organic plastic solar cells. *Appl. Phys. Lett.* **2001**, *76*, 841–843.
- (351) Heeger, A. J. Semiconducting and Metallic Polymers: The Fourth Generation of Polymeric Materials. *J. Phys. Chem. B* **2001**, *105*, 8475–8491.
- (352) Gomez-Romero, P. Hybrid organic-inorganic materials - In search of synergic activity. *Adv. Mater.* **2001**, *13*, 163–174.
- (353) Breeze, A. J.; Schlesinger, Z.; Carter, S. A.; Brock, P. J. Charge transport in TiO<sub>2</sub>/MEH-PPV polymer photovoltaics. *Phys. Rev. B* **2001**, *64*, art. no.-125205.
- (354) Hoppe, H.; Sariciftci, N. S. Organic solar cells: An overview. *J. Mater. Res.* **2004**, *19*, 1924–1945.
- (355) Yu, G.; Gao, J.; Hummelen, J. C.; Wudl, F.; Heeger, A. J. Polymer Photovoltaic Cells - Enhanced Efficiencies Via a Network of Internal Donor-Acceptor Heterojunctions. *Science* **1995**, *270*, 1789–1791.
- (356) Pientka, M.; Dyakonov, V.; Meissner, D.; Rogach, A.; Vanderzande, D.; Weller, H.; Lutsen, L.; Vanderzande, D. Photoinduced charge transfer in composites of conjugated polymers and semiconductor nanocrystals. *Nanotechnology* **2004**, *15*, 163–170.
- (357) Gregg, B. A. Excitonic Solar Cells. *J. Phys. Chem. B* **2003**, *107*, 4688–4698.
- (358) Sariciftci, N. S. Role of buckminsterfullerene, C<sub>60</sub>, in organic photoelectric devices. *Prog. Quant. Electr.* **1995**, *19*, 131–59.
- (359) Brabec, C. J.; Sariciftci, N. S.; Hummelen, J. C. Plastic Solar Cells. *Adv. Funct. Mater.* **2001**, *11*, 15–26.
- (360) Salafsky, J. S. Exciton dissociation, charge transport, and recombination in ultrathin, conjugated polymer-TiO<sub>2</sub> nanocrystal intermixed composites. *Phys. Rev. B* **1999**, *59*, 10885–10894.
- (361) Drew, K.; Girishkumar, G.; Vinodgopal, K.; Kamat, P. V. Boosting the Fuel Cell Performance with a Semiconductor Photocatalyst. TiO<sub>2</sub>/Pt-Ru Hybrid Catalyst for Methanol Oxidation. *J. Phys. Chem. B* **2005**, *109*, 11851–11857.
- (362) Carrette, L.; Friedrich, K. A.; Stimming, U. Fuel cells: Principles, types, fuels, and applications. *ChemPhysChem* **2000**, *1*, 162–193.
- (363) Wasmus, S.; Kuver, A. Methanol oxidation and direct methanol fuel cells: a selective review. *J. Electroanal. Chem.* **1999**, *461*, 14–31.
- (364) Maynard, H. L.; Meyers, J. P. Miniature fuel cells for portable power: Design considerations and challenges. *J. Vacuum Sci. Technol. B* **2002**, *20*, 1287–1297.
- (365) Eikerling, M.; Iasevich, A. S.; Komyshev, A. A. How good are the electrodes we use in PEFC? *Fuel Cells.* **2004**, *4*, 131–140.